

BACTERIA AS DRUG DELIVERY VEHICLES

by

SEBASTIAN OLIVER WENDEL

Dipl.Ing., FH University of Applied Sciences Giessen, 2011

AN ABSTRACT OF A DISSERTATION

submitted in partial fulfillment of the requirements for the degree

DOCTOR OF PHILOSOPHY

Department of Chemical Engineering
College of Engineering

KANSAS STATE UNIVERSITY
Manhattan, Kansas

2015

Abstract

Both chemotherapy for cancer treatment and antibiotic therapy for bacterial infections require systemic applications of the drug and a systemic application is always linked to a number of disadvantages. To circumvent these a targeted drug delivery system was developed. It utilizes the ability of phagocytes from the hosts own immune system to recognize and internalize antigens. Deactivated *M. luteus*, a non-pathogenic gram positive bacteria was loaded with high concentrations (exceeding the IC₅₀ at least 60 fold in local intracellular concentration) the chemotherapeutics doxorubicin or DP44mt or with the bactericidal chlorhexidine. The modified bacteria is fed to phagocytes (Monocytes/Macrophages or neutrophils) and serves as protective shell for the transporting and targeting phagocyte. The phagocyte is recruited to the tumor site or site of infection and releases the drug along with the processed *M. luteus* via the exosome pathway upon arrival.

The chlorhexidine drug delivery system was successfully tested both *in vitro* and *in vivo*, reducing the pathogen count and preventing systemic spread of a *F. necrophorum* infection in a mouse model. The doxorubicin drug delivery system reduced the viability of 4T1 cancer cells to 20% over the course of four days *in vitro*.

BACTERIA AS DRUG DELIVERY VEHICLES

by

SEBASTIAN OLIVER WENDEL

Dipl.Ing., FH University of Applied Sciences Giessen, 2011

A DISSERTATION

submitted in partial fulfillment of the requirements for the degree

DOCTOR OF PHILOSOPHY

Department of Chemical Engineering
College of Engineering

KANSAS STATE UNIVERSITY
Manhattan, Kansas

2015

Approved by:

Major Professor
Stefan H. Bossmann

Copyright

SEBASTIAN OLIVER WENDEL

2015

Abstract

Both chemotherapy for cancer treatment and antibiotic therapy for bacterial infections require systemic applications of the drug and a systemic application is always linked to a number of disadvantages. To circumvent these a targeted drug delivery system was developed. It utilizes the ability of phagocytes from the hosts own immune system to recognize and internalize antigens. Deactivated *M. luteus*, a non-pathogenic gram positive bacteria was loaded with high concentrations (exceeding the IC₅₀ at least 60 fold in local intracellular concentration) the chemotherapeutics doxorubicin or DP44mt or with the bactericidal chlorhexidine. The modified bacteria is fed to phagocytes (Monocytes/Macrophages or neutrophils) and serves as protective shell for the transporting and targeting phagocyte. The phagocyte is recruited to the tumor site or site of infection and releases the drug along with the processed *M. luteus* via the exosome pathway upon arrival.

The chlorhexidine drug delivery system was successfully tested both *in vitro* and *in vivo*, reducing the pathogen count and preventing systemic spread of a *F. necrophorum* infection in a mouse model. The doxorubicin drug delivery system reduced the viability of 4T1 cancer cells to 20% over the course of four days *in vitro*.

Table of Contents

List of Figures	x
List of Tables	xiii
Acknowledgements.....	xiv
Chapter 1 - Introduction.....	1
Characteristics of Tumor Physiology	2
Differences between tumor tissue and healthy tissue	2
Tumor Hypoxia.....	2
Cancer treatment strategies.....	3
Chemotherapy	3
Endocrine therapy	4
Targeted therapy	4
Anti-angiogenic therapy.....	4
Virotherapy	5
Solid tumors and the immune system.....	5
Antibiotic and antimicrobial resistance, a global threat	6
Development of MDR.....	7
Drug delivery systems (DDS).....	8
Liposomes and similar particulate carriers	9
Enhanced Permeability and Retention (EPR) effect.....	10
Active targeting systems for synthetic delivery systems	12
Cell based drug delivery systems.....	12
Monocytes and macrophages	12
Erythrocytes	13
Bacterial ghosts.....	13
Summary.....	14
Phagocytes	14
Discovery and sub-classification	14
Available antibacterial and antiviral pathways	15

Activation of phagocytes	16
Chapter 2 - Cell-Types and Active Components Used in the Drug Delivery System.....	18
Monocytes.....	18
Macrophages.....	18
The Macrophage life cycle.....	19
Neutrophil granulocytes.....	19
Active Components.....	20
DPP44mt.....	20
Doxorubicin	21
Chlorhexidine.....	21
Chapter 3 - Abbreviations.....	23
Chapter 4 - Materials and Methods.....	25
Materials	25
Buffers	25
PBS	25
Lysis Buffer	26
Strong Lysis Buffer.....	26
<i>M. luteus</i> Culture.....	26
Loading of <i>M. Luteus</i> with Chlorhexidine.....	26
Indirect measurement.....	27
Direct measurement	28
Time Resolved Loading of CHX	28
Zeta Potential Measurements	28
CHX Retention.....	29
Thioglycollate Induced Peritonitis for ex vivo use of Neutrophils.....	29
Flow Cytometry Analysis of Neutrophils.....	29
PI-Annexin-V Assay to determine neutrophil survival	30
In Vitro drug delivery against <i>E. coli</i> and <i>F. necrophorum</i>	30
Loading of Doxorubicin (DOX) in <i>M. luteus</i>	31
DOX Retention	32
MTT assay for cell viability measurements.....	33

4T1 Cancer Cell Assay with Conditioned Medium	33
DP 44 mt	34
DP44mt Retention.....	34
DP44mt Analogue – CHX Conjugate.....	34
Conjugate Retention.....	35
In vivo Studies	35
Preliminary toxicity Study	35
Mouse-treatment Study.....	36
Chapter 5 - Characterization of Loaded <i>M. luteus</i> , <i>ex vivo</i> Loading of Neutrophils and <i>in vitro</i>	
Drug Delivery Testing	37
<i>M. luteus</i> loaded with chlorhexidine.....	37
Characterization of the loaded bacterial cells	37
Neutrophil loading and survival <i>ex-vivo</i>	41
Evaluation of Oxygen Consumption and Supply in the <i>ex vivo</i> loading procedure.....	43
In-Vitro Results.....	46
<i>M. luteus</i> loaded with doxorubicin	48
Characterization of the loaded bacterial cells	48
Retention of DOX	51
In vitro cell assays of Mo/Ma cell survival.....	52
In vitro cell assays with 4T1 cancer cells and conditioned medium.....	53
<i>M. luteus</i> loaded withDP44mt	56
Characterization of the loaded bacterial cells	56
In vitro cell assay for Mo/Ma cell survival.....	59
CHX-DP44mt analogue conjugate	60
Conclusions.....	62
Chapter 6 - <i>In vivo</i> Mouse Studies of the Cell Based Antibacterial Drug Delivery System Against	
<i>F. necrophorum</i> Infections	64
Preliminary mouse toxicity study	64
Mouse study for antibacterial drug delivery against <i>F. necrophorum</i> infections.....	64
Conclusions.....	66
References.....	68

Appendix A - R-code for student's t-test..... 89

List of Figures

Figure 1: Schematic of the proposed drug delivery system.....	1
Figure 2: Example for the setup of the 96 well plate for UV/Vis analysis.....	27
Figure 3: Example for the setup of the 96 well plate for DOX analysis in the <i>M. luteus</i> cell lysate	32
Figure 4: Comparison of the <i>M. luteus</i> absorption with and without CHX. The loaded sample ● shows the distinctive peak for CHX at 635nm while the unloaded sample ● does not.....	37
Figure 5: Time resolved loading of <i>M. luteus</i> with CHX. While the average spectral absorption for intracellular CHX increases over time, the difference between the time steps is not significant ($p>0.05$).....	38
Figure 6: Zeta potential data (surface charge) for <i>M. luteus</i> loaded with CHX-hydrochloride over a range of concentrations from 0 μ g/ml to 1000 μ g/ml CHX. The data has been normalized (0%-100% equals an increase of the zeta potential from -32.86 \pm 1.88 mV to -9.63 \pm 2.22 mV).	39
Figure 7: Correlation of the measured zeta potential (x-axis) with the measured absorption of CHX in the lysate (y-axis). A linear trend with an R^2 value of 0.9045 is visible.	40
Figure 8: Analysis of CHX retention in <i>M. luteus</i> over the course of 5 days. There is no detectable increase in the amount of free, extracellular CHX (average value over 5 days is 15 μ g), while the intracellular CHX stays constant at an average of 490 μ g.	41
Figure 9: Comparison of the yellow fluorescence of an unloaded neutrophil population with a neutrophil population loaded with rhodamine-modified <i>M. luteus</i>	42
Figure 10: Neutrophil survival after 3 and 6 hours for ratios of 10, 20 and 100 bacteria/neutrophil determined by PI/annexin 5 apoptosis assay and flow cytometry.	43
Figure 11: <i>In vitro</i> tests of the cell based CHX drug delivery system on <i>E. coli</i> C600N. Here <i>E. coli</i> C600N was exposed to the following test groups: A is the CHX - <i>M. luteus</i> – Neutrophil granulocyte delivery system, B is the first control group with Neutrophil granulocytes loaded with unmodified <i>M. luteus</i> , C is the second control group with just unmodified Neutrophil granulocytes and D is the third control group with plain RPMI culture medium.	47

Figure 12: *In vitro* tests of the cell based CHX drug delivery system on *Fusobacterium necrophorum* subspecies *necrophorum*. Here *Fusobacterium necrophorum* subspecies *necrophorum* was exposed to the following test groups: A is the CHX - *M. luteus* – Neutrophil granulocyte delivery system, B is the first control group with Neutrophil granulocytes loaded with unmodified *M. luteus*, C is the second control group with just unmodified Neutrophil granulocytes and D is the third control group with plain RPMI culture medium. 48

Figure 13: Typical UV/Vis absorption spectrum for several DOX concentrations..... 49

Figure 14: Calibration curves for DOX in PBS and in lysis buffer. Lysis buffer reduces the absorption for samples of the same concentration by a factor of 3.3..... 50

Figure 15: Mass balance for doxorubicin loaded *M. luteus*. The difference between intracellular & unloaded sample compared with the initial DOX concentration is not significant. Measurements for DOX in lysis buffer resulted in a larger standard deviation, a behavior not seen for the calibration curve. Approximately 36% of the initially provided DOX was internalized by bacterial cells..... 51

Figure 16: DOX retention over the course of seven days. The bacterial cells have released 38% of the initially internalized DOX. 52

Figure 17: MTT assay to determine the survival of Mo/Ma cell cultures when exposed to bacterial samples and bacteria loaded with DOX. While the viability decreases significantly for both sample types it remains at 80% after 72 hours. This is a sufficient value since Mo/Ma cells should be able to reach their target within 24 hours..... 53

Figure 18: The 4T1 breast cancer cell line is exposed to conditioned medium from Mo/Ma-DOX cells or Mo/Ma cells loaded with DOX modified bacteria. Only the conditioned medium from the Mo/Ma - bacterial carrier system was able to reduce 4T1 cell viability. It drops from 95% to less than 20% within 4 days..... 54

Figure 19: DOX released from Mo/Ma cells loaded with free DOX or DOX in a bacterial carrier. The amounts of DOX released from the bacterial carrier system are significantly higher than the DOX released from the bacteria free system. Data was acquired via IVIS fluorescence. 55

Figure 20: The fluorescence of Mo/Ma cells loaded with DOX-bacteria decreases over the course of five days as DOX is released from the cells. Flow cytometry registers DOX-specific

fluorescent cells of the total Mo/Ma population. Initially 70% of the Mo/Ma population showed DOX-specific fluorescence. This value decreases to 20% after five days.	56
Figure 21: Typical UV/Vis spectrum for various concentrations of DP44mt	57
Figure 22: Calibration curve for quantification of intracellular DP44mt	57
Figure 23: The left image shows the mass balance for the loading process of DP44mt. The sum of DP44mt found in the various cell associated samples exceeds the initially provided amount by 7.4 µg. The right image shows the spectra for the intracellular DP44mt and DP44mt in the washing step. While the signal is weak the specific peak for DP44mt at 320 nm can still be seen.	58
Figure 24: DP44mt is not retained by <i>M. luteus</i> cells. The complete amount of initially intracellular DP44mt is released after 48 hours allowing the cytotoxic effects of DP44mt to affect the transporting Mo/Ma cells.	59
Figure 25: Mo/Ma cell viability observed over 72 hours. DP44mt is not contained by its bacterial carrier and shows similar cytotoxicity as the free DP44mt.	60
Figure 26: The left graph shows the UV/Vis spectrum for the conjugate while the right spectrum shows the spectra for the individual pure components. While the general shape of the conjugate absorption curve resembles the CHX-hydrochloride curve the conjugate spectrum is red-shifted in comparison due to the influence of the DP44mt analogue.	61
Figure 27: The conjugates retention in <i>M. luteus</i> was measured over the course of 6 days. Consistently large absorption for extracellular conjugate due to its poor water solubility make it unclear if the retention of the conjugate is better in comparison to DP44mt.	62
Figure 28: Results of the <i>in vivo</i> experiment. MP + CH is the treatment group containing neutrophils loaded with CHX modified <i>M. luteus</i> . MP + DOXY is the treatment group containing neutrophils loaded with doxycycline modified bacteria. The PBS group is the control group containing pure RPMI medium while PMN and PMN + MP represent the neutrophil control groups without and with unmodified <i>M. luteus</i>	65
Figure 29: Image of a mouse liver from the PBS control group showing lesions caused by <i>F. necrophorum</i> subspecies <i>necrophorum</i>	66

List of Tables

Table 1: Oxygen consumption for different cell types under phagocytotic stress. Values were obtained from references 224 and 232.....	46
Table 2: Standard deviations for the DOX calibration curves	50
Table 3: Values for the DP44mt calibration curve including standard deviations	58
Table 4: Bactericidal properties of the synthesized conjugate.....	61

Acknowledgements

I first would like to thank my advisor Dr. Stefan Bossmann for four exciting years full of crazy ideas and, sometimes, even crazier results. Working for and with you, and all the things that happen along the way (conference trips, delicious food parties, becoming a movie star on the K-State channel) make me miss the time in your group before it's even over and really leave me with nothing much to say other than: Thank you!!!

Of course I wouldn't have had the chance to go to K-State in the first place if it weren't for Dr. Peter Czermak who offered me this opportunity in 2009 and accompanies me to this day as a member of my committee. Thank you very much.

I'd also like to thank my committee members Dr. Peter Pfromm and Dr. Deryl Troyer for their ideas, their help and input along the way.

Furthermore I thank Hamad for his help with the *in vitro* and *ex vivo* experiments and his friendship. Sailesh and Dr. Narayanan, for their help and their efforts during the *in vitro* experiments with *F. necrophorum* and especially for the time during the *in vivo* experiment when my capabilities were impaired by my broken ankle!

I am also grateful for the help, the exchange of knowledge and ideas with all Bossmann group members, especially Hongwang, Aruni and Thilani. This also includes my undergrads Jenny and Lauren whom I wish all the best for their grad school careers.

When you live in one place for four years you'd expect to make some good friends. I made some great ones and thanks to Ronny that happened on my first day here. Josh, Vika, Celine, Deisy and Sigi, thank you all. Kevin, I met you a bit later but you and your family have done more for me than I can possibly list here, thank you for everything!

My final thanks goes to my family, my mom and dad and my sister. Your support means everything to me.

Chapter 1 - Introduction

The goal of this work is to utilize phagocytes, part of the unspecific immune system, to carry chemotherapeutics or antimicrobial drugs to the tumor or site of infection respectively. This targeted approach aims to circumvent a systemic application of a drug and rather relies on a high local concentration at the site where the drug is needed. However to avoid cytotoxic effects on the phagocyte by the drug and to enhance uptake the drug is first loaded into the nonpathogenic bacterium *M. luteus*. *M. luteus* provides a protective shell that retains the drug within the bacterium and enhances uptake with its antigen covered surface. The following sections aim to give a general overview of current drug delivery systems and to show which type of phagocyte and drug is suited for this application.

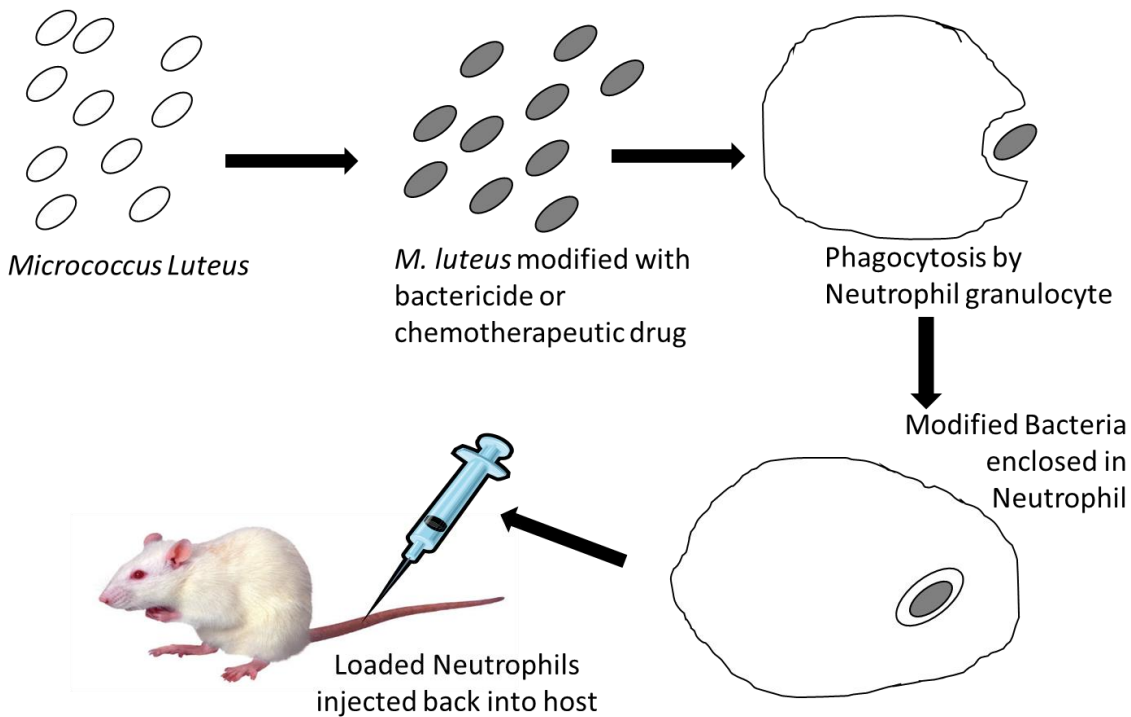


Figure 1: Schematic of the proposed drug delivery system

Characteristics of Tumor Physiology

Differences between tumor tissue and healthy tissue

One big challenge of the cytotoxic mechanisms of non-surgical anticancer methods is their non-specificity. To a certain degree both radio- and chemo-therapy are limited in their effect because they kill healthy cells as well. Radiation therapy tries to counteract by an increased precision and focus of the beam towards the tumor and its immediate surroundings. Yet these efforts are limited if the tumor is located deep because the surrounding tissue blocks the radiation dose.

Chemotherapy drugs can achieve a degree of specificity by targeting DNA synthesis and therefore being more lethal to rapidly dividing cells. This however includes bone marrow cells (precursor cells to the immune system), hair follicles and epithelial cells of the gastrointestinal tract, causing severe side effects for chemotherapy patients.

The underlying difference in solid tumors separating them from healthy tissue is the tumor vasculature. A tumor is supplied by two types of vessels:

- Preexisting vessels from the healthy tissue that the tumor invaded
- Microvessels from neovascularization as a result of proangiogenic factors secreted by the tumor cells

In 1979 Endrich et al. ¹⁾ described *in vivo* tumor blood flow for the first time and noted its heterogeneity and leakiness. Structural abnormalities like wider endothelial gaps were later identified as the reason for the altered flow patterns ^{2,3)}.

The newly formed blood vessels proved to be highly irregular, including dead ends, random branching and a lack of smooth muscle or nerve supply ⁴⁾.

Tumor Hypoxia

Tumor hypoxia is a common feature of solid tumors in mammals ⁵⁾. These hypoxic tumor areas can render cancer treatment ineffective, ⁶⁾ for example has shown that the success of radiation therapy depends on the available oxygen supply. Oxygen has a diffusion distance of approximately 150 μ m with typical intercapillary oxygen tensions and oxygen consumption rates ⁴⁾.

Hypoxic tumor cells have also a slower rate of proliferation due to their limited oxygen supply ^{7,} ⁸⁾ and additionally must be the most distant cells from drug distributing blood vessels. Both factors cause chemotherapeutics that target rapidly dividing cells to lose their effectiveness because on the one hand hypoxic cells are down-regulated and on the other hand the drug concentration drops with distance to the blood vessel.

Two causes for hypoxia are known. The general case is the model with limited oxygen diffusion distance ⁹⁾. Acute hypoxia can occur due to temporary obstructions of the blood flow in tumor blood vessels ¹⁰⁾. Hypoxia offers new methods to attack cancer cells, for example with drugs that show cytotoxicity towards hypoxic cells like quinine antibiotics or nitroimidazoles ^{11, 12, 13)}. Siim et al. illustration demonstrates a hypothetical synergistic effect of traditional/hypoxic tumor treatment.

Cancer treatment strategies

There are three major types of available cancer treatments. Surgery is the oldest and, if possible, most effective strategy since it is a zero order kinetic effectively removing the diseased cells from the body and therefore eliminating 100% of the threat. In contrast the other two types, radiotherapy and chemotherapy, can only kill a fraction of the tumor cells with each treatment cycle, making them effective complementary therapies. With 45% of all newly diagnosed cancer cases receiving radiotherapy ¹⁴⁾ the most common therapeutic pathway is radiotherapy with either a complementary chemo therapy or surgery. If surgery is the complementary treatment a postoperative radiotherapy is preferred ¹⁵⁾.

Chemotherapy

Chemotherapy is the systemically administration of cytotoxic drugs that mostly target a cell's DNA, a valid target for rapidly dividing cells like cancer cells. The drug is often administered in high, but not life threatening dosages called maximum tolerated dose (MTD) ^{16, 17)}. This kind of treatment requires extended treatment-free periods to allow the patient to recover from the side effects, taking the cytotoxic pressure off of surviving cancer cells and increasing the risk of the development of drug resistant cancer cells ¹⁸⁾.

Endocrine therapy

Newer treatment strategies emerge as the understanding of different cancer types is improved. Endocrine treatments for hormone related cancers ¹⁹⁾ such as breast and prostate cancer represent a new pathway to enhance traditional treatment methods. Selective estrogen inhibitors ²⁰⁾ and the newer aromatase inhibitors ²¹⁾ have increased the 10 year survival rate by 11% for endocrine receptor positive breast cancer patients ²²⁾.

Targeted therapy

Targeted therapy aims to find common targets that are universal for as many types of cancer as possible. There are two general types of targeting molecules: Monoclonal antibodies (mAb) and small molecular inhibitors. A possible route is to deplete the tumor of essential growth factors through binding them with specialized mAb. Anti HER-2 mAb ²³⁾ for example bind to the HER-2/neu trans membrane receptor that is mediating cell growth, differentiation and survival. The HER-2/neu receptor is overexpressed in 20-25% of all breast cancer cases ²⁴⁾ constituting an especially aggressive form with short disease free periods after postoperative chemotherapy cycles.

The findings led to trastuzumab, a mAb against the HER-2/neu receptor, blocking the outside domain and inducing an antibody dependent immune cytotoxic response ²⁵⁾. In cases where the trastuzumab treatment proved ineffective a small molecule inhibitor (lapatinib) can be used to inhibit the activity of the intracellular tyrosine kinase domain of the HER-2/neu receptor ²⁶⁾.

Anti-angiogenic therapy

As the tumor growth progresses the process of angiogenesis is crucial for tumor survival and to avoid hypoxia and starvation ²⁷⁻²⁹⁾. It was first hypothesized in 1971 that anti-angiogenic therapeutics are an effective pathway for cancer treatment ³⁰⁾. Angiogenesis is a process induced by cytokines such as VEGF, bFGF, PIGF and IL-8 and does not solely involve tumor cells. Surrounding tissue cells may be manipulated to produce these cytokines while the angiogenic process itself is carried out by cells of the immune system ³¹⁾.

A way to combat tumor angiogenesis is metronomic chemotherapy where low but frequent non-toxic dosages (rather than the usual high and infrequent) of chemotherapeutics are applied. These target the endothelium of the tumor vasculature or tumor stroma rather than the tumor itself ¹⁷⁾.

Virotherapy

Viral therapy exploits the ability of retroviruses to insert genes into a host cell. This mechanism can be used to manipulate tumor cells so that they express prodrug activating enzymes causing the administered prodrug to only become active within the tumor environment. An example is the use of herpes simplex in combination with the gene for thymidine kinase and the drug ganciclovir or cytosine deaminase with 5-fluorocytosine ³²⁾. However the immune system as well as a dense tumor stroma may prevent the virus from reaching all tumor cells.

Solid tumors and the immune system

This section focusses on the relationship between cancerous cells and the immune system, most importantly monocytes, macrophages and neutrophils. Neutrophils make up a large portion of the leukocyte count found in a wide variety of human cancers ^{33, 34)}. Neutrophil granulocytes have three options to take influence on tumor growth and invasiveness:

- Chemokines and cytokines to regulate cell activity of both the tumor and the immune system
- Cytotoxic reactive oxygen species (ROS). ROS have been shown to induce tumor establishment by causing gene-damage to host cells ³⁵⁾. Adversely ROS cytotoxicity has been shown to damage tumor cells ³⁶⁾
- Proteases for the degradation of cell-matrix or extracellular matrix proteins

These examples underline the multilayered role of immune cells in the tumor microenvironment. Fridlender et al. ³⁷⁾ have shown that two different phenotypes of tumor associated neutrophils (TAN) exist. Depending on their configuration they are distinguished as TAN-N1 and TAN-N2, anti and pro tumor neutrophils respectively.

The phenotype TAN-N1 shows anti-tumor activity by cytotoxicity through reactive oxygen species ³⁷⁻³⁹⁾, reduced tumorigenesis by MMP-8 secretion ⁴⁰⁾, induction of apoptosis ⁴¹⁾ and activation of the immune system through chemokines and cytokines ^{37, 42)}.

TAN-N2 promotes the tumor by MMP-9 secretion (anti-apoptotic) ^{43, 44)} Extravasation (collagenase, heparanase) ⁴⁵⁻⁴⁷⁾ angiogenesis (MMP-9) ⁴⁸⁻⁵⁰⁾ and immune suppression (arginase → T-cell inhibition) ⁵¹⁾.

Generally the presence of (TAN) correlates with a disadvantageous prognosis as well as increased mortality^{33, 34)}. An important factor associated with a high TAN count is the IL-8 level of a patient. High IL-8 levels correlate with both, high TAN count and poor survival⁵²⁾.

An important task of TANs is the remodeling of the immediate surroundings of the tumor, called immunosculpting or immunoediting. Here neutrophils are activated by tumor cells to remove healthy tissue surrounding the tumor, making space for new tumor cells^{53, 54)}. This is achieved by the neutrophils wide arsenal of proteinases. These proteinases are used to degrade different cytokines, chemokines, integrins as well as their receptors and extracellular matrix proteins (collagen, elastin) to aid proliferation and angiogenesis. The most prominent proteases are

- Neutrophil elastase: it makes up 2% of the neutrophil dry weight⁵⁵⁾ and has a broad substrate specificity. It is meant to clean up cell from invading organisms or cell debris⁵⁶⁾ but can also process the aforementioned protein spectrum, aiding tumor angiogenesis⁵⁷⁾
- MMP-9 or gelatinase-B: neutrophil associated MMP-9 is not inhibited by TIMP-1 molecule allowing an easier activation and a higher activity in the tumor environment⁵⁵⁾.
- MMP-8

Neutrophils are actively recruited into the tumor microenvironment through IL-8 secretion by the tumor cells themselves. Then tumor cells can use the ICAM-1 receptor to bind to neutrophils and escape into circulation where they migrate to new, healthy tissues to form metastases⁵⁸⁾.

Antibiotic and antimicrobial resistance, a global threat

With the release of the World Health Organization's (WHO) report on the status of antimicrobial resistance in April 2014 it becomes increasingly clear that the broad application of antibiotics in the health systems and food production cycles around the world has initiated the transition towards a post antibiotic era. In this scenario common diseases like pneumonia from Streptococcus or Klebsiella infections, diarrhea from Salmonella or Shigella infections or blood infections from E. coli or Staphylococcus pose a serious threat to the health system and economy through their acquired multi drug resistances (MDR). MDR is defined as a resistance against typical first line drugs (Doxycycline, Azithromycin, from CDC antibiotic treatment guidelines⁵⁹⁾. Diseases like Tuberculosis (TB) or cystic fibrosis have advanced even further and reached a

stage of extensive drug resistance (XDR). Organisms that have reached a drug resistance against at least one or two of the most powerful antimicrobial drugs (e.g. mycobacterium tuberculosis (MTB) and its resistance against fluoroquinolone) are classified XDR. XDR-TB cases have been found in 92 countries and an estimated 6% of all TB cases are caused by MDR-TB ⁶⁰.

Pneumonia patients face an even more severe situation with XDR-pathogens against cephalosporin and carbapenems due to a class of enzymes called extended spectrum β -lactamases (ESBL) ⁶¹.

WHO has selected seven pathogens for an extensive report on and a prolonged surveillance of their drug resistance development. The data was compiled of the available resources from national official agencies, national and international antimicrobial resistance surveillance networks and scientific literature from 2008 on with a decreasing respective order of importance. WHO has also evaluated the economic impact of this threat caused by prolonged treatment times, decreased drug effectiveness and more sick days resulting in a loss of 20 billion \$ in the United States alone as indicated by the 2013 CDC report.

Development of MDR

Even if dosages and treatment times were sufficient, microorganisms have developed resistances due to the following factors:

- Suppressed immune functions of the patient
- Poor drug bioavailability
- Increased drug metabolism ⁶⁰

The pathways over which these resistances were acquired are called primary resistance (when the pathogen was resistant to the drug before it had contact with it) and secondary resistance. The secondary resistance, or acquired resistance, is developed by selective pressure on the pathogen after it had an encounter with the drug ^{62, 63}. It can be divided in three sub-categories depending on their severity:

- Intrinsic resistance or MDR. Characterized by a resistance against first line drugs (e.g. rifampicine or fluconazole ⁶²)
- Extensive resistance. Characterized by a resistance against the most powerful antimicrobials (e.g. fluoroquinolone ^{64,65})

- Clinical resistance. This is the case if the invading pathogen is only inhibited by drug concentrations higher than the MTD ⁶²⁾

The general mechanisms of action of antibiotic drugs are inhibition of metabolic pathways like nucleotide synthesis, DNA/RNA synthesis or protein synthesis as well as a competition with the substrates for cell wall synthesis for enzymes like chitin synthase ⁶⁶⁾. The problem with mechanisms that target the biochemistry of the cell is that mutations in the genome and the selective pressure on the pathogen population bare the risk that pathogens develop appropriate countermeasures ⁶⁰⁾. These may include alterations in the membrane composition that reduce permeability, uptake and susceptibility to antibiotics ^{62, 66, 67)}. An example is the reduced ergosterol content in fungal plasma membranes. Gene mutations in genes that encode the targeted protein can lead to structural changes in the protein's 3D configuration of the peptide chain. While the proteins biochemical function is retained, this can cause decreased susceptibility to the drug because the new conformation hinders the drug-protein interaction ^{62, 66, 68)}. Or the pathogen starts an overexpression of the drug target to bypass inhibition ⁶⁹⁾.

A more active form of pathogen defense against antibiotics is the expression of enzymes that inactivate or degrade the drug by ester- or amide-bond formation in the drug molecule or acetylation, phosphorylation, adenylation, glycosylation and hydroxylation ⁶⁰⁾

Drug delivery systems (DDS)

Traditional chemo-therapy as well as antibiotic treatments rely on a systemic administration of the drug. This system has the flaw that large quantities of the active component are required to achieve therapeutic concentration at the diseased site. A systemic application also means that the drug reaches healthy regions of the host body possibly leading to severe side effects. Targeted drug therapy follows the idea to confine and focus the drug distribution to the diseased area as much as possible. The market has 30 main drug delivery products available and generates 33\$ billion annual revenue with an estimated annual growth of 15% ⁷⁰⁾. Current technologies can be split in two groups:

Soluble macromolecules

- Monoclonal antibodies
- Soluble synthetic polymers
- Polysaccharides
- Biodegradable polymers

Complex particulate multicomponent structures

- Microcapsules/-particles
- Lipoproteins
- Liposomes
- Cell ghosts
- Cells

A hypothetical ideal drug delivery system is the phagocyte, a nanorobot capable of delivering drugs directly to the diseased cell ⁷¹⁾. With current technology a cell based drug delivery approach is the closest available targeting system ⁷²⁾.

The following sections are intended to give an overview of current synthetic and cell based drug delivery systems.

Liposomes and similar particulate carriers

Macromolecular carriers are limited in their drug carrying capacity (1:1 ratio for immunoconjugates and 1:10 ratio for polymer conjugates) and therefore require more potent drugs since higher dosages of carrier material aren't always an option due to the risk of carrier toxicity ⁷³⁾. Liposomes don't face this problem due to their super-molecular structure and usually provide carrier to drug ratios of 1:10000 unless the liposome is designed very small for enhanced biodistribution (BD) while a large therapeutic molecule such as a protein is the payload ⁷⁴⁾. On the other hand liposome systems, while offering good retention characteristics for hydrophilic molecules, may struggle with the retention of neutral hydrophobic intermediate solubility drugs ⁷⁵⁾. Macromolecular carrier-drug conjugates don't face this problem since the drug is generally covalently linked to the carrier ⁷⁶⁾. To overcome this hurdle pH or chemical gradients can help with loading and retaining drugs like doxorubicin or vincristine into liposomes ^{77,78)}.

Early generation liposomes were detected by the immune system and the majority were captured by the reticuloendothelial system (RES) of the liver. Polyethylene glycol (PEG) coated liposomes brought a major improvement with a loss of only 10%-15% to the RES ⁷⁹⁾.

General positive effects of carrier systems are a decreased drug clearance and in consequence an increased half-life of the drug. The volume of distribution decreases, possibly minimizing side effects on healthy body parts and the area under the concentration versus time curve increases, granting a prolonged time over the minimal therapeutic concentration (MTC). ⁷⁶⁾.

The rate of drug release from a larger (50-200nm) liposomal carrier is detrimental for the drugs BD pattern. A slow drug release confines the drug's pharmacokinetics (PK) and BD approximately to the volume of plasma, giving it the same pattern as for the carrier itself while a rapid release shifts the PK and BD towards the pattern of a free drug, although improvements in unwanted toxicity may be seen ⁸⁰⁾. A too slow rate of release may lead to an impaired therapeutic effect when compared to the free drug due to drug concentrations under the MTC ⁸¹⁾. Most actual systems are in between those two extremes, making the rate of drug release the major balancing factor for the drugs PK and BD ⁷⁶⁾.

The use of a liposomal carrier can also affect the maximum tolerated dose (MTD) in three possible ways:

- MTD is increased (e.g. the kidney toxicity of amphotericin B can be controlled when administered in a liposomal carrier, leading to larger quantities of amphotericin B ⁸²⁾
- MTD stays the same (e.g. liposomal vincristine where the MTD stays the same while the drugs potency is increased ⁸³⁾
- MTD is decreased (e.g. liposomal carriers protect topotecan from metabolism, lowering the amount that can be administered without severe toxic side effects ⁸⁴⁾

A special case are drugs that are inactive while associated with the carrier. For example doxorubicin linked to N2-hydroxypropyl methacrylamide copolymers leads to a large increase of the MTD due to reduced cardiotoxicity ⁸⁵⁾.

Enhanced Permeability and Retention (EPR) effect

EPR is a passive targeting effect for larger particulate carriers ⁸⁶⁾. Certain pathological conditions like inflammation or solid tumors increase the permeability of the tissue vasculature by widening the gap size (up to 600-800nm) between the endothelial cells. This allows larger carriers that

would normally be retained in the blood stream to escape the blood vessel into the tissue environment⁸⁷⁾. This condition is induced by cytokines released from inflamed or tumorous tissue to allow leukocyte extravasation for an immune/inflammatory or tumor angiogenesis response respectively^{88, 89)}.

Especially in tumors the combination of the EPR effect with an impaired lymphatic drainage of the tumor tissue can lead to a concentration of carrier particles in the interstitial regions of the tumor environment of up to ten fold^{90, 91, 92, 93)} The EPR effect does however not guarantee a homogeneous distribution of the carrier particles within the tumor or inflammatory site. It is not yet fully understood what causes this rather focal distribution of carrier particles⁹⁴⁾. Several factors have been identified playing a role in carrier distribution throughout the target area⁷⁶⁾:

- Average size of the drug delivery systems (DDS) particles
- DDS half-life in circulation (DDS particle concentration peaks at the tumor site 1-3 days after the injection)
- Degree of tumor vascularization
- Degree of angiogenesis
- Epithelial pore size

With the rate and level of bioavailable drug as a detrimental factor for a successful DDS therapy relying on the EPR effect a long carrier half-life is desirable to ensure an optimal accumulation of carrier particles in the diseased tissue⁹⁵⁾. The strong dependence of DDS on rate and amount of released drug lead to further developments such as triggered release mechanisms or the delivery of prodrugs in combination with drug activating signals. Examples for investigated triggered release mechanisms are pH or temperature shifts, magnetic fields, sensitivities to specific enzyme levels and radiofrequency^{96, 97)}. An example for an activatable prodrug is Visudyne in combination with the liposomal photosensitizer verteporfin⁹⁸⁾.

Some carrier systems do not rely on the EPR effect but rather on a sustained drug release into blood circulation. This system is comparable to an IV drug infusion but with less inconvenience for the patient⁹⁹⁾.

Active targeting systems for synthetic delivery systems

The most recent efforts in DDS research have focused on the use of targeting moieties on the surface of carrier particles. These targeting moieties, mostly short signaling peptides, are intended to increase the site specific action of the DDS (“Ligand mediated targeting”) by adding an active targeting mechanism to the system rather than to rely on the passive EPR effect ⁷³⁾.

Cell based drug delivery systems

Monocytes and macrophages

Drug delivery systems that are based on live, biologically active cells exist in two forms: Transduced cells, which are genetically altered to express the pharmaceutically relevant molecules and cell carriers that are loaded with drugs and are intended to release the drug either in circulation or at a specific site they target ⁷⁰⁾.

Examples for transduced cells are monocytes and macrophages that deliver immunomodulatory molecules at the site of interest ¹⁰⁰⁾ or stem-cells that have targeted brain metastases from melanoma ¹⁰¹⁾.

Macrophages and monocytes have been investigated as drug carriers ^{102, 103)}. After an ex vivo loading with an antiretroviral drug the macrophages were observed in lung, liver, kidney and spleen. HIV-Ip 24 antigen levels were reduced by 23-51%.

The loading of macrophages with nanoparticulate drug carriers has also been investigated ¹⁰⁴⁻¹¹³⁾ revealing several possible uptake routes for carrier types:

- Polysaccharides ¹¹⁴⁾
- Endotoxins ¹¹⁵⁾
- Immunoglobulins (via the Fc receptor) ¹¹⁶⁾
- Low density lipids (LDL, via scavenger receptors) ¹¹⁷⁾

Depending on the receptor pathway of the uptake of particulate nanomaterials the monocytes reaction may alter, having an influence of endosome maturation, endosome-lysosome fusion and inflammatory response ¹⁰⁸⁾. This may affect parameters such as drug release, metabolism and bioavailability.

The characteristics of particulate carriers play an important role for the readiness of macrophages to take them up ^{119, 120)}:

- Surface charge of the particle (negative surface charge is beneficial for uptake)
- Hydrophobicity
- Morphology
- Chemical structure

Overloading monocytes with nanoparticulate carriers may lead to cell death via respiratory burst (121, 122).

Another example of cell based drug delivery is the encapsulation of catalase by monocytes. The enzyme is intended to combat reactive oxygen species at inflammatory sites in atherosclerosis patients (123).

Erythrocytes

Since erythrocytes that have exceeded their life span are recycled by monocytes/macrophages in liver and spleen they can be used to target specifically these cell types to treat diseases like Leishmaniasis (70). Old erythrocytes are recognized via the reticuloendothelial system (RES) by monocytes and macrophages. If erythrocytes are used as a DDS the RES-signal can be artificially induced for loaded erythrocytes to trigger a rapid uptake and drug delivery to the monocytes and macrophages (124, 125). The loading mechanism for erythrocytes relies on osmotic pressure to conserve the functionality and integrity of the cell which in turn limits the range of drugs that can be loaded to water soluble molecules.

Bacterial ghosts

Bacterial ghosts are bacterial cells with a genetically induced pore that causes the depletion of all cytoplasm and its contents while surface antigenicity and morphology are conserved. The ghost cell can then be loaded with chemotherapeutics or immunoglobulins targeting tumors. Due to the large pore size this DDS is limited to molecules that associate strongly with the bacterial membrane, membrane proteins or cell wall to achieve acceptable retention of the drug (126, 127).

Summary

DDS have been criticized for their complexity and higher costs, however microparticulate systems not involving viruses or transduced cells can be cost competitive ¹²⁸⁾ especially when toxicity management and side effect mediation are considered ^{129, 130)}. Negative side effects of DDS are possible hypersensitivity ¹³¹⁾, a reaction of the immune system against the carrier and/or drug ¹³²⁾ and possible stronger drug side effects due to an altered PK and BD ^{133,134)}.

Phagocytes

Discovery and sub-classification

Phagocytic cells are part of the mammalian immune system. Their primary task is to protect the host organism from harmful invading foreign objects (e.g. Viruses, bacteria, fungi, parasites, toxins) by ingestion of the invaders ¹³⁵⁾. They are the higher organism's first line of defense in the fight against any infection and help in the development of the immune systems specific response and subsequent immunity via antigen presentation ¹³⁶⁾. Their antibacterial properties were first discovered by Nobel Prize laureate Ilya Mechnikov in 1882 ¹³⁷⁾.

Phagocytes can be categorized into two sub groups, professional and non-professional phagocytes ^{138, 139)}. Examples for professional phagocytes are:

- Neutrophil granulocytes
- Monocytes/Macrophages
- Mast cells
- Dendritic cells

While non-professional phagocytes are represented by:

- Lymphocytes
- Epithelial cells
- Natural killer cells
- Endothelial cells
- Fibroblasts
- Erythrocytes

The differentiation of the two sub groups is based on the presence of specialized receptors (e.g. IgG Fc receptors (Fc γ R) and complement receptors) that can recognize and bind foreign objects which present antigens on their surface ¹⁴⁰. These receptors can only be found in professional phagocytes.

Available antibacterial and antiviral pathways

In case of an infection phagocytes are recruited from the blood stream into the inflamed tissue by a chemical signal cascade called chemotaxis ^{141,142}. The signaling molecules, chemokines, can originate from the invading organism, the invaded tissue or phagocytes already present at the site of the infection ¹⁴³. The chemokines then create a concentration gradient that the phagocytes travel along towards its origin. Notable chemokines are:

- Interleukin 8 (IL-8) for neutrophils ^{144, 145}
- Chemokine ligand 5 (CCL5) for monocytes and macrophages ^{144, 145}

After arrival at the site of inflammation and upon contact with the pathogen phagocytes begin the engulfment of the foreign organism. This process is called endocytosis ¹⁴⁴. Phagocytes then can kill the internalized organism with reactive oxygen species or nitric oxide ¹⁴⁶. Some phagocytes are specialized to present parts of the digested pathogen on their cell-surface to other cells of the immune system. This triggers the specific immune response and leads to the mass production of monoclonal antibodies (mAb) by lymphocytes, specifically tailored to the invading pathogen ¹⁴⁷. Phagocytes can rely on three different ways to kill or inactivate pathogens ¹⁴⁸:

- Oxygen dependent intracellular
- Oxygen independent intracellular
- Extracellular

The oxygen dependent intracellular pathway, or respiratory burst, is characterized by an increased oxygen uptake of the phagocyte upon endocytosis of the pathogen ¹⁴⁹. The produced reactive oxygen species are toxic to both, the invading cell and the phagocyte and therefore require compartmentalization to minimize host cell damage. There are two types of reactive oxygen species used by phagocytes. The first type, superoxide (O₂⁻) ¹⁵⁰, is enzymatically converted by superoxide dismutase to hydrogen peroxide (H₂O₂) ^{151, 152}. Furthermore superoxide

and H₂O₂ can produce hydroxyl radicals (HO) that assist in killing the pathogen. The second type is solely used by neutrophil granulocytes and results in the formation of hypochlorite (=bleach) by myeloperoxidase ¹⁵³. The oxygen dependent intracellular pathway is the most effective tool of phagocytes against invading pathogens.

The oxygen independent pathway is not as effective but knows four different types:

- Charged peptides that damage the membrane of endocytosed bacteria ¹⁵⁴
- Lysozyme, an enzyme specialized in breaking down bacterial cell walls ¹⁵⁵
- Lactoferrins that deplete the bacterium of essential iron ¹⁵⁶
- Proteases and hydrolases that digest bacterial proteins ¹⁵⁷

This pathway is activated once the endosome fuses with the lysosome, a vesicle containing these different types of digestive enzymes.

The extracellular killing pathway relies on the release of nitric oxide (NO) by the phagocyte into the extracellular medium. Nitric oxide is produced enzymatically produced by interferon-gamma (IFN γ) stimulated macrophages and causes DNA damage to the pathogen by de-aminating its nucleobases. Cells secreting the IFN γ stimulant are T-cells, B-cells, natural killer cells, monocytes, dendritic cells and other macrophages ¹⁵⁸.

Activated macrophages also produce tumor necrosis factor (TNF), a signaling molecule that can induce apoptosis to cancer cells or virus infected cells in the immediate environment of the macrophage ¹⁵⁹.

Activation of phagocytes

Phagocytes exist in varying degrees of readiness throughout the body and require different activation pathways to reach their full anti-pathogenic potential. Macrophages for example usually exist in a semi resting state in anchored positions throughout the tissue. In case of an infection they are activated and recruited to the infection site by IFN γ emitted from the infected host cells ¹⁶⁰. Additional macrophages can be recruited by the attraction of monocytes from the bloodstream that differentiate to macrophages upon the arrival at the inflammation site. This recruitment process occurs in a timeframe of several hours to a day ¹⁶¹. However in case of a sudden direct contact with a pathogens endotoxins in combination with high levels of IFN γ , macrophages become hyper-activated causing them so solely focus on an increased phagocytic activity ¹⁶².

Neutrophils primarily float with the blood stream until activated by signaling molecules (mostly IL-8) emitted from inflamed tissue or responding tissue anchored macrophages. Once activated they leave the bloodstream through endothelial gaps, responding to an invading organism within minutes making them the first line of defense in the unspecific immune response ¹⁶³).

In this work we specifically investigated the role of Monocytes, Macrophages and most importantly neutrophils as a targeting component in a cancer or anti-bacterial drug delivery system. The following section will provide more detailed information on these three phagocyte cell types.

Chapter 2 - Cell-Types and Active Components Used in the Drug Delivery System

Monocytes

Monocytes represent the largest type of white blood cell and constitute 2%-10% ¹⁶⁴⁾ of all white blood cells. Upon activation they respond to inflammatory signals within 6-18 hours ¹⁶⁵⁾ via extravasation from the blood stream and tissue migration. Upon arrival at the infection site they differentiate into macrophages or dendritic cells ¹⁶⁶⁾, fulfilling three main functions:

- Phagocytosis
- Antigen presentation to trigger a specific immune response
- Cytokine production (TFN, IL-1, IL-12) to recruit other immune cells to the infection site

There exist three different phenotypes of monocytes characterized by various levels of CD14 and CD 16 surface receptors. CD14 serves as a receptor for bacterial antigen recognition while CD16 is involved in the activation of natural killer cells ¹⁶⁷⁾.

Macrophages

The name macrophage means big eater and describes their primary role in the unspecific immune response. With an average diameter of $21.2 \pm 0.3\mu\text{m}$ ¹⁶⁸⁾ they are able to phagocytize invading foreign organisms and particles up to a size of $20\mu\text{m}$ ¹⁶⁹⁾. After phagocytosis macrophages can present parts of the digested and processed invading organism ¹⁷⁰⁾ to CD4+ T-cells that regulate the activity of the adaptive immune system for a specific immune response ¹⁷¹⁾, most essentially B-cell antibody class switching. The macrophage presents the processed antigen (usually a surface protein of the pathogen) on an MHC class II receptor (major histocompatibility complex) ¹⁷²⁾.

Macrophages have the unique ability to metabolize arginine for the production of nitric oxide, used as an extracellular bactericidal molecule. Alternatively ornithine, a cellular repair molecule is produced which allows the differentiation of macrophages into two sub categories: M1

macrophages or “killer macrophages” which secrete the pro-inflammatory IL-12 or M2 “repair macrophages” which secrete the anti-inflammatory IL-10¹⁷³⁾.

The Macrophage life cycle

The life cycle of a macrophage begins when a monocyte is triggered to leave the bloodstream. With that it starts the differentiation process towards a macrophage. Unlike the short lived neutrophils, macrophages have a survival time of several months if they are semi dormant and anchored in tissue¹⁷⁴⁾. While at this stage their primary role is to clean up dead host cells and host cell debris like aged neutrophils via the CD31 receptor^{175, 176)}.

Once a macrophage responds to inflammatory signals sent out by inflamed tissue or neutrophil first responders it becomes mobile and starts to migrate towards the origin of inflammation using pseudopods in an amoeboid movement^{177, 178)}. Activated macrophages have an average life time of 15 days.

Neutrophil granulocytes

Neutrophil granulocytes are the immune system’s first response to an invading organism¹⁷⁹⁾.

They have a short average life time of 5.4 days in their dormant stage¹⁸⁰⁾ (although this value is also reported as 24-48h^{179, 181)} and disputed claiming a life span 10 hours in blood circulation elsewhere¹⁸²⁾ and exhibit a very high motility enabling them to respond to inflammatory signals and reaching the inflamed tissue region within minutes¹⁸³⁾. They represent the most abundant

white blood cell type with approximately 50-70% of all white blood cells being neutrophils¹⁸⁴⁾.

With a spherical shape their size ranges from 8-12 μ m when dormant¹⁸⁵⁾ and approximately $16 \cdot 10^{10}$ neutrophils are produced daily in humans^{186, 187)}. The most important molecule class for neutrophil activation and recruitment are cytokines with IL-8 and IFN γ as the most prominent examples. When activated via chemotaxis the neutrophils extravasate from the blood stream and fight the invading pathogen at the source of inflammation for 1-2 days. The short lifetime may be intended to limit propagation of parasitic bacteria as well as damage to the host tissue by antimicrobial products during inflammatory neutrophil response¹⁸⁸⁾.

Neutrophils are specialized in the fight against pathogenic microbes and have three ways to fight infections:

- Phagocytosis and respiratory burst
- Release of soluble antimicrobial granules ¹⁸⁹⁻¹⁹¹⁾
- Neutrophil extracellular traps (NETs) ¹⁹²⁾

While the phagocytic pathway works similar as in the previously discussed macrophages the other two ways are unique to neutrophils. Antimicrobial granules can be categorized as primary, secondary and tertiary granules ¹⁸⁹⁾.

Primary granules contain peroxidases, bactericidal/permeability increasing protein (BPI), defensins, serine proteases and cathepsin G. Secondary granules contain alkaline phosphatase, lysozyme, collagenase and lactoferrin. Tertiary granules contain cathepsins and gelatinase ¹⁸⁹⁻¹⁹¹⁾.

Neutrophil extracellular traps were discovered fairly recently in 2004 and are antimicrobial proteins distributed on a DNA scaffold designed to entrap and immobilize pathogens.

Macrophages, as the secondary wave of the unspecific immune response then clean up the NETs along with entrapped bacteria or fungi upon their arrival at the site of inflammation ¹⁹²⁾.

Active Components

DP44mt

DP44mt is an iron and copper chelator designed for anti-tumor activity. Buss et al and Kalinowski et al ^{193, 194)} have shown that depriving a solid tumor of the essential nutrient and physiological trace element iron can inhibit the growth of cancer cells and iron chelating drugs like Triapine have entered clinical trials ¹⁹⁵⁾. This is of particular interest since cytotoxic iron chelators like DP44mt don't rely on the apoptosis inducing factor p53 ¹⁹⁶⁾, that is often defective in a wide variety of cancer cells ^{197, 198, 199)}. The rate limiting step of DNA-synthesis for example is catalyzed by ribonucleotide reductase, an enzyme relying on iron to remain active ²⁰⁰⁾.

Richardson et al. ²⁰¹⁾ have developed a new class of di-2-pyridylketone thiosemicarbazones (DpT backbone) of which DP44mt (di-2-pyridylketone-4, 4-dimethyl-3-thiosemicarbazone) showed the most promising results *in vitro*. In a study with 28 different cancer cell types DP44mt's average IC₅₀ was 0.03 ± 0.01 μM with a range from 0.005 to 0.4 μM. These results were

significantly lower than the IC₅₀ for Triapine ($1.41 \pm 0.37 \mu\text{M}$) or DOX ($0.62 \pm 0.35 \mu\text{M}$, range 0.02-0.6 μM) and DP44mt outperformed DOX on 26 out of 28 cell lines ²⁰¹).

In addition to the inhibition of iron-dependent enzymes DP44mt has shown to up-regulate the N-myc downstream regulated gene I (NdrGI) ²⁰², a gene known to inhibit primary tumor growth and the formation of metastasis ²⁰³).

However due to its high cytotoxicity DP44mt can induce cardiac fibrosis in a dose dependent manner (doses above 0.75 mg/kg, ²⁰¹). This effect might be mediated with appropriate dosing of the drug (it shows significant tumor growth inhibition at 0.3 mg/kg ²⁰⁴).

Further investigation of DP44mt's mechanism of action showed that the drug can chelate both, iron ²⁰⁵) and copper ²⁰⁶) ions. Both complexes have redox potential and attack the lysosomal membrane ²⁰⁷). The copper complex shows greater activity than the iron complex or the DP44mt ligand alone but copper is not successfully scavenged from the tumor cells ²⁰⁷). The drug could be administered in its copper complex form to exploit the higher activity.

Doxorubicin

Doxorubicin, also called Adriamycin, is an anthracycline antibiotic ²⁰⁸). Its effectiveness in cancer treatment has been studied for both animals ²⁰⁹) and humans ²¹⁰). Doxorubicin binds to free nucleic acids and inhibits DNA- and RNA polymerases ²¹¹⁻²¹³) which results in a blocked DNA or RNA synthesis and cell death for fast proliferating cells. Its application is limited by a dose dependent cardiac dysfunction ²¹⁴).

Chlorhexidine

Chlorhexidine is a bactericidal and bacteriostatic as well as a topical disinfectant. It is commonly used in mouthwash and contact lens cleaning solutions and its mechanism of action is membrane disruption ^{215, 216}). The positively charged drug recognizes bacteria by their overall negative surface charge from the cell wall molecules, and attaches to the bacterial surface. Then it begins with the disruption of parts of both cell –wall and membrane causing leakage of the cytoplasm and uncontrolled ion flow that ultimately lead to the bacteria's death. Its IC₅₀ varies depending on the attacked organism but lies between 0.01 and 0.1 Mg/kg (CHX MSDS sheet). Because of this rather physical then biochemical approach especially gram positive microorganisms (like

MRSA) have difficulties do develop effective countermeasures and resistances, although rises in the minimum inhibitory concentration may be observed ^{217, 218}).

Chlorhexidine is in the WHO list of essential medicines (WHO Model List of Essential Medicines, 18th list, April 2013)

Chapter 3 - Abbreviations

ATCC - American Type Culture Collection
BD - Biodistribution
bFGF - Basic fibroblast growth factor
BPI - Bactericidal/permeability increasing protein
CCL - Chemokine ligand
CD receptor - Classification determinant receptor
CDC - Centers for Disease Control and Prevention
CFU - Colony forming unit
CHX - Chlorhexidine
DDS - Drug delivery system
DIEA - N,N-Diisopropylethylamine
DMF - Dimethylformamine
DMSO - Dimethyl sulfoxide
DNA - Deoxyribonucleic acid
DOX - Doxorubicin
DOXY - Doxycycline
EDC - 1-Ethyl-3-(3-dimethylaminopropyl)carbodiimide
EPR - Enhanced permeability and retention
ESBL - Extended spectrum β -lactamases
HER-2/neu - Receptor tyrosine-protein kinase erbB-2
HIV - Human immunodeficiency virus
HOBT - Hydroxybenzotriazole
IC - Inhibitory concentration
IFN γ - Interferon gamma
IgG - Immunoglobulin G
IL - Interleukin
IV - Intravenous
IVIS - In vivo imaging system
LDL - Low density lipid

mAb - Monoclonal antibody
MDR - multi drug resistant
ML - Micrococcus luteus
MMP - Matrix metalloproteinase
MOI - Multiplicity of infection
MPN - Most probable number
MRSA - Multiresistant Staphylococcus aureus
MSDS - Material safety data sheet
MTC - Minimal therapeutic concentration
MTD - Maximum tolerated dose
MTT - 3-(4,5-Dimethylthiazol-2-yl)-2,5-Diphenyltetrazolium Bromide
NdrnI - N-myc downstream regulated gene
NETs - Neutrophil extracellular traps
OD - Optical density
PBS - Phosphate buffered saline
PEG - Polyethylene glycol
PI - Propidium Iodide
PIGF - Phosphatidylinositol-glycan biosynthesis class F protein
PK - Pharmacokinetics
PMN - Polymorphonuclear neutrophils
PRAS-BHI - Pre Reduced Anaerobically Sterilized Brain Heart Infusion broth
RES - Reticuloendothelial system
RNA - Ribonucleic acid
ROS - Reactive oxygen species
rpm - revolutions per minute
RPMI - Roswell Park Memorial Institute
SDS - Sodium dodecyl sulfate
TAN - Tumor associated neutrophils
TB - Tuberculosis
TNF - Tumor necrosis factor
UV/Vis - Ultraviolet/Visible

VEGF - Vascular endothelial growth factor

WHO - World Health Organization

XDR - Extensive drug resistance

Chapter 4 - Materials and Methods

Materials

Chlorhexidine-gluconate (CHX, 2% solution, MW: 897.75 g/mol) was purchased from Bimeda (IL). Chlorhexidine-diacetate hydrate (>98% purity, MW: 625.55 g/mol) was purchased from Acros Organics (NJ). Doxorubicin-hydrochloride (DOX, >99% purity, MW: 579.98 g/mol) was purchased from TSZ Chem (MA). DP44mt was synthesized by Dr. Tej B. Shrestha²⁰⁴. Doxycycline (DOXY, >99% purity, MW: 444.43 g/mol) was purchased from Clontech (CA). LB-broth, Miller was purchased from Acros Organics (NJ). RPMI1640 medium was purchased from Sigma-Aldrich (MO). PI/Annexin V dead cell apoptosis kit for flow cytometry was purchased from lifetechnologies (NY). Rhodamine-B (analytical grade, MW: 479.02 g/mol) was purchased from Fisher Chemical (MA). All other chemicals were purchased of analytical grade. *Micrococcus luteus* was purchased from Carolina Biological Supply Company (NC). RAW 264.7 Monocyte/Macrophage co-culture (Mo/Ma cells) was purchased from American Type Culture Collection (ATCC) (VA). 4T1luc2 cancer cell line was purchased from Caliper Life Sciences (MA).

Buffers

PBS

Concentrated 10x PBS stock solution was made by dissolving 79g NaCl, 3.4g KCl, 14.4g Na₂HPO₄ and 2.4g KH₂PO₄ in 1000ml of purified water (B-Pure Water Purification System, Barnstead, Van Nuys, CA). After complete dissolution of all material the pH was adjusted to 7.4 using NaOH (pH meter: Orion 2 Star, Thermo Scientific, Waltham, MA). To reach the 1x working concentration 100ml of 10x PBS were mixed with 900ml of purified water.

Lysis Buffer

Lysis buffer was made by dissolving 6.057g (50mM) of Tris in 1000ml of purified water. After the complete dissolution of Tris, 1% (w/v) Triton-X 100 was added and the pH was adjusted to 7.4.

Strong Lysis Buffer

Strong lysis buffer is a modification of lysis buffer with 3% (w/v) Triton-X 100 and 1% (w/v) SDS added to the buffer and the pH adjusted to 7.4.

M. luteus Culture

In a 225ml KIMAX culture flask 2g LB broth substrate were dissolved in 100ml purified water and autoclaved for 45 min at 121°C and 1bar (Autoclave: Yamato Sterilizer SM200, Japan). The sterile medium was inoculated with 100 µl of a *M. luteus* suspension and the culture was grown for 12 hours at 37 °C and 200 rpm (New Brunswick scientific heated shaker, Enfield, CT). The cells were separated from the medium via centrifugation at 10000g (Thermo Scientific Sorvall Legend RT+ centrifuge, Waltham, MA) and washed twice with phosphate buffered saline (PBS) by replacing the supernatant with fresh buffer and resuspending the cells through vortexing. To proceed with the loading of the various active components, 1 ml of the cell suspension was transferred into a 1.5 ml Eppendorf reaction tube and centrifuged at 14000 rpm (Eppendorf centrifuge 5415C, Germany). The supernatant was removed so that the cell pellet was ready for resuspension in a solution of the respective active component. This procedure was repeated for the desired number of samples.

Loading of *M. Luteus* with Chlorhexidine

To load *M. luteus* with chlorhexidine, the cell pellet of 1 ml cell-suspension was resuspended in concentrated chlorhexidine-gluconate (the stock solution is 2% w/v). A total of 5 samples was prepared. The chlorhexidine-cell suspension was placed on the thermo rocker overnight. After 12-18 hours the samples were centrifuged at 14000rpm, washed with PBS once and both supernatant and cell pellet were kept for further analysis.

An initial characterization of loaded and unloaded *M. luteus* suspensions was done using the UV/Vis plate reader (Synergy H1 micro-plate reader BioTek, Winooski, VT) and analysis software Gen5 v2.05 (BioTek Winooski, VT). The absorbance spectrum for five loaded and five

unloaded samples of *M. luteus* were measured by plating 100µl of the respective samples in wells on a 96 well plate and measuring the absorbance in the region from 550nm to 700nm with a 2nm step size.

To quantify the amount of CHX taken up by *M. luteus* two methods were employed: An indirect measurement that keeps the actual cell-sample intact for further experiments and a direct measurement where CHX is released from the cells by disrupting the cells with lysis buffer.

Indirect measurement

M. luteus cells were loaded with CHX as previously described. After loading the cells were separated from the remaining CHX stock solution (loading supernatant) by centrifuging at 14000rpm. The absorbance spectrum of the loading supernatant was measured from 550 to 700 nm. The absorption peak of CHX occurring at 635 nm was used for calibration and data analysis. The loading supernatant’s absorbance at 635nm is analyzed using UV/Vis spectroscopy and compared to the absorbance of unaltered CHX stock solution at 635nm.

	Loading Sup	Cell Frag	3	4	5	6	
A	SPL1	SPL2					Well ID
							Conc/Dil
B	SPL1	SPL2					Well ID
							Conc/Dil
C	SPL1	SPL2					Well ID
							Conc/Dil
D	SPL1	SPL2					Well ID
							Conc/Dil
E	SPL1	SPL2					Well ID
							Conc/Dil
F	BLK						Well ID
							Conc/Dil
G	STD1 0	STD2 400	STD3 800	STD4 1200	STD5 1600	STD6 2000	Well ID
							Conc/Dil
H	STD1 0	STD2 400	STD3 800	STD4 1200	STD5 1600	STD6 2000	Well ID
							Conc/Dil

Figure 2: Example for the setup of the 96 well plate for UV/Vis analysis

The supernatant is expected to have a significantly lower absorbance in comparison to the stock solution and the amount of CHX accumulated in the cells can be calculated via spectral subtraction.

Direct measurement

M. luteus cells were loaded with CHX as previously described. The cells were separated from the remaining CHX solution via centrifugation at 14000rpm and washed with PBS. To measure intracellular CHX directly the samples were centrifuged at 14000rpm and the cell pellet was resuspended in 1 ml lysis buffer and placed in a 40 °C sonication water bath for 30 minutes. The cell fragments were centrifuged off subsequently and the supernatant was removed. Cell fragments were resuspended in 1 ml PBS buffer and both the cell fragment suspension as well as the lysate were analyzed for their CHX concentration. The absorbance spectra were measured from 550 to 700 nm. The absorption peak of CHX occurring at 635 nm was used for data analysis.

Time Resolved Loading of CHX

M. luteus cells were loaded as previously described with the modification that the loading time was controlled and 1, 2, 3 and 4 hours of loading were allowed for the respective samples. The cells were separated from the remaining CHX solution via centrifugation at 14000rpm after the defined loading time was up and washed with PBS. To measure intracellular CHX directly the samples were centrifuged at 14000rpm and the cell pellet was resuspended in 1 ml lysis buffer and placed in a 40 °C sonication water bath for 30 minutes. The cell fragments were centrifuged off subsequently and the supernatant was removed. The absorbance spectra of the supernatant was measured from 550 to 700 nm. The absorption peak of CHX occurring at 635 nm was used for data analysis.

Zeta Potential Measurements

A dilution series of a 1000µg/ml CHX-diacetate stock solution in PBS was produced to acquire the desired concentrations and *M. luteus* was loaded as previously described with the serial dilution of CHX-diacetate instead of CHX-gluconate stock solution. A loading time of 12h was allowed. Zeta potential measurements were performed using the ZetaPALS Zeta Potential Analyzer (Brookhaven Instruments Corporation, Austin TX), as described previously²²¹. *M. luteus* was characterized in 1 X PBS-CHX-diacetate solution at and at $8 \cdot 10^8$ cells/ml. The influence of CHX on the zeta potential was studied over a range of concentrations from 0µg/ml to 1000µg/ml CHX in increments of 100 µg/ml. In order to correlate the zeta potential data with the amount of CHX found intracellular, the samples were recovered and centrifuged to separate

cells from the PBS-CHX-diacetate solution. The cells were resuspended in lysis buffer and placed in a 40 °C sonication water bath for 30 minutes. The cell fragments were centrifuged off subsequently and the absorbance of the supernatant after lysis was measured as described earlier in the direct measurement section.

CHX Retention

To measure the retention of CHX over the course of five days 30 ml of a *M. luteus* cell suspension were centrifuged at 10000g. The supernatant was removed and replaced by 30ml of CHX-gluconate stock solution (2% w/v). Loading was allowed for 12 hours. The cells were separated by centrifugation at 10000g, the cell pellet was washed once with PBS and subsequently resuspended in 30 ml PBS buffer. First, five 1ml samples were taken and the cells were separated by centrifugation at 14000 rpm. The supernatant was removed and stored for analysis. The cell pellet of each sample was resuspended in 1ml lysis buffer and both supernatant and lysate were analyzed immediately using UV/Vis spectroscopy as previously described. The procedure was repeated every 24h for five days.

Thioglycollate Induced Peritonitis for ex vivo use of Neutrophils

Syngeneic mice were used to isolate circulating leukocytes for loading with appropriate antimicrobials. Mice were injected with 2.5 ml of autoclaved, aged thioglycollate medium (Fisher Scientific, Waltham, MA) intraperitoneally. Twelve hours later, mice were placed under isoflurane anesthesia (2.0%-4.0%) and circulating neutrophils were isolated by peritoneal lavage with PBS. Following the procedure the mice were euthanized.

Flow Cytometry Analysis of Neutrophils

The extracted neutrophil granulocytes were counted using a hemocytometer. The cells were centrifuged at 500g (accuSpin 3r, Fisher Scientific, Waltham, MA) resuspended in RPMI medium to match a concentration of $5 \cdot 10^5$ cells/ml (cut-off for the flow cytometer). A cell-pellet from a 1ml *M. luteus* suspension was exposed to a 0.5 mg/ml stock solution of rhodamine-B for 12 hours. The cells were separated via centrifugation at 14000 rpm and washed with PBS until the supernatant is colorless and then resuspended in PBS. After counting the bacterial cells the suspension was diluted to a concentration of $5 \cdot 10^7$ cells/ml. 200 μ l of rhodamine-B modified *M. luteus* suspension were added to 1ml of neutrophils in RPMI and the sample was incubated for 2

hours at 37°C. In preparation for analysis the sample was centrifuged at 500g and the supernatant was replaced with 1ml PBS. Flow cytometry (Guava easy cyte plus, Guava Technologies, Chicago, IL, Software: easy cyte 2.2.2) was used to determine the amount of neutrophils showing fluorescence from rhodamine-B. An unloaded neutrophil control group was used to calibrate the horizontal cutoff on a yellow fluorescence vs. side scatter readout and 5000 cells were counted per measurement. Each measurement was repeated three times.

PI-Annexin-V Assay to determine neutrophil survival

Neutrophils were prepared as described in the previous section. *M. luteus* was loaded with CHX as described earlier, counted and diluted to a concentration of $2.5 \cdot 10^8$ cells/ml. Two sets (3h and 6h incubation time) of neutrophil-samples (5 ml suspension per sample) were subsequently incubated with CHX-modified *M. luteus* with 10, 20 and 100 bacterial cells per neutrophil granulocyte (100 μ l, 200 μ l, 1000 μ l respectively). The cell cultures were incubated for two hours at 37°C in a 50ml conical tube with filter cap. Then the protocol for the PI/annexin 5 apoptosis assay was carried out²²⁰⁾ and the samples were analyzed via flow cytometry. An unloaded sample of neutrophils was used to calibrate the vertical and horizontal cutoff on a red fluorescence (PI) vs. green fluorescence (Annexin-V) readout and 5000 cells were counted per sample. Each measurement was repeated three times.

In Vitro drug delivery against E. coli and F. necrophorum

The extracted neutrophils (PMN) were loaded with 20 bacteria per neutrophil ($4-6 \cdot 10^6$ neutrophils per sample). The samples were incubated at 37°C for two hours as previously described. Sample types were PMN + ML (Neutrophils + *M. luteus*), PMN + ML modified with CHX, PMN (Neutrophils + CHX-modified *M. luteus*) and RPMI buffer.

A starter culture of *E. coli* was grown overnight from a single colony in LB broth containing Ampicillin at a final concentration of 50ng/ml and Nalidixic acid at a final concentration of 12ng/ml. 0.1ml of the overnight culture was added to 5ml of fresh LB broth containing no antibiotics, and grown to and O.D.600 of 0.3. The bacteria were spun down to pellet out the bacteria. The bacterial pellet was resuspended in 1X PBS to achieve $1 \cdot 10^7$ CFU/ml. The bacteria were then incubated with 10% v/v complement inactivated mouse serum for 20 minutes at 37°C to opsonize the bacteria. The opsonized bacteria were then mixed with equal amount of PMNs (1:1 MOI and 1:1 volume of each) and incubated at 37°C for 90 minutes, on a rocker platform.

The tubes were then spun down at 5,000 RPM for 5 minutes, the supernatant was discarded and the pellet was resuspended in 100µl of 1X PBS. 100µl of 1% Triton was added to the resuspended pellet to lyse the eukaryotic cells, and was gently mixed to ensure that no bubbles were formed. This mixture was allowed to sit at room temperature for 5 minutes. 800µl of LB broth was added to the mixture to bring up the final volume to 1ml, which was then serially diluted and plated on LB agar plates containing a final concentration of 50ng/ml Ampicillin and 12ng/ml Nalidixic acid to enumerate the bacteria.

A starter culture of *F. necrophorum* subsp. *necrophorum* strain 8L1 was grown overnight from a single colony in Pre Reduced Anaerobically Sterilized Brain Heart Infusion broth (PRAS-BHI). 0.3 ml of the overnight culture was added to 10ml of fresh PRAS-BHI broth and grown to an O.D.600 of 0.7. The bacteria were spun down to pellet out the bacteria. The bacterial pellet was resuspended in 1X PBS to achieve $1 \cdot 10^7$ CFU/ml. The bacteria were then incubated with 10% v/v complement inactivated mouse serum for 20 minutes at 37°C to opsonize the bacteria. The opsonized bacteria were then mixed with equal amount of PMNs (1:1 MOI and 1:1 volume of each) and incubated at 39°C for 90 minutes, on a rocker platform. The tubes were then spun down at 5,000 RPM for 5 minutes, the supernatant was discarded and the pellet was resuspended in 100µl of 1X PBS. 100µl of 1% Triton was added to the resuspended pellet to lyse the eukaryotic cells, and was gently mixed to ensure that no bubbles were formed. This mixture was allowed to sit at room temperature for 5 minutes in an anaerobic chamber. 800µl of PRAS-BHI was added to the mixture to bring up the final volume to 1ml, which was then serially diluted and plated on blood agar plates (Thermo Scientific), and incubated in an anaerobic chamber to enumerate the bacteria.

Loading of Doxorubicin (DOX) in *M. luteus*

A DOX stock solution was prepared by dissolving 2.5 mg DOX in 50ml PBS in a 50ml-size conical tube. The *M. luteus* cell pellets described in the previous section are resuspended in 1ml of the 0.05 mg Doxorubicin/ml PBS buffer solution. The cell suspension was placed on the LabLine thermo rocker overnight. This procedure was repeated five times to create five samples.

	1	2	3	4	5
A	Lysate	Lysate	Lysate	Lysate	Lysate
B	BLK	BLK			
C	STD1 0	STD2 12.5	STD3 25	STD4 37.5	STD5 50
D	STD1 0	STD2 12.5	STD3 25	STD4 37.5	STD5 50
E	STD1 0	STD2 12.5	STD3 25	STD4 37.5	STD5 50

Figure 3: Example for the setup of the 96 well plate for DOX analysis in the *M. luteus* cell lysate. After 12-18h the samples were centrifuged (Eppendorf centrifuge 5415C, Germany) and the supernatant was replaced by 1ml of PBS buffer and washed once. To quantify the uptake of DOX in the cell pellet the loaded cells were lysed using the strong lysis buffer and a 40 °C sonication water bath (Cole-Parmer, Vernon Hills, IL) for 30 minutes. After exposing the cells for 40 minutes to the strong lysis buffer the sample was centrifuged at 14000rpm to remove cell fragments and the supernatant was kept for analysis. The amount of DOX in the supernatant was determined by UV/Vis spectroscopy (BioTek Synergy H1 micro-plate reader, Winooski, VT). The spectrum was measured from 400 to 500nm with a step size of 5nm. The samples were analyzed on a 96 well plate and 100µl were plated per sample. A calibration curve was established by measuring the absorption of DOX in PBS as well as in strong lysis buffer from 0 to 50 µg in increments of 12.5 µg (3 repetitions for each increment). Both lysate (DOX in strong lysis buffer) and the supernatant after loading (DOX in PBS) were analyzed with the respective blanks and the amount of DOX was determined using the respective calibration curve.

DOX Retention

To measure the retention of DOX over time 10 ml of a *M. luteus* cell suspension were centrifuged at 10000g (Thermo Scientific Sorvall Legend RT+ centrifuge, Waltham, MA). The supernatant was removed and replaced by 10ml of a 0.05 mg DOX/ml PBS solution for 12 hours. The cells were centrifuged off at 10000G, the cell pellet was washed once with PBS and subsequently resuspended in 10 ml PBS buffer. First, five 1ml samples were taken and analyzed immediately to serve as initial reference of the total amount of DOX loaded. The remaining 5 ml of DOX loaded cell suspension were placed on a shaker. After seven days the cells were centrifuged off and a 1 ml sample was taken from the supernatant and analyzed for its DOX

concentration. UV/Vis analysis was carried out as described above, with PBS as blank and using the DOX-PBS calibration curve.

All samples were measured in groups of five repetitions to evaluate the standard deviation.

MTT assay for cell viability measurements

M. luteus was loaded with DOX as described in the previous section. Mo/Ma cells were plated in concentrations of 8000-10000 cells per well in 100 μ l of RPMI1640 medium supplemented with 10% fetal bovine serum one day in advance. With three different groups and ten repetitions for each group a total of 30 wells were plated in three rows of ten wells on a 96 well plate. Row one was the control group and received no additional treatment. Row two received 10 μ l of the 2×10^7 cells/ml *M. luteus* suspension (20 bacterial cells/Mo-Ma cell). Row three received 10 μ l of the 2×10^7 cells/ml DOX-modified *M. luteus* suspension (20 bacterial cells/Mo-Ma cell). The samples were incubated for 72 hours and the MTT assay was carried out according to reference²¹⁹).

4T1 Cancer Cell Assay with Conditioned Medium

The tumor cell line 4T1 from the mouse mammary gland adenocarcinoma were grown in PMII640 medium supplemented with 10% fetal bovine serum (FBS; Sigma–Aldrich, St. Louis, MO). Cells were plated in concentrations of 8000-10000 cells per well with 100 μ l RPMI medium for MTT assays. Three plates with four rows and ten filled wells each for a total of 120 wells was prepared. Conditioned medium for the *in vitro* testing of released DOX from Mo/Ma cells on 4T1 cells was produced by plating 80000 loaded cells per well with 1.5 ml RPMI in five wells on a 24 well plate. Each well was incubated with 100 μ l of an 8×10^7 bacterial cells/ml suspension of DOX-modified *M. luteus*. Two control groups were plated in similar fashion but were not incubated with DOX-modified bacteria. One control group received only RPMI medium and one received 100 μ l of 0.05 mg DOX/ml PBS buffer solution. The medium was collected each day from each well and replaced with 1.5ml of fresh medium. The collected conditioned medium was then complemented with 1 ml fresh medium and added to 4T1 cancer cell cultures grown on a 96 well plate in portions of 100 μ l. Each day the 4T1 cell vitality was evaluated by executing the MTT assay as previously described on one row on each of the 96-well plates. The procedure was repeated over the course of four days.

Simultaneously the fluorescence increase in the collected conditioned-medium was measured over the course of five days in an IVIS Lumina-II imaging system (Caliper Life Sciences) to

monitor the release of DOX from the Mo/Ma cells during the production of conditioned medium. After the Mo/Ma incubated with DOX-modified *M. luteus* produced conditioned medium they were lifted by trypsination and flow cytometry was used to determine the fraction of fluorescent Mo/Ma cells. The RPMI-control group was used to adjust the cutoff bar on the yellow fluorescence vs. side scatter readout.

DP 44 mt

To solubilize DP 44 mt 1.8 mg were first dissolved in 20 μ l of DMSO and vortexed for 30 min. 9980 μ l of PBS buffer (pH 7.4) were added subsequently and the sample was centrifuged to detect and separate the solution from possible insoluble parts. If no insoluble parts were detected by eye the solution was labeled as 0.18 mg DP44mt/ml PBS.

Aliquots of 1ml were drawn from a *M. luteus*-PBS suspension and placed in 1.5ml Eppendorf reaction tubes for a total of five samples. They were centrifuged at 14000rpm and the supernatant was replaced by the DP 44 mt solution. After resuspending the cell pellet the samples were kept on the shaker overnight. After 12-18 hours the cells were centrifuged off at 14000rpm and the supernatant was stored for further analysis. The cell pellet was washed with PBS once and the washing supernatant was also stored for further analysis. The cells then were lysed with 1% Triton-X lysis buffer to release the loaded DP44mt into the lysis buffer and all samples were analyzed using UV/Vis spectroscopy (BioTek Synergy H1 micro-plate reader, Winooski, VT). The absorption spectrum was measured from 300nm to 400nm with a step size of 1nm. DP44mt's peak at 322nm was used to determine the concentration of DP44mt in solution and the amount of DP44mt loaded per sample.

DP44mt Retention

To measure the retention of DP44mt a 15 ml cell suspension was centrifuged and the supernatant was replaced by 10 ml DP44mt-PBS stock solution (0.18 mg/ml). After a loading period of 18 hours the cell suspension was centrifuged and the supernatant was replaced by 15 ml PBS buffer pH 7.4. On day 0, 1 and 2 five 1 ml samples were taken and analyzed using UV/Vis spectroscopy. The plate reader settings were the same as described in the previous section.

DP44mt Analogue – CHX Conjugate

The conjugate was synthesized following this procedure:

Coupling of thiosemicarbazone (N'-(Di-pyridin-2-yl-methylene)-hydrazinecarbodithioic acid methylester) (DP44mt analogue of the DP family) to chlorhexidine was done in DMF with two equivalence each of EDC (1-Ethyl-3-(3-dimethylaminopropyl)carbodiimide), HOBT (Hydroxybenzotriazole) and 2.5 equivalence of DIEA (N,N-Diisopropylethylamine). The reaction solution was reacted for four days under argon. After the completion, DMF was evaporated by air oxidation. The synthesis product was a brown solid.

The conjugate shows a decreased water solubility to an extent that the preparation of a stock solution with known concentration was impossible. To get an aqueous solution of the conjugate the synthesis product was first dissolved in pure DMSO and centrifuged to separate the solution from insoluble parts. 20 µl of the clear conjugate-DMSO solution were then added to 1 ml PBS which resulted in a precipitation of some material that was prone to stick to the reaction tubes wall. The sample was then placed on the rocker for 24 hours at 45 °C in order to re-solubilize the precipitate partially. After 24 hours the sample was centrifuged to separate the solution from remaining precipitate. The supernatant was of light brown color and was transferred to a new tube. Loading of *M. luteus* with the aqueous conjugate solution was similar to the loading with DP44mt. The sample preparation for analysis was again done with 1% Triton-% buffer and the lysate was analyzed spectroscopic. The conjugate's stock solution of unknown concentration showed no specific peak but a very strong absorption in the region below 350 nm. Dilutions of the stock solution showed a specific peak at 290 nm. This was utilized to measure the retention of the conjugate over the course of 6 days.

Conjugate Retention

To measure the retention 6 individual aqueous 1 ml conjugate solutions were prepared as previously described. All *M. luteus* samples were exposed to the conjugate solution for 18 hours after which the supernatant was replaced by PBS and the conjugate specific absorption at 290 nm was measured over the course of 6 days using one sample each day with 5 repetitions plated.

In vivo Studies

Preliminary toxicity Study

Neutrophils were loaded with *M. luteus* modified with 1% or 2% CHX as described earlier in the in vitro tests against *F. necrophorum*. The loaded neutrophils were centrifuged at 500g for

30 minutes to separate them from the RPMI medium and resuspended in PBS to reach a concentration of 1×10^6 cells/ml.

In order to determine whether chlorhexidine gluconate was toxic to mice, we conducted in-vivo toxicity assays. Briefly, ten week old BALB/c mice were given tail vein intra-venous (IV) injections containing approximately one million neutrophils carrying *M. luteus* loaded with either 1% or 2% chlorhexidine gluconate. Additionally a control group was injected with PBS. The three groups were assigned three animals per group. The animals were observed for 5 days post challenge to see if they demonstrated any clinical signs of toxicity. At the end of 5 days, the mice were euthanized and their kidneys, liver, brain, lung, spleen and heart were fixed in 10% formalin for histopathological evaluation.

Mouse-treatment Study

F. necrophorum subsp. *necrophorum* strain 8L1 was grown overnight from a single colony in PRAS-BHI. 0.3ml of the starter culture was added to 10ml of fresh PRAS-BHI broth and grown to an O.D.600 of 0.7. 1 ml of this culture was diluted 1:40 to achieve a final concentration of approximately 4×10^6 CFU/ml²²²). 400µl of the diluted bacteria was injected intraperitoneally into 10 week old BALB/c mice. The mice were observed for two days before they were treated with neutrophils carrying antimicrobial cargo.

10 week old BALB/c mice were randomly assigned into 6 groups with 9 mice per group. On day zero, all mice were infected intraperitoneally with an infectious dose of *F. necrophorum*. On day 3 of the experiment, all mice were given intravenous tail injections containing 100µl of the following treatments or controls- mice in group 1 were treated with one million neutrophils containing *M. luteus* loaded with chlorhexidine, mice in group 2 were treated with one million neutrophils containing *M. luteus* loaded with doxycycline (4.4mg/kg body weight), mice in group 3 were treated with one million neutrophils containing empty microparticles, mice in group 4 were treated with one million neutrophils and mice in group 5 were treated with 1X PBS. The animals were monitored for clinical signs for 5 days after treatment and were euthanized if any clinical signs developed. The mice were euthanized 5 days post treatment and all mice were examined post mortem for abscesses in the livers. Livers of the mice were weighed and homogenized in a tissue homogenizer for 1 min in modified lactate (ML) broth. The *F. necrophorum* bacterial load in the homogenate was enumerated using most probable number

(MPN) analysis²²³) using ML broth. Homogenized liver tissue samples were streaked on blood agar plates for bacterial isolation and identification using Rapid ANAI system (Thermo Scientific). Liver, lung and spleen were fixed in formalin for histopathological evaluation.

Chapter 5 - Characterization of Loaded *M. luteus*, *ex vivo* Loading of Neutrophils and *in vitro* Drug Delivery Testing

M. luteus loaded with chlorhexidine

Characterization of the loaded bacterial cells

The CHX-loaded *Micrococcus luteus* was analyzed qualitatively using the CHX specific UV/Vis absorption at 635nm wavelength. Figure 4 shows the CHX peak at 635nm is clearly visible in the loaded sample and the average absorption is increased by roughly 0.1 for equal bacterial concentrations of 8×10^8 cells/ml.

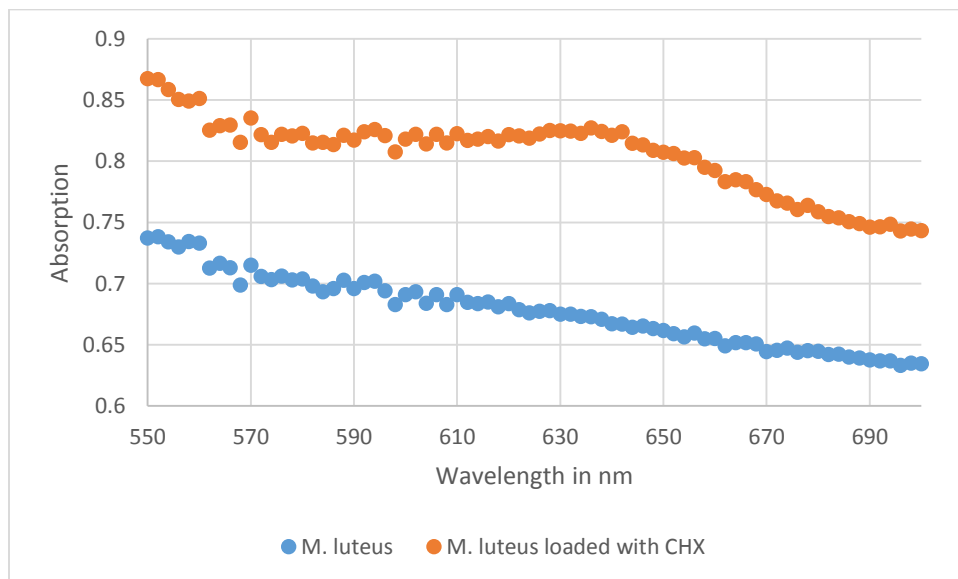


Figure 4: Comparison of the *M. luteus* absorption with and without CHX. The loaded sample ● shows the distinctive peak for CHX at 635nm while the unloaded sample ● does not.

The amount of CHX loaded was determined by lysing the cells with a Triton-X/Tris buffer system in order to establish a mass balance. Samples that were needed for further experiments can be analyzed indirectly by measuring the CHX concentration in the supernatant after loading the cells and calculating the amount of CHX loaded via spectral subtraction of a CHX reference. Both methods have shown to be accurate with standard deviations under 10% of the measured value. The results show that 1.81 ± 0.11 mg of CHX are taken up by an average 40mg/ml wet cell mass sample of *M. luteus*. This is an uptake of 9% of the initially provided amount of CHX (20mg/ml stock solution). No traces of CHX were found in the washing steps or the lysed cell fragments.

The uptake of CHX loading also was observed over a 4h timeframe in one hour increments showing that with an increased loading time more CHX is taken up. The results however are not significant ($p>0.05$) and all samples for in-vitro and in-vivo experiments have been loaded for 24h to ensure a steady state.

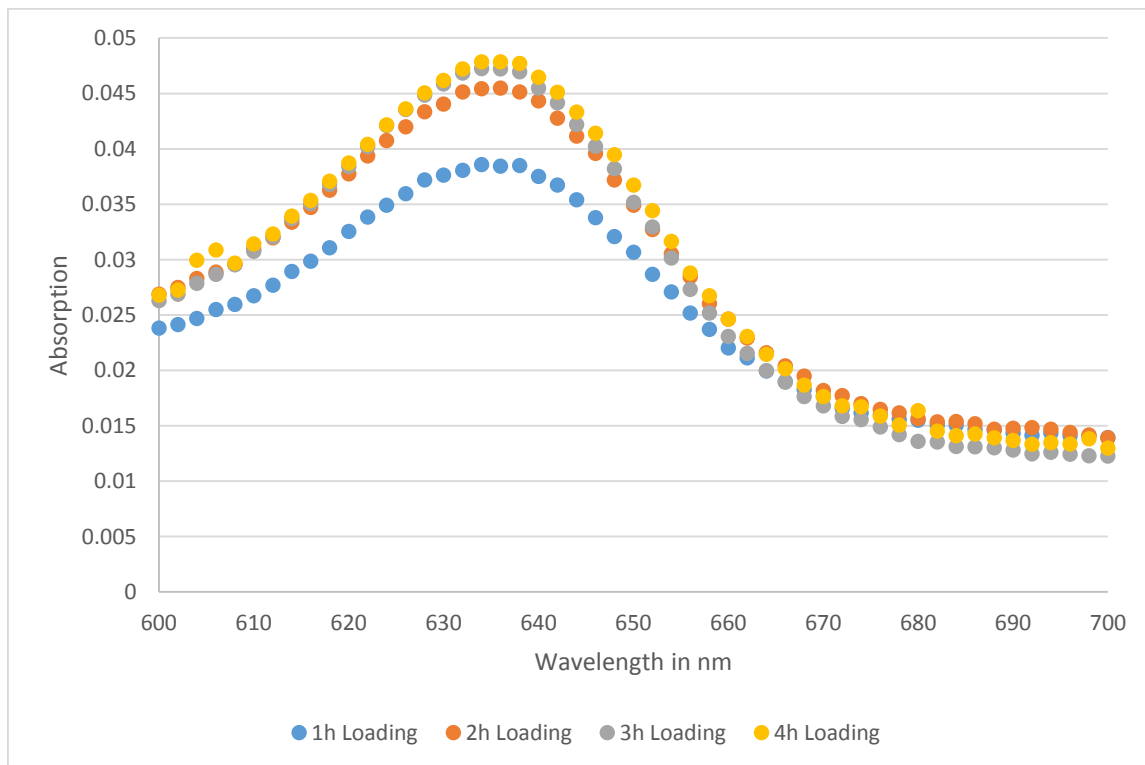


Figure 5: Time resolved loading of *M. luteus* with CHX. While the average spectral absorption for intracellular CHX increases over time, the difference between the time steps is not significant ($p>0.05$)

Another method to assess CHX loading and, more importantly, where in the bacterial cell CHX is located is a correlation of zeta potential measurement and UV-Vis analysis of loaded CHX. Since the mechanism of action for CHX is governed by the attraction of the positively charged CHX molecule to the negative surface charge of the bacterial cell an increase of this surface charge can be measured. Figure 6 shows the increased zeta potential for a CHX-hydrochloride concentration from 0 $\mu\text{g/ml}$ to 1000 $\mu\text{g/ml}$ loading stock solution in 100 $\mu\text{g/ml}$ increments. The data has been normalized to allow a nonlinear regression of the underlying logarithmic shape of this dataset. The zeta potential reaches from -32.86 ± 1.88 mV (0%) at 0 $\mu\text{g/ml}$ CHX to -9.63 ± 2.22 mV (100%) at 1000 $\mu\text{g/ml}$ CHX.

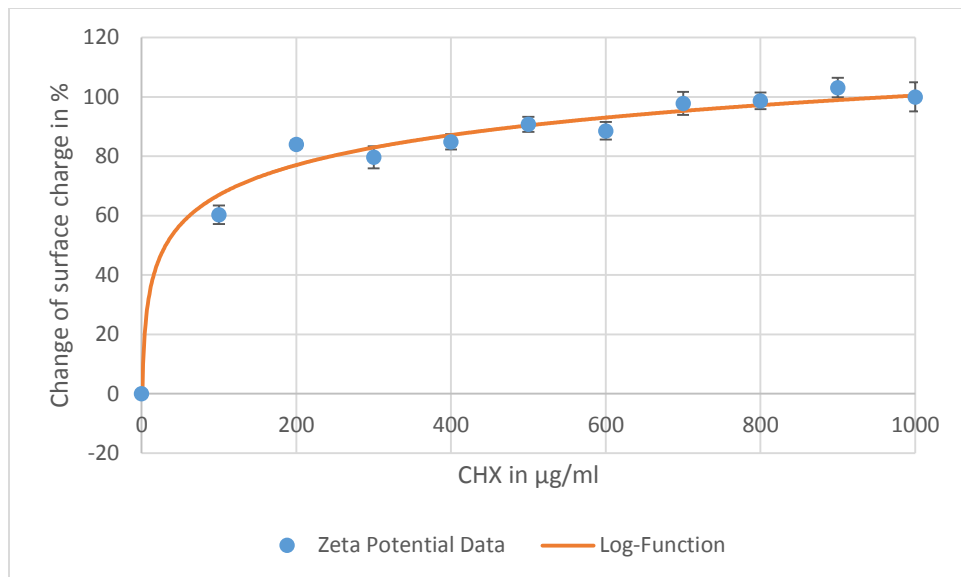


Figure 6: Zeta potential data (surface charge) for *M. luteus* loaded with CHX-hydrochloride over a range of concentrations from 0 $\mu\text{g/ml}$ to 1000 $\mu\text{g/ml}$ CHX. The data has been normalized (0%-100% equals an increase of the zeta potential from -32.86 ± 1.88 mV to -9.63 ± 2.22 mV).

We subsequently correlated the zeta potential data to the actual amount of CHX loaded into the cell as we detect it by lysing the cells and measuring the CHX concentration in the lysate. The detected linear correlation in Figure 7 suggests that most of the CHX is bound on the surface of the cells or integrated into the cell wall rather than taken up into the cells cytoplasm. If CHX would enter the cytoplasm a further increase of CHX concentration in the cell lysate would be

expected, while the zeta potential is maintained at its upper limit of roughly -10mV. However this is not the case. A possible explanation is that the negative surface charge has reached a level too weak to further attract the positively charged CHX molecules.

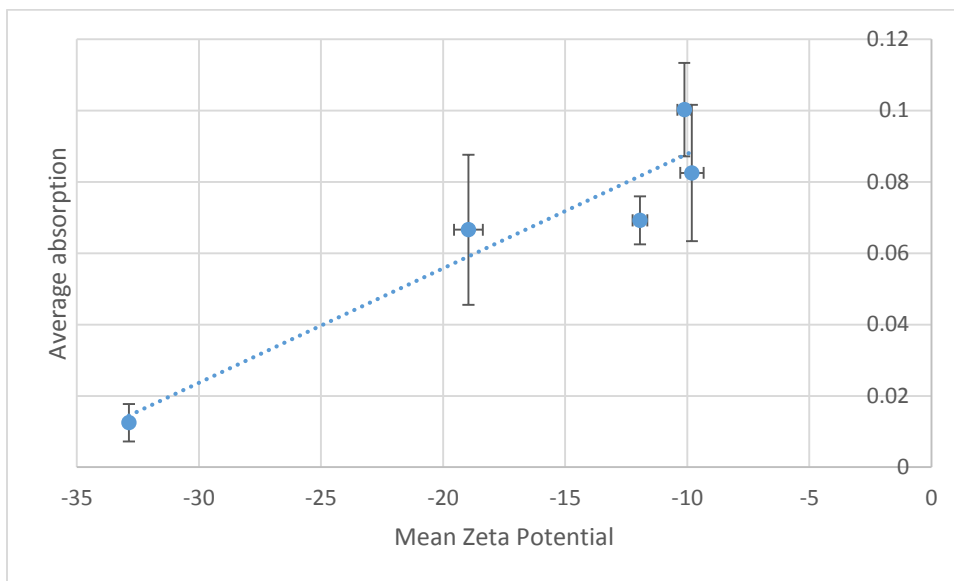


Figure 7: Correlation of the measured zeta potential (x-axis) with the measured absorption of CHX in the lysate (y-axis). A linear trend with an R^2 value of 0.9045 is visible.

The ability of *M. luteus* to retain CHX it has taken up is vital to ensure that the neutrophil granulocyte's quality as a drug carrier is not impaired by cytotoxic effects of released CHX on the way to the site of the infection.

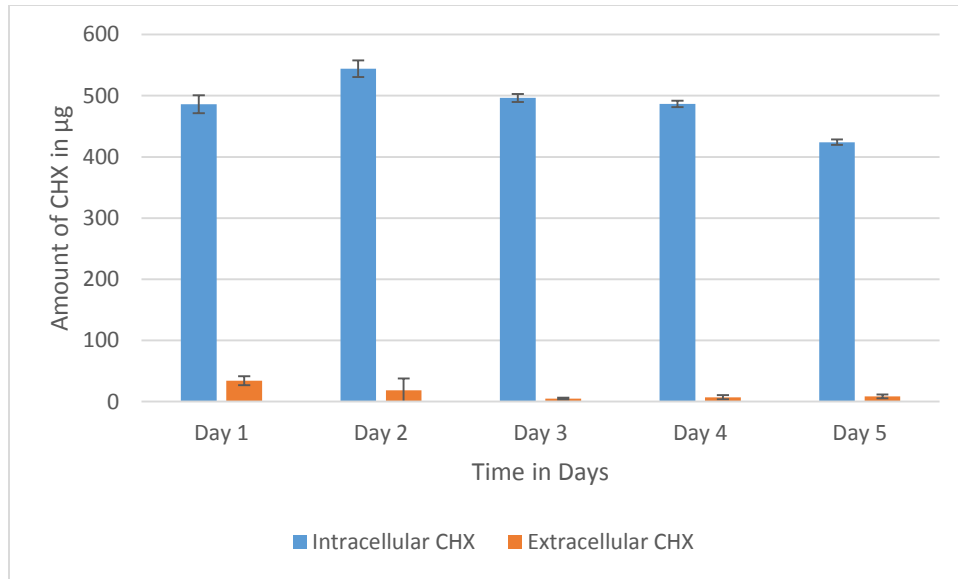


Figure 8: Analysis of CHX retention in *M. luteus* over the course of 5 days. There is no detectable increase in the amount of free, extracellular CHX (average value over 5 days is 15µg), while the intracellular CHX stays constant at an average of 490µg.

Figure 8 shows that after 5 days 5% of the loaded CHX are released by the cells into the buffer. Given the average lifetime of neutrophil granulocytes of 5.4 days¹⁸⁰⁾ this presents a satisfying result in terms of protecting the carrier cell from cytotoxic CHX effects.

Neutrophil loading and survival ex-vivo

To determine the ex-vivo neutrophil loading efficiency for modified bacteria, *M. luteus* was loaded with a fluorescent rhodamine dye. The neutrophil sample was analyzed via flow cytometry and compared to an unloaded neutrophil sample. Figure 9 shows that approximately 70% of the neutrophil population had taken up the rhodamine-modified *M. luteus* after a 2h loading period.

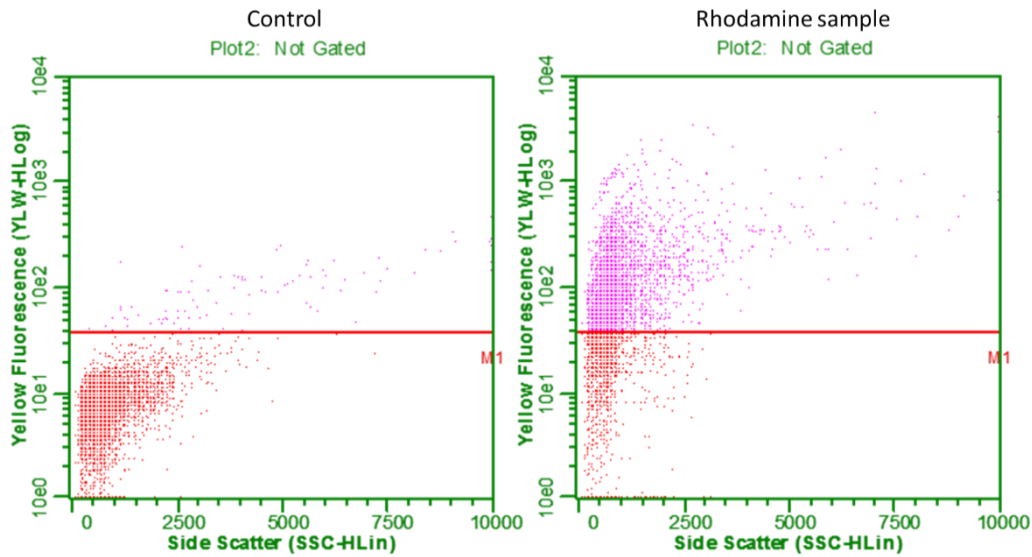


Figure 9: Comparison of the yellow fluorescence of an unloaded neutrophil population with a neutrophil population loaded with rhodamine-modified *M. luteus*.

Ex-vivo neutrophil survival during the loading phase is detrimental for this drug delivery mechanism. Neutrophil granulocytes don't survive for more than a day ex-vivo and additional stress by exposure to bacterial sample can further reduce the survival time dramatically. It has been shown that phagocytic activity increases the oxygen consumption of neutrophils by the factor of two²²⁴). Figure 10 shows that ratios of 10-20 bacteria per neutrophil granulocyte give reasonable survivability of the neutrophil when compared to the control group. If exposed to a ratio of 100 bacteria per neutrophil the survival drops below 10% for both time points.

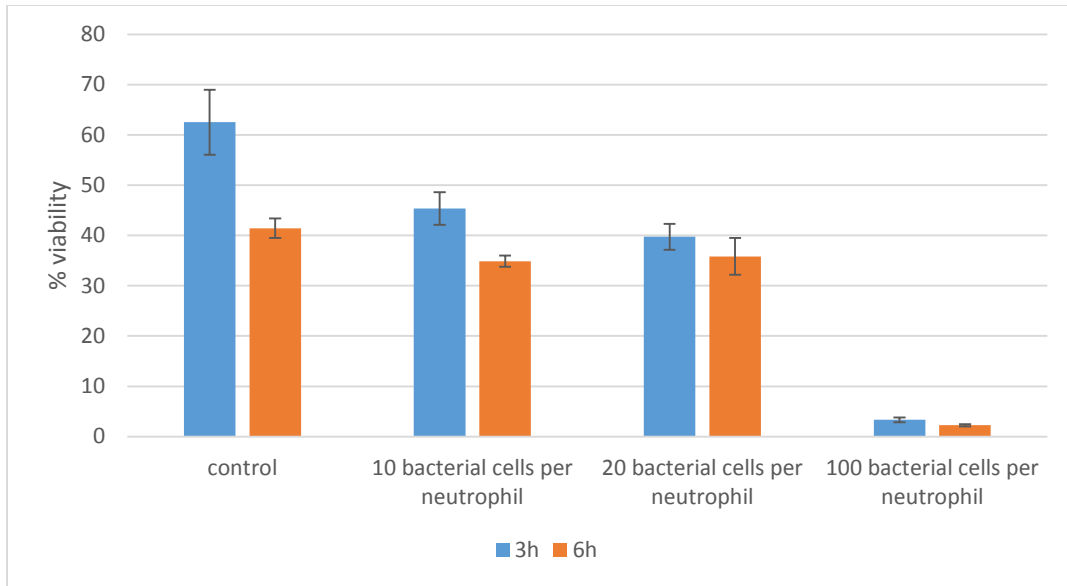


Figure 10: Neutrophil survival after 3 and 6 hours for ratios of 10, 20 and 100 bacteria/neutrophil determined by PI/annexin 5 apoptosis assay and flow cytometry.

Evaluation of Oxygen Consumption and Supply in the ex vivo loading procedure

The loading ex vivo is carried out in a filter capped reaction tube with 18-20 million cells at the concentration of $1 \cdot 10^6$ cells/ml. The system is neither aerated nor mixed so oxygen transport occurs only at the air-liquid interface. This implies that the governing equation for oxygen transport into the system is Fick's law for diffusion where the driving force for mass transport is the concentration gradient between the oxygen concentration in the interphase layer and the bulk liquid.

If we assume steady state the accumulation term of the mass balance is zero and the mass balance becomes:

$$\text{Input} = \text{Consumption}$$

Or:

Equation 1

$$A \cdot J = OUR$$

With:

Equation 2

$$J = -D \frac{\delta c}{\delta x}$$

- J is the diffusion flux in mol/(m²·s)
- D is the diffusion coefficient in m²/s
- C is the concentration in mol/m³
- X is the position in m
- A is the surface area of the liquid

The values of oxygen consumption (OUR) for phagocytosing monocytes, macrophages and neutrophils were obtained from the literature ^{224, 232}).

Wilke et al. (1955) ²³²) have developed a correlation to estimate the diffusion coefficient in liquids:

Equation 3

$$D_{O_2} = 7.4 * 10^{-8} \frac{T(A_{H_2O} * M_{H_2O})^{\frac{1}{2}}}{\mu * V_{O_2}^{0.6}}$$

- T is the absolute temperature in K
- A_{H₂O} is an association parameter for the solvent (value = 2.26)
- M_{H₂O} is the molecular mass of water
- μ is the viscosity of water in centipoise (value = 0.682 cp)
- V_{O₂} is the molar volume of oxygen (value = 25.6 cm³/g-mole)

The diffusion coefficient for oxygen at 37 °C was calculated to be 3.067·10⁻⁵ cm²/s, and is comparable to ²³⁴).

The oxygen concentration on the liquid side of the gas-liquid interface, c*, can be described by the partial pressure of oxygen in the gas phase and the Henry coefficient for low oxygen concentrations ²³⁵):

Equation 4

$$c_{O_2}^* = \frac{P_{O_2}}{H_{O_2}}$$

- P_{O_2} is the partial pressure of oxygen in the gas phase (value = 0.21 atm, partial pressure for oxygen in air)
- H_{O_2} is the Henry constant

The Henry coefficient strongly depends on temperature and ion – concentration in the medium and has a range of 900-1300 bar*L/mol for media ²³⁵). Its temperature and salinity dependence is described by Benson and Krause (1984) ²³⁶) with following equation:

Equation 5

$$H_{O_2} = e^{\left(3.71814 + \frac{5596.17}{T} - \frac{1049668}{T^2} + S\left(0.0225034 - \frac{13.6083}{T} + \frac{2565.68}{T^2}\right)\right)}$$

- T is the absolute temperature in K
- S is the salinity at physiological level (value = 5)

This gives a Henry coefficient of 53990 atm or 0.972 atm·m³/mol and a surface oxygen concentration c^* of 0.216 mol/m³.

Since the oxygen concentration in the bulk liquid is unknown the critical oxygen concentration for eukaryotic cell culture of 0.05% ²³⁷) of the saturation concentration was used for the bulk liquid concentration in Fick’s law. This is reasonable since we are interested in the onset of cell death due to hypoxia and want to compare literature values for the oxygen uptake rates (OUR) of monocytes, macrophages and neutrophils under phagocytic conditions with the oxygen transfer rate (OTR) into the system.

Integrating Fick’s law and inserting upper and lower boundaries gives:

Equation 6

$$J = -D \frac{(c_{O_2,l} - c_{O_2}^*)}{(x_{top} - x_{bottom})}$$

- $C_{O_2,l}$ is the lowest oxygen concentration in the liquid
- $C^*_{O_2}$ is the oxygen concentration in the liquid at the gas-liquid interface
- X_{top} is the height of the liquid column (0.046 m), X_{bottom} is 0

J is 1.37·10⁻⁴ mol/(m² s) and that gives an influx of oxygen of 8.21·10⁻⁸ mol/s when multiplied with the area of the gas-liquid interface of 5.73·10⁻⁴ m².

The following values of cell specific OUR for monocytes, macrophages and neutrophils with and without phagocytic stress were found:

Table 1: Oxygen consumption for different cell types under phagocytotic stress. Values were obtained from references 224 and 232.

All values in mol _{O2} /(10 ⁻⁶ cells·s)	Monocytes ²²⁴⁾	Macrophages ²³²⁾	Neutrophils ²²⁴⁾
No phagocytotic stress	1.667·10 ⁻¹²	1.267·10 ⁻¹⁰	1.833·10 ⁻¹¹
Phagocytotic stress	2.66·10 ⁻¹¹	5.733·10 ⁻¹¹	3.883·10 ⁻¹¹

For neutrophil samples with a total cell count of $20 \cdot 10^6$ cells as used in the neutrophil survival experiments this means a total oxygen uptake of $7.77 \cdot 10^{-10}$ mol/s. This is two orders of magnitude below the supplying rate of oxygen so the increased oxygen uptake by neutrophils during phagocytosis is not the determining factor of cell survival. Instead other factors like auto-cytotoxicity from the produced antimicrobial reactive oxygen species ²³⁸⁾ or induced apoptosis ²³⁹⁾ from antigen recognition may be the driving force for neutrophil cell death and the limiting parameters for phagocytic capacity.

In-Vitro Results

The delivery system was tested *in vitro* on *E. coli* and *F. necrophorum* cultures. In both cases the targeted bacterium was eradicated completely by the treatment group. Control groups containing neutrophils or neutrophils loaded with unmodified *M. luteus* reduced the bacterial count when compared to the medium-control group but failed to effectively battle the bacteria leaving viable CFUs in the range of 10^6 - 10^8 . This drop in the CFU count can be attributed to the increased release of bactericidal reactive oxygen species from neutrophil granulocytes as shown by Reiss et al. ²²⁴⁾ Figure 11 shows the results for *in vitro* tests of the drug delivery system on *E. coli* C600N. The CHX treatment group was able to eradicate all *E. coli* C600N so that in a CFU count

no colonies were found. Similarly Figure 12 shows the complete eradication of *Fusobacterium necrophorum* subspecies *necrophorum* by the cell based CHX delivery system. Again the control groups containing live neutrophil granulocytes show a reduced CFU count that can likely be attributed to the bactericidal properties of the phagocyte.

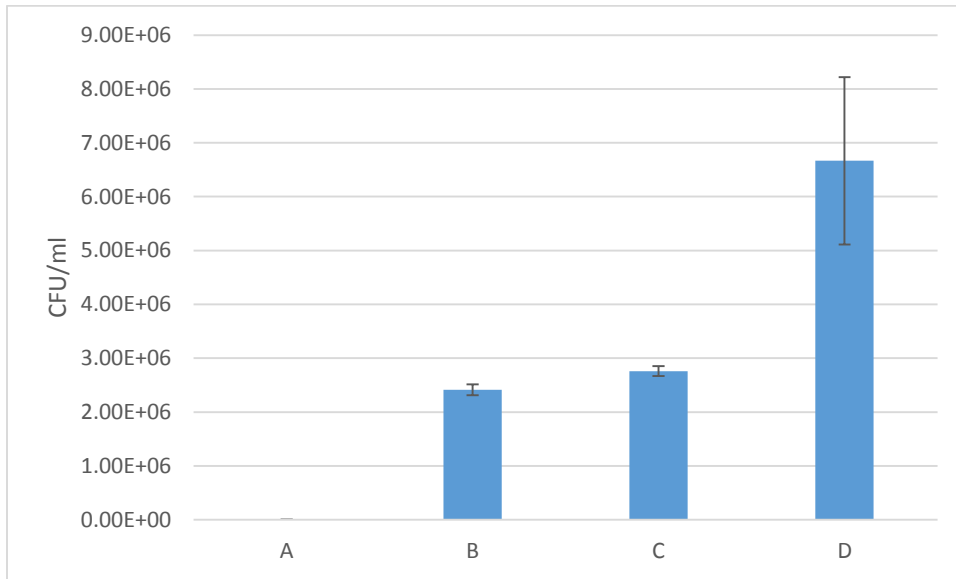


Figure 11: *In vitro* tests of the cell based CHX drug delivery system on *E. coli* C600N. Here *E. coli* C600N was exposed to the following test groups: A is the CHX - *M. luteus* – Neutrophil granulocyte delivery system, B is the first control group with Neutrophil granulocytes loaded with unmodified *M. luteus*, C is the second control group with just unmodified Neutrophil granulocytes and D is the third control group with plain RPMI culture medium.

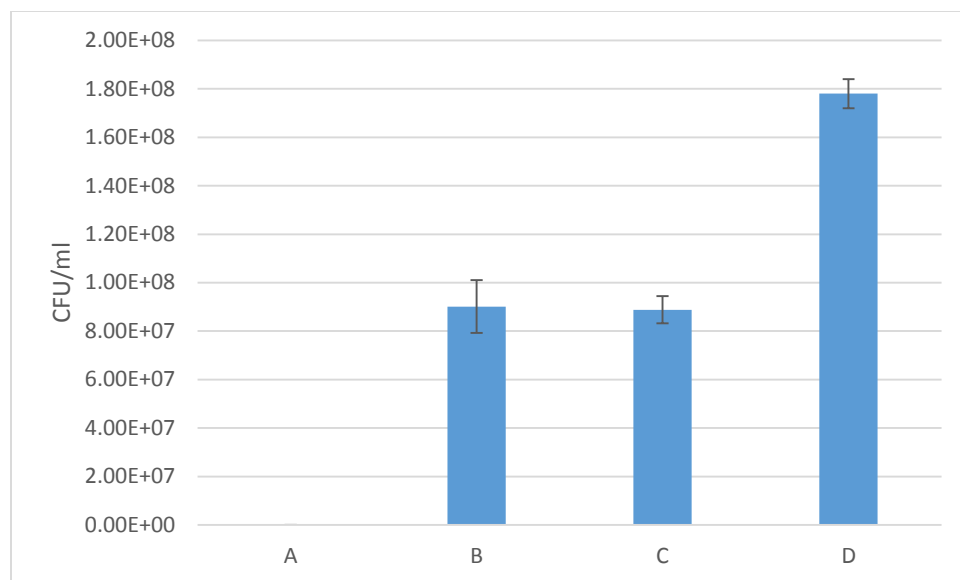


Figure 12: *In vitro* tests of the cell based CHX drug delivery system on *Fusobacterium necrophorum* subspecies *necrophorum*. Here *Fusobacterium necrophorum* subspecies *necrophorum* was exposed to the following test groups: A is the CHX - *M. luteus* – Neutrophil granulocyte delivery system, B is the first control group with Neutrophil granulocytes loaded with unmodified *M. luteus*, C is the second control group with just unmodified Neutrophil granulocytes and D is the third control group with plain RPMI culture medium.

***M. luteus* loaded with doxorubicin**

Characterization of the loaded bacterial cells

Doxorubicin (DOX) proved to be easily water-soluble within the relevant concentration range of 12.5 to 50 µg/ml. Although it is listed as an anthracycline antibiotic it was ineffective at killing or inhibiting *M. luteus* in the previously mentioned concentration range. Its bright orange color allows an easy first assessment of the success of the loading procedure. Loaded *M. luteus* will accumulate in a bright orange pellet at the bottom of the tube after centrifugation when previously exposed to a DOX-PBS solution for 24 hours.

UV-Vis spectroscopy was chosen to determine the DOX concentrations since DOX is self-quenching making fluorescence measurements inconvenient especially after loading, when DOX is confined to the volume of the cell. The strong association of DOX with the bacterial cell or cell fragments, even after using 1% Triton-X lysis buffer and 40 minutes of sonication, made it

necessary to use a stronger lysis buffer with 3% Triton-X and 1% SDS. This however alters the absorption response of DOX molecules when compared to the PBS buffer and makes it necessary to employ individual calibration curves for the respective buffer systems. Figure 13 shows the exemplary absorption spectrum of DOX in PBS in the range of 400 – 600 nm and its peak maximum at 480 nm that was used to establish a calibration curve.

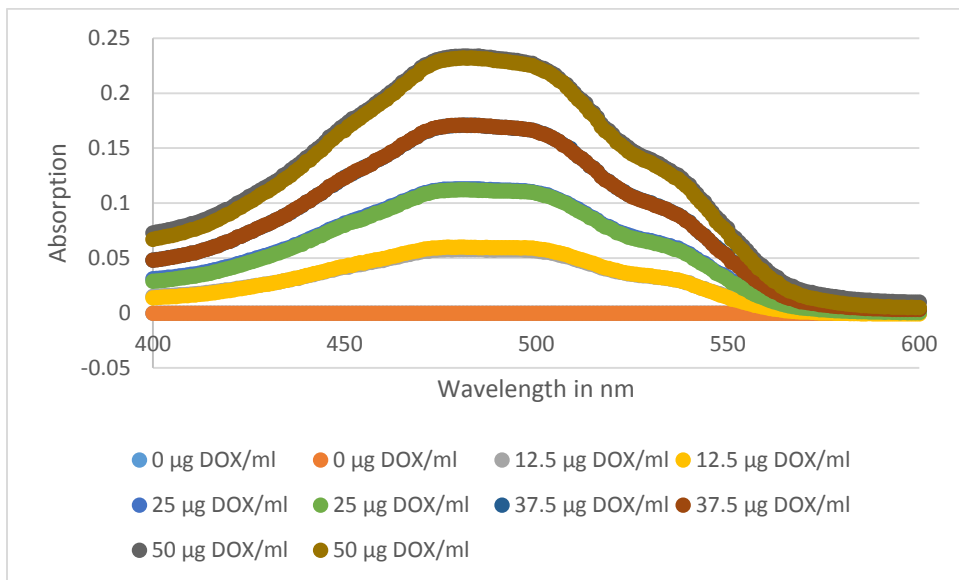


Figure 13: Typical UV/Vis absorption spectrum for several DOX concentrations

The spectrum for DOX in strong lysis buffer retains the distinctive peak and absorption maximum at 480 nm, the absorption signal itself however is dampened as shown in Figure 14, the comparison of calibration curves for the lysis buffer-DOX system and the PBS-DOX system. The standard error for the calibration is given in Table 2 since the error bars were too small to be visible in the graph.

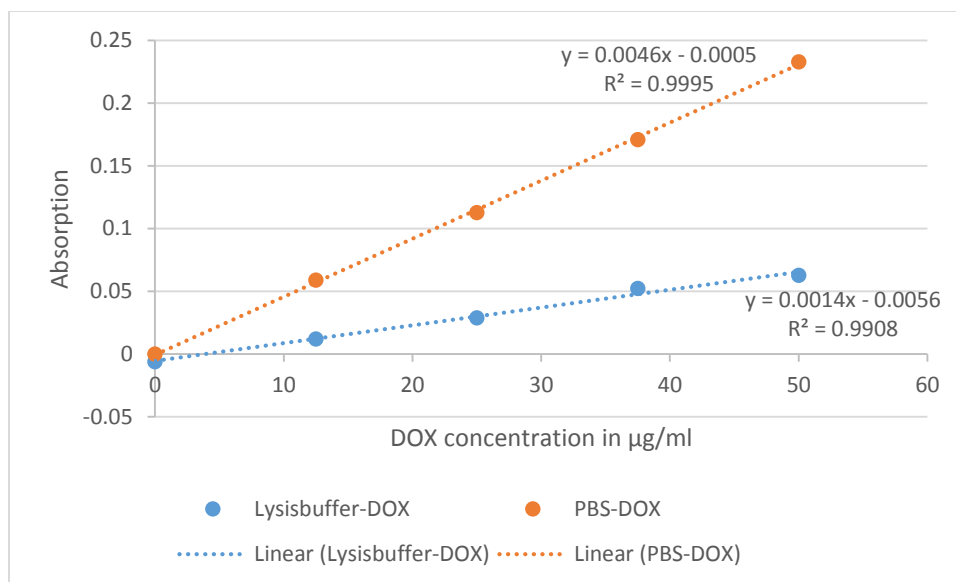


Figure 14: Calibration curves for DOX in PBS and in lysis buffer. Lysis buffer reduces the absorption for samples of the same concentration by a factor of 3.3

Table 2: Standard deviations for the DOX calibration curves

Lysis buffer - DOX	0.0014	0.0014	0.0023	0.0009	0.0011
PBS - DOX	0	0.0096	0.0032	0.002	0.0064

There are two parameters of interest at this stage: how much DOX has been loaded into the *M. luteus* cell sample and how well do these cells retain DOX. A mass balance for DOX was established showing the amount of DOX initially provided compared with the amount found intracellular after lysing the cells with strong lysis buffer and the amount of DOX that was not taken up and remained in the PBS buffer after the 24 hour loading period. No detectable amount of DOX was found in the washing step.

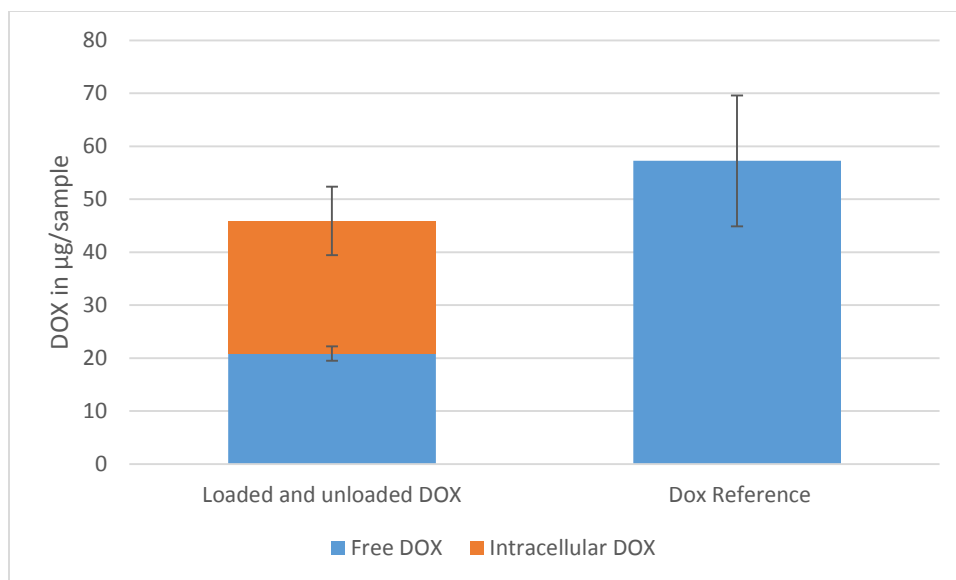


Figure 15: Mass balance for doxorubicin loaded *M. luteus*. The difference between intracellular & unloaded sample compared with the initial DOX concentration is not significant.

Measurements for DOX in lysis buffer resulted in a larger standard deviation, a behavior not seen for the calibration curve. Approximately 36% of the initially provided DOX was internalized by bacterial cells.

A t-test shows no significant difference ($p > 0.1$) between the sum of intracellular DOX and unloaded DOX compared to the reference, the initial DOX concentration provided. Samples measured in lysis buffer (Intracellular and reference DOX) are however associated with a higher error, a phenomenon not seen for the calibration curve. Approximately 36.5% of the DOX provided were cell associated and released only by using the strong lysis buffer.

Retention of DOX

DOX retention by the bacterial cells is important to ensure the protection of neutrophil or monocyte/macrophage carrier cells. The retention was observed over a time period of seven days and showed that over this time period of the $20.8 \pm 1.4 \mu\text{g}$ intracellular DOX 38% ($7.9 \pm 0.8 \mu\text{g}$) were released into the buffer.

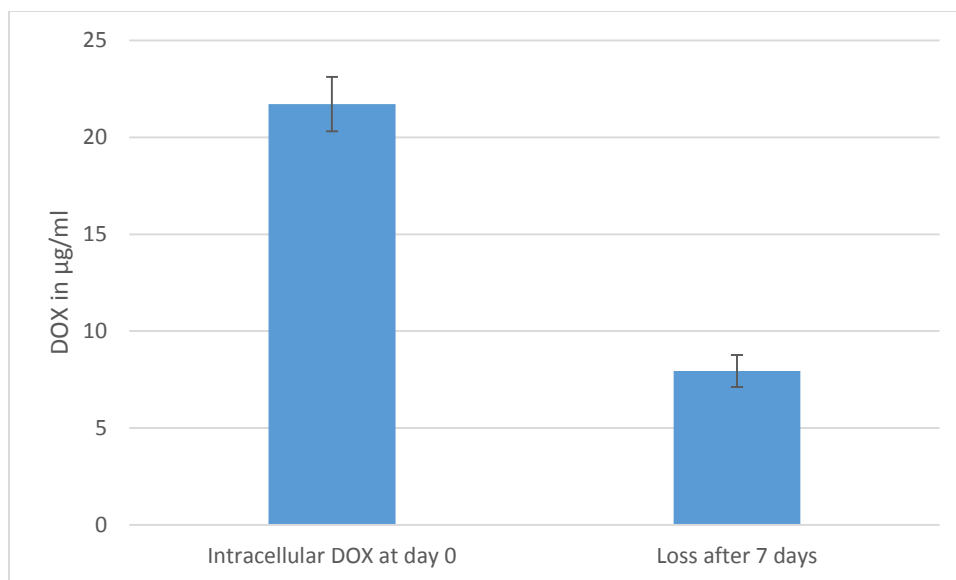


Figure 16: DOX retention over the course of seven days. The bacterial cells have released 38% of the initially internalized DOX.

The bacterial ghost system for example loses 40% of its DOX payload within the first 24h. While still acceptable when compared to the work of Lubitz et al. ^{126, 127)} this is a surprisingly high value given the strong association of DOX to the cells when we tried to release it with normal lysis buffer. DOX might need the interaction with bacterial DNA, of which bacterial ghosts are stripped, therefore causing the short retention time. The fact that DOX does not kill *M. luteus* as we had initially assumed might be point towards a mechanism to remove DOX from the cell.

The amount of DOX (MW of doxorubicin hydrochloride: 579.98 g/mol) carried by a bacterial sample of 0.2 ml volume and $8.8 \cdot 10^8$ cells/ml (sample size applied later in the chlorhexidine-mouse study) is 7.17 µM and exceeds the IC₅₀ systemic concentration of 0.62 µM more than 60 fold making *M. luteus* a very effective carrier for DOX ²⁰¹⁾, especially for a targeted drug delivery that confines DOX closely to the tumor boundaries. Compared with lysosomal carriers that typically exhibit a carrier to drug ratio of 1:10000 ⁷⁶⁾ the bacterial carrier achieves a ratio of $1:2.25 \cdot 10^8$.

In vitro cell assays of Mo/Ma cell survival

The survival of the transport cell is paramount to the success of the delivery system. Mo/Ma cell survival was tested for bacteria and bacteria loaded with DOX to ensure that the exposure to

bacterial antigens as well as the drug carrying bacteria does not affect the Mo/Ma cells vitality. The cells were exposed to their respective samples for 72 hours and their survival was measured via MTT assay. The results are shown in Figure 17.

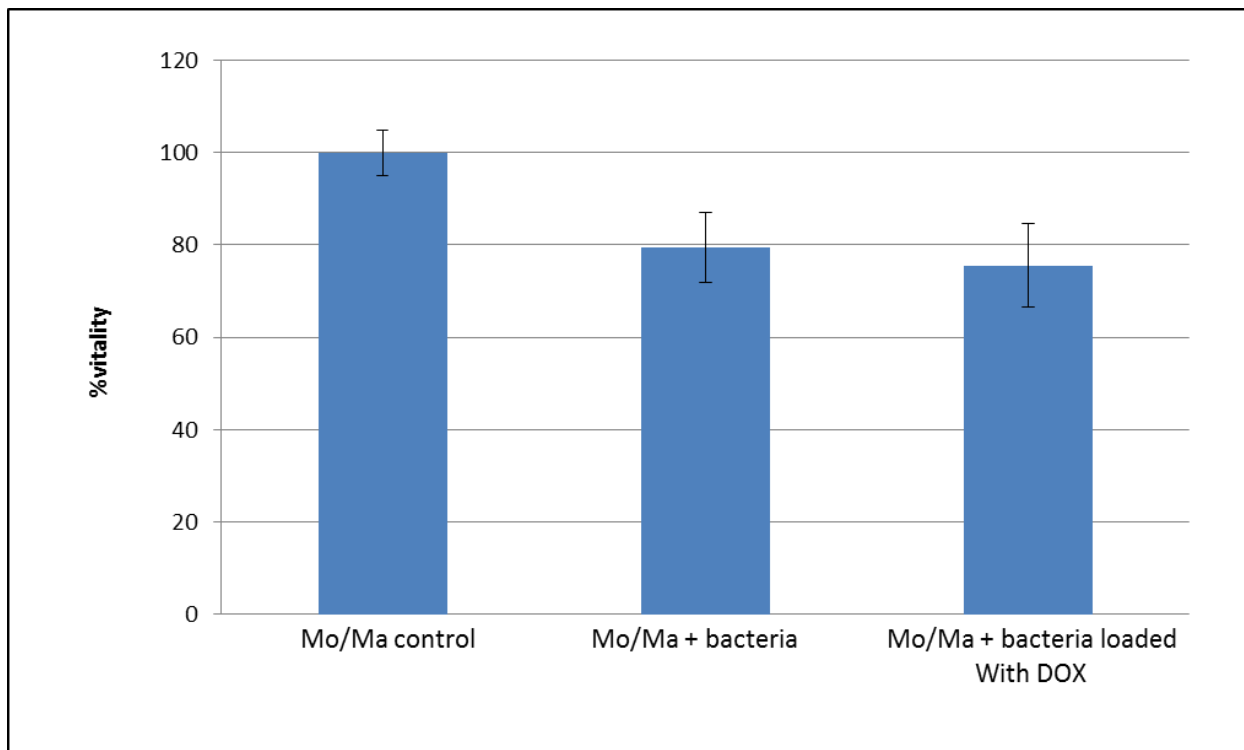


Figure 17: MTT assay to determine the survival of Mo/Ma cell cultures when exposed to bacterial samples and bacteria loaded with DOX. While the viability decreases significantly for both sample types it remains at 80% after 72 hours. This is a sufficient value since Mo/Ma cells should be able to reach their target within 24 hours.

Both samples, Mo/Ma + bacteria and Mo/Ma + loaded bacteria have a significantly decreased viability ($p < 0.01$) but average viabilities of 80% when compared to the control group after 72 hours are acceptable results since Mo/Ma cells should be capable of reaching their target in 24 hours or less ¹⁶⁵.

In vitro cell assays with 4T1 cancer cells and conditioned medium

After a sufficient survival of Mo/Ma cells that had taken up DOX carrying bacteria was shown medium was conditioned by Mo/Ma cells loaded with DOX modified bacteria. After 24 hours the conditioned medium was complemented with fresh medium of the same volume and 4T1 breast cancer cells were exposed to the conditioned medium. This leads to a significant decrease

in 4T1 cell viability when exposed to medium conditioned by the Mo/Ma + DOX modified bacteria group over the course of 4 days while the 4T1 control group maintains a viability of 100%. The other control group, conditioned medium from Mo/Ma cells loaded with 12.5 $\mu\text{g/ml}$ DOX directly, did not course a drop in 4T1 cell viability.

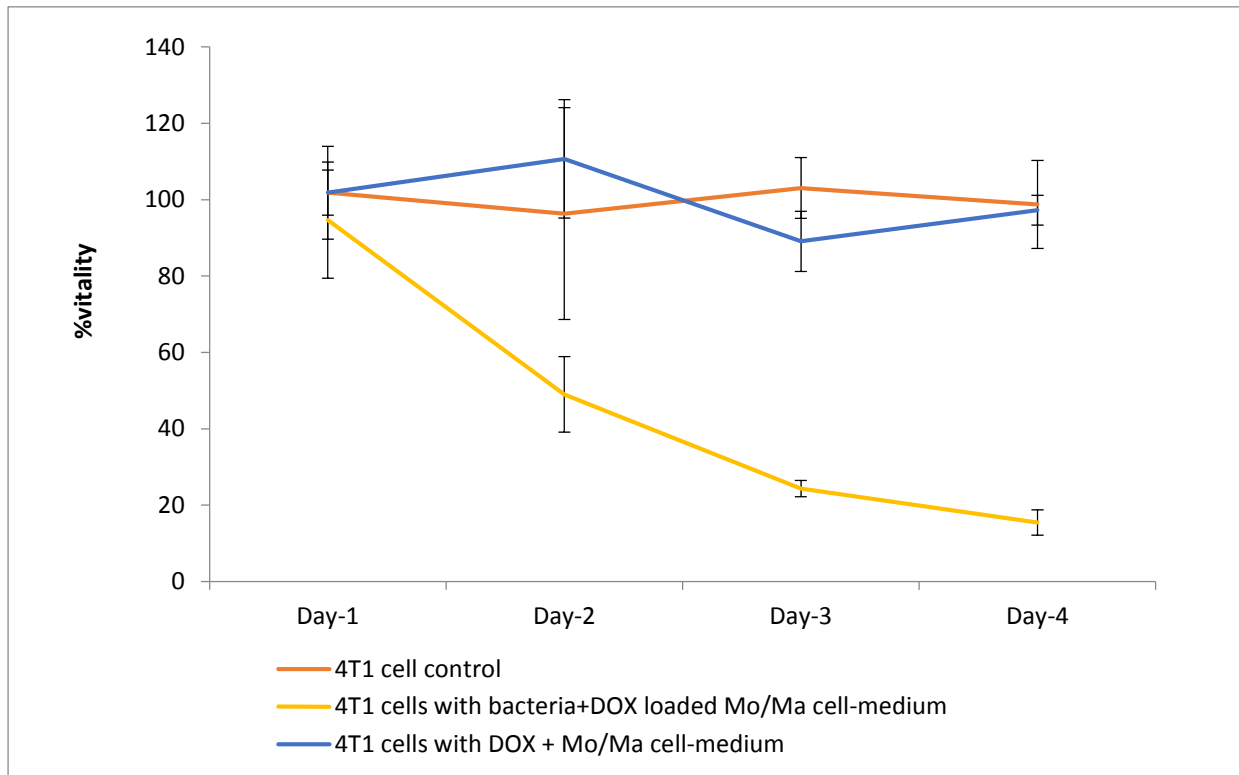


Figure 18: The 4T1 breast cancer cell line is exposed to conditioned medium from Mo/Ma-DOX cells or Mo/Ma cells loaded with DOX modified bacteria. Only the conditioned medium from the Mo/Ma - bacterial carrier system was able to reduce 4T1 cell viability. It drops from 95% to less than 20% within 4 days.

A possible explanation is that free DOX associates with components of Mo/Ma cells, particularly DNA and free nucleotides²⁰⁸⁾, so strongly that it isn't released from the cells. The DOX specific fluorescence was measured in the medium to determine if DOX is released from the cells.

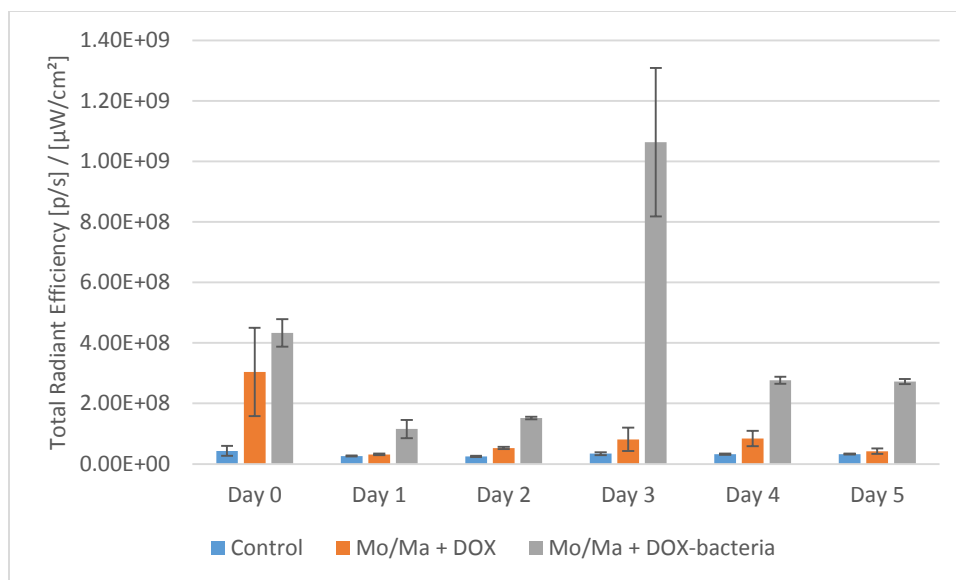


Figure 19: DOX released from Mo/Ma cells loaded with free DOX or DOX in a bacterial carrier. The amounts of DOX released from the bacterial carrier system are significantly higher than the DOX released from the bacteria free system. Data was acquired via IVIS fluorescence.

The Mo/Ma DOX-bacteria system shows a higher release of DOX over the observed time course, confirming that free DOX is not easily released from Mo/Ma cells once taken up, while DOX taken up via a bacterial carrier is probably released through an exosome. This is furthermore confirmed via flow cytometry, showing that the fluorescence of loaded Mo/Ma cells decreases over time from initially 70% fluorescent cells right after the loading process to 20% fluorescent cells at day 5.

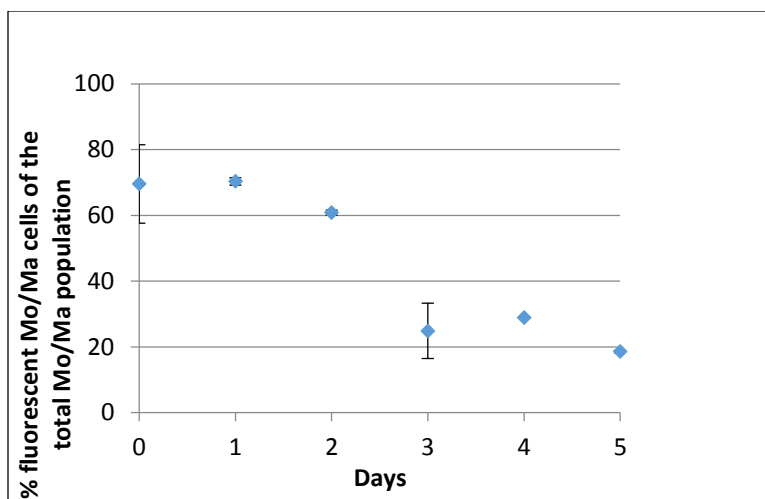


Figure 20: The fluorescence of Mo/Ma cells loaded with DOX-bacteria decreases over the course of five days as DOX is released from the cells. Flow cytometry registers DOX-specific fluorescent cells of the total Mo/Ma population. Initially 70% of the Mo/Ma population showed DOX-specific fluorescence. This value decreases to 20% after five days.

***M. luteus* loaded with DP44mt**

Characterization of the loaded bacterial cells

Solid DP44mt is of bright yellow color but stock solutions with solubilized DP44mt are colorless not allowing an easy assessment of the loading as it was the case for DOX. DP44mt is poorly water-soluble and two different methods were tested for solubilization. The first solvent tested is a 50%/50% mix of poly-propylene glycol (PPG) and PBS and allowed concentrations up to 0.1 mg/ml DP44mt. The second system uses 20 μ l of DMSO to dissolve the initial DP44mt crystals (up to 2 mg) and then dilute the sample with the desired amount of PBS making solutions with higher concentrations possible. DP44mt was tested for antibacterial activity and proved ineffective in killing bacteria, however the 50/50 PPG-PBS mix was toxic to bacteria reducing the CFU count from more than 400 countable colonies for *M. luteus* in PBS to 2. All following work used the DMSO-PBS system because of the higher maximum concentration. DP44mt shows a distinct peak in the UV/Vis absorption spectrum at 322 nm as shown in Figure 21.

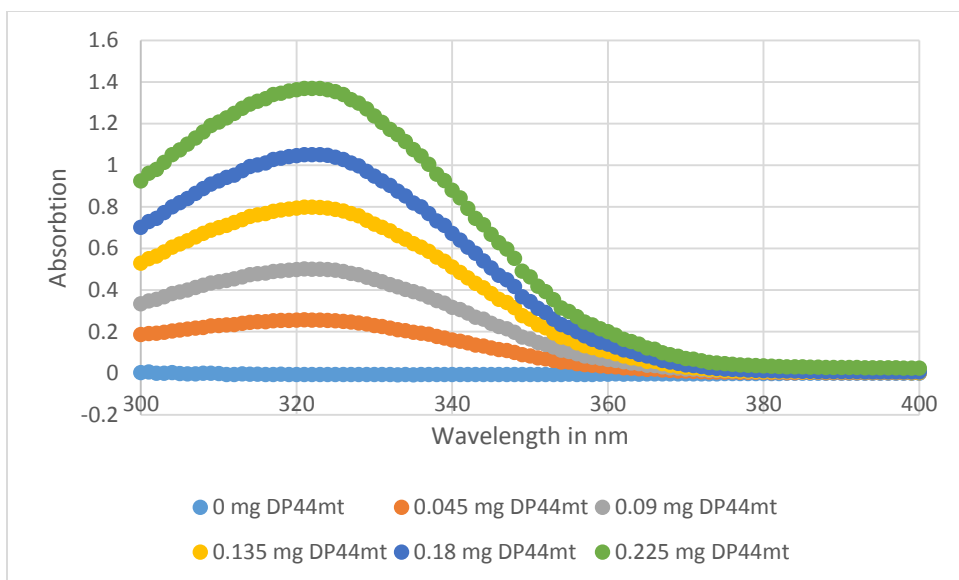


Figure 21: Typical UV/Vis spectrum for various concentrations of DP44mt

Similarly to DOX this distinct peak is used for a calibration curve to determine DP44mt concentrations in samples like cell lysates and supernatants of unloaded DP44mt.

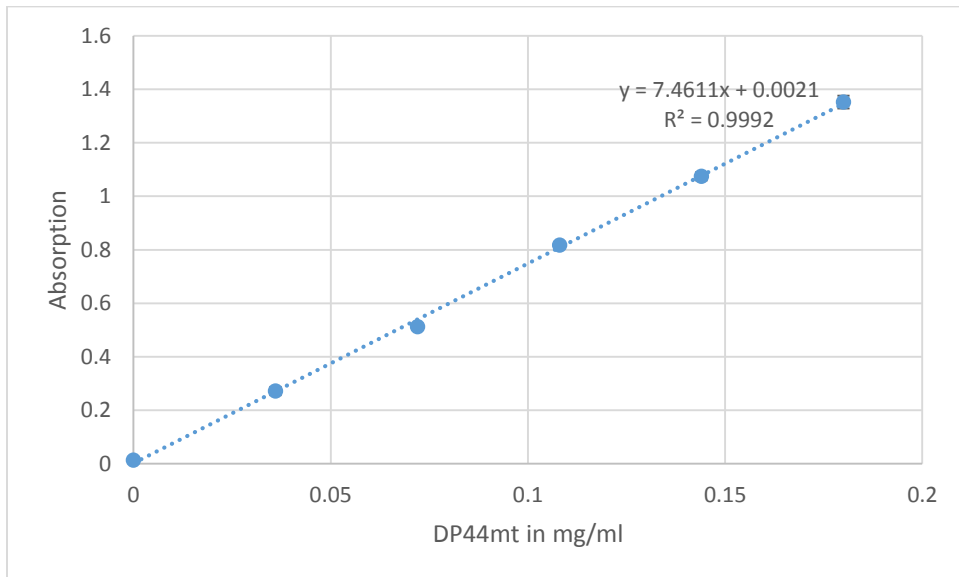


Figure 22: Calibration curve for quantification of intracellular DP44mt

Table 3: Values for the DP44mt calibration curve including standard deviations

DP44mt Calibration						
DP44mt concentration in mg/ml	0	0.036	0.072	0.108	0.144	0.18
Average absorption	0.0138	0.272	0.5128	0.817	1.0746	1.3516
StDev	0.011498	0.015556	0.008468	0.012021	0.015372	0.024037

Again the parameters of interest are the amount of DP44mt loaded and the retention capabilities of the cell. The loading efficiency for a 0.18mg/ml stock solution is 8.8% with a total amount of 16.8 ± 1.4 μg /sample loaded.

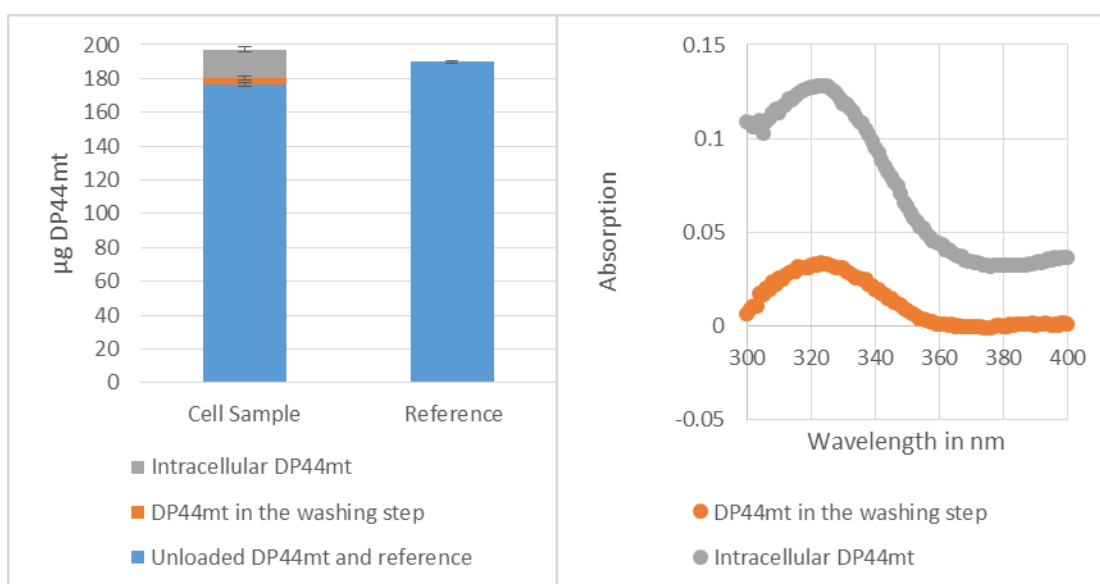


Figure 23: The left image shows the mass balance for the loading process of DP44mt. The sum of DP44mt found in the various cell associated samples exceeds the initially provided amount by 7.4 μg . The right image shows the spectra for the intracellular DP44mt and DP44mt in the washing step. While the signal is weak the specific peak for DP44mt at 320 nm can still be seen.

The mass balance however shows a significant difference ($p < 0.005$) of the sample parts that were exposed to cells when compared to the reference sample with a total amount of 197.2 ± 3.3 μg DP44mt found in samples that were exposed to cells and the reference sample with 189.9 ± 0.8 μg DP44mt. This results in a difference of 7.4 μg DP44mt, which are unaccounted for. The retention of DP44mt was tested over the course of three days showing that DP44mt is not well retained by *M. luteus* cells. While 16.8 ± 1.4 μg /sample can be found intracellular right after

the 24 hour loading process this value drops to $5.1 \pm 0.6 \mu\text{g}/\text{sample}$ after 24 hours and after 48 hours the amount of intracellular DP44mt is below the detection limit. Why the amount of extracellular DP44mt after 24 hours exceeds the amount of DP44mt initially associated with the cell sample (both in- and extracellular) by approximately $17 \mu\text{g}$ is unclear.

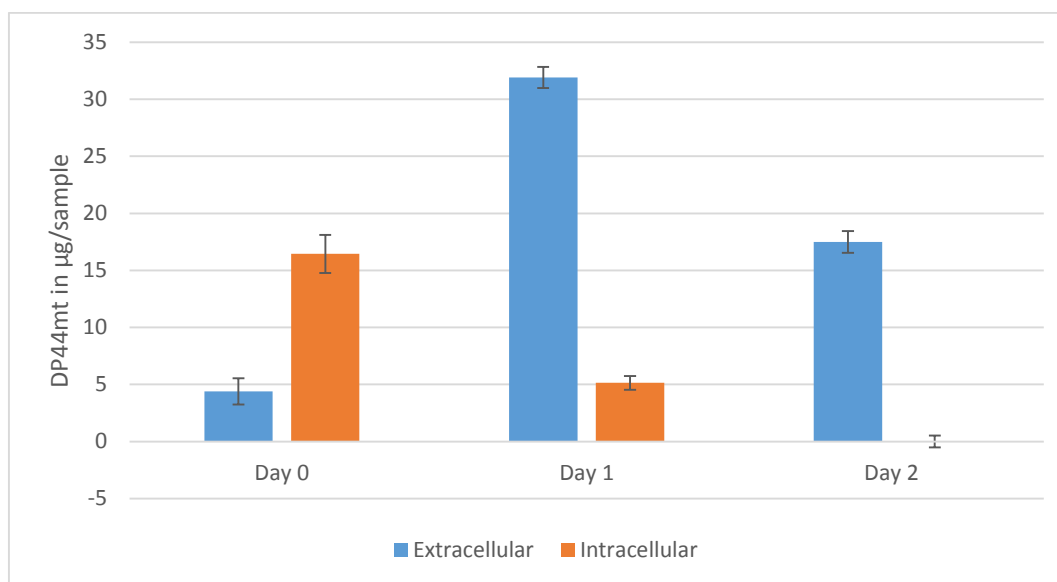


Figure 24: DP44mt is not retained by *M. luteus* cells. The complete amount of initially intracellular DP44mt is released after 48 hours allowing the cytotoxic effects of DP44mt to affect the transporting Mo/Ma cells.

DP44mt (molecular weight 285.37 g/mol) has an average IC_{50} of $0.03 \mu\text{M}$ for a total of 28 cancer cell lines tested. The amount initially loaded in the experiments here is the equivalent of $11.2 \mu\text{M}$ for a 0.2 ml sample, exceeding the average IC_{50} of $0.03 \mu\text{M}$ more than 370 fold allowing the system to transport substantial amounts of DP44mt. The poor retention however fails to protect the monocyte/macrophage carrier cells from the cytotoxic effects of DP44mt as will be shown later in the *in vitro* cell culture section. A DP44mt analogue-chlorhexidine conjugate was synthesized to exploit the excellent retention of chlorhexidine and combine it with the high cytotoxicity of DP44mt.

In vitro cell assay for Mo/Ma cell survival

The MTT assay shows that bacteria loaded with DP44mt don't have any protective effect compared to free DP44mt. Cell viability drops from 80% to 40% within 48 hours. The reason is

the insufficient retention of the drug by the bacterial cells allowing the released DP44mt to unfold its cytotoxic effects within the Mo/Ma cells.

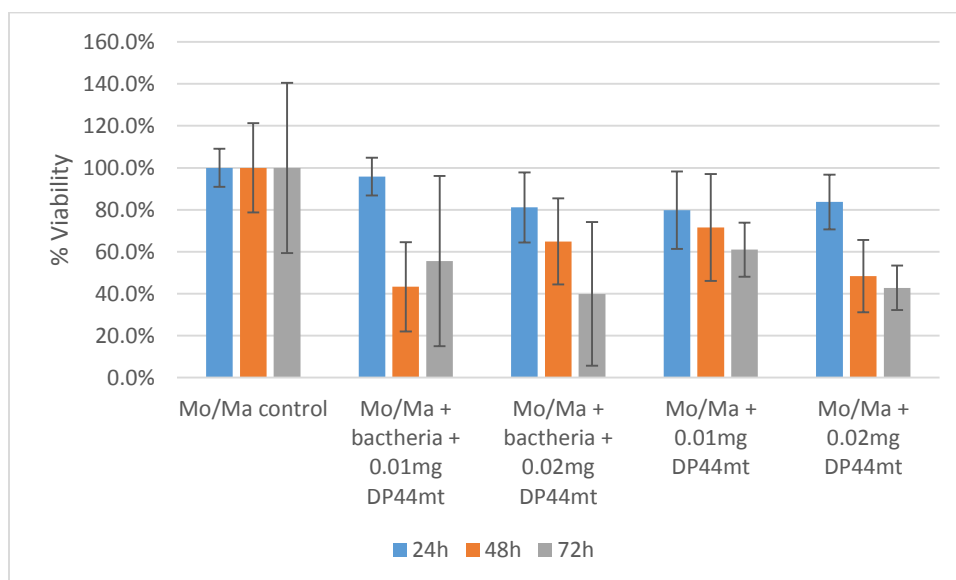


Figure 25: Mo/Ma cell viability observed over 72 hours. DP44mt is not contained by its bacterial carrier and shows similar cytotoxicity as the free DP44mt.

CHX-DP44mt analogue conjugate

The synthesized conjugate showed extremely poor water solubility. In order to solubilize a fraction of the conjugate it was first dissolved in pure DMSO, which wouldn't result in a complete dissolution of the conjugate. Part of the DMSO-conjugate solution was then added to PBS resulting in a partial precipitation of the conjugate. The precipitate free fraction of the PBS-DMSO-conjugate system was then analyzed via UV/Vis and compared with the pure individual components to verify the quality of the synthesis product. The poor solubility made it impossible to establish a calibration curve for quantification since producing a stock solution of known concentration was impossible. Other than pure DP44mt the conjugate is an effective bactericidal, completely deactivating the *M. luteus* population.

Table 4: Bactericidal properties of the synthesized conjugate

	<i>M. luteus</i> in PBS	<i>M. luteus</i> exposed to conjugate in PBS
Cells/ml	2.80E+11	0
StDev	5.97E+10	0

CHX hydrochloride only absorbs in the region below 320nm while the DP44mt analogue has its peak maximum at 350nm. In the conjugate this results in a shift of the onset from the predominant CHX hydrochloride absorption from 320 nm to approximately 355 nm and tailing of the absorption up to 480 nm. This indicates that the DP44mt analogue has been linked to CHX hydrochloride.

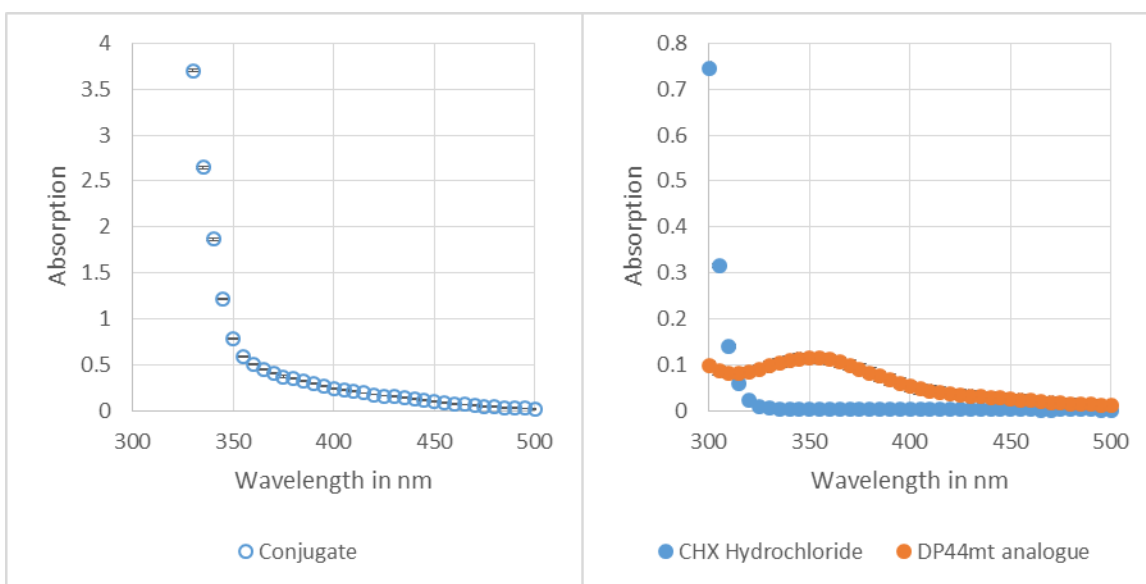


Figure 26: The left graph shows the UV/Vis spectrum for the conjugate while the right spectrum shows the spectra for the individual pure components. While the general shape of the conjugate absorption curve resembles the CHX-hydrochloride curve the conjugate spectrum is red-shifted in comparison due to the influence of the DP44mt analogue.

The retention of the conjugate was measured over the course of six days by lysing loaded cells and measuring the spectra from 280 to 360 nm. While the conjugate showed an increased retention through a consistent absorption in the cell lysate compared to pure DP44mt it also showed a consistently high absorption for the conjugate in the extracellular buffer. A possible explanation is that the conjugate further precipitated during the 24 hour loading process or that

not all of the precipitate was removed. Overall the conjugates poor solubility in the solvents used was a major obstacle for a good characterization of conjugate loaded cells and made a quantification impossible.

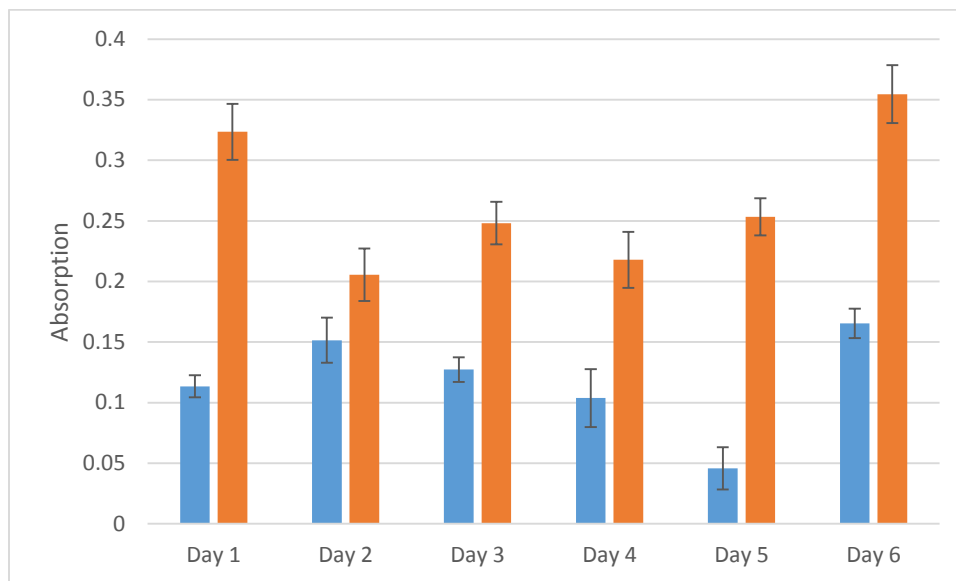


Figure 27: The conjugates retention in *M. luteus* was measured over the course of 6 days. Consistently large absorption for extracellular conjugate due to its poor water solubility make it unclear if the retention of the conjugate is better in comparison to DP44mt.

Intracellular conjugate is found consistently over the course of six days, but it remains unclear if the retention properties have improved since higher concentrations of the conjugate were found in the extracellular buffer simultaneously.

Conclusions

Chlorhexidine loaded bacterial samples perform well in all aspects. Due to the blue color of CHX-gluconate loading success can easily be determined from the color change of the cell pellet. Uptake is rapid and the cells are fully loaded within 4 hours. CHX is well retained by the cells providing good protection for the transporting neutrophil granulocytes. The zeta potential experiments have shown that CHX associates with the cell surface rather than being internalized. While this is unfortunate in terms of achieving the best possible loading by using the full volume of the cell, the in-vitro experiment show that the amount loaded is sufficient to kill gram negative

pathogenic bacteria. CHX is probably not internalized because of the lack of a driving force once most of the negatively charged surface positions are occupied. Ex vivo loading of neutrophil granulocyte transport cells was successfully tested. It is detrimental for neutrophil survival not to overload the cells with too many bacteria. *In vitro* drug delivery tests on *E. coli* and *F. necrophorum* were very successful and resulted in the complete eradication of the pathogen cultures.

Doxorubicin is easily loaded into bacterial cells and, like CHX, loading success can be determined from the color of the cell pellet after loading due to DOX bright orange color. A strong lysis buffer using both Triton-X and SDS as detergents is required to release the full amount of DOX from the cells again. This results in larger errors in the DOX quantification because DOX seems to interact with the lysis buffer, which alters the absorption pattern. Bacterial DOX shows a better release from Mo/Ma cells when compared to free DOX loaded into Mo/Ma cells. This may be the result of an uptake/release via endosome/exosome for bacterial DOX rather than a diffusion through the Mo/Ma cells membrane and possible interaction with DNA or nucleotides for free DOX. Ma/Ma cells loaded with bacterial DOX were able to reduce 4T1 breast cancer viability to 20% of the initial level.

The poor water solubility of DP44mt is likely the cause of numerous problems with the component or the later synthesized conjugate. The mass balance for DP44mt leaves a significant gap between the amount of DP44mt initially provided and the sum of DP44mt associated with various stages of the cell samples. It is not well retained by the bacterial cell and its absorption behavior is influenced when in contact with bacterial cells as shown in the progression of the retention experiment. A conjugate of CHX and a DP44mt analogue was synthesized to exploit the excellent retention characteristics of CHX and combine it with the high cytotoxicity of DP-class iron chelators. This conjugate however shows even poorer water solubility and makes an accurate quantification impossible. Unlike pure DP44mt it is bactericidal and may be retained by the bacterial cell, although the amount of extracellular conjugate found during the 6 day retention experiment does not allow a definitive conclusion since the conjugate might be in an equilibrium between in- and extracellular concentration rather than attached to negatively charged elements of the cell as it was shown for CHX-gluconate.

Chapter 6 - *In vivo* Mouse Studies of the Cell Based Antibacterial Drug Delivery System Against *F. necrophorum* Infections

Preliminary mouse toxicity study

Two *in vivo* studies were carried out. The first one was a small 9-mouse study to determine toxic side effects of the drug delivery system, particularly toxic effects from free *M. luteus* and chlorhexidine itself.

The mouse behavior was observed but no signs of lethargy unusual grooming behavior was found. Kidneys, liver, brain, lung, spleen and heart were collected for a histopathological evaluation of the tissues and showed no signs of tissue damage from CHX mediated toxic side effects.

Mouse study for antibacterial drug delivery against *F. necrophorum* infections

In the final *in vivo* mouse experiment the CHX treatment group showed significant results ($p < 0.05$, Pairwise Two-Sided Multiple Comparison Analysis; Dwass, Steel, Critchlow-Fligner Method²²⁵⁻²²⁷) against all control groups. Each mouse in the CHX treatment group received a dose of 0.056 mg CHX. The CFU count was reduced by an order of magnitude from an average of approximately $2 \cdot 10^6$ in the control groups to $1 \cdot 10^5$. The treatment group using doxycycline modified *M. luteus* showed significant results as well but the results might be distorted due to two early deaths in this group that raised the bacterial count for this particular group. Figure 28 shows the CFU count results of homogenized and plated liver samples.

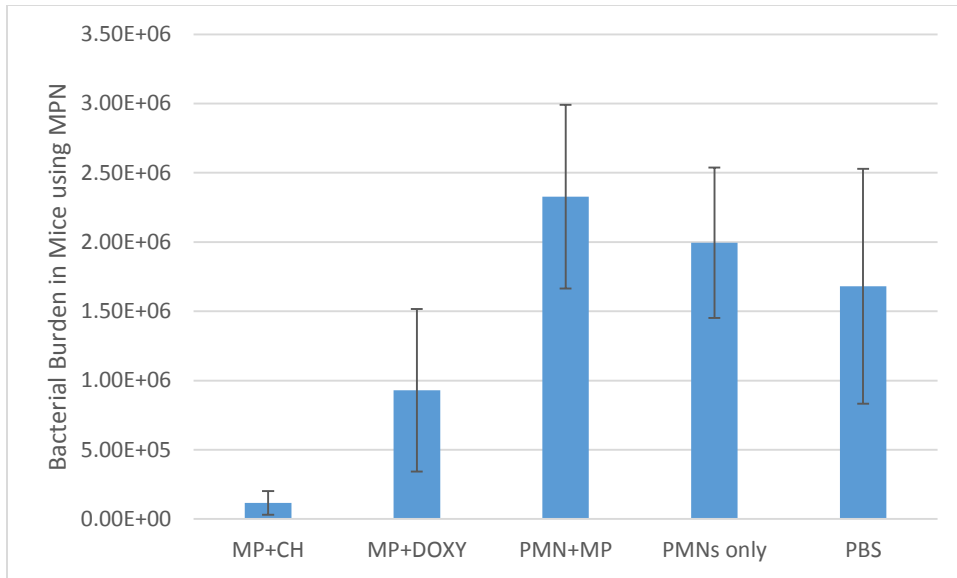


Figure 28: Results of the *in vivo* experiment. MP + CH is the treatment group containing neutrophils loaded with CHX modified *M. luteus*. MP + DOXY is the treatment group containing neutrophils loaded with doxycycline modified bacteria. The PBS group is the control group containing pure RPMI medium while PMN and PMN + MP represent the neutrophil control groups without and with unmodified *M. luteus*.

A subsequent spectroscopic analysis of the mouse liver samples showed no traces of residual CHX five days after the treatment injection. The damage caused to an untreated liver by *Fusobacterium necrophorum* subspecies *necrophorum* can be seen in Figure 29



Figure 29: Image of a mouse liver from the PBS control group showing lesions caused by *F. necrophorum* subspecies *necrophorum*.

Conclusions

The *in vivo* mouse treatment study shows that:

- A non-pathogenic bacterium (*Micrococcus luteus*) can be used as a vector for efficiently loading neutrophils with drugs *ex-vivo*
- Chlorhexidine (a broad spectrum disinfectant) or doxycycline (a tetracycline antibiotic) can be efficiently taken up and trapped by the bacteria
- Mouse neutrophils containing the therapeutic cargo can kill *Fusobacterium necrophorum* *in-vitro*
- Mouse neutrophils loaded *ex-vivo* with the *M. luteus* containing antimicrobial drugs can be used as vehicles for targeted therapy of liver abscesses in mice caused by *Fusobacterium necrophorum*

Thus, the bacterium *M. luteus* is used as a liposome-like protective shell for the active ingredient, chlorhexidine. It protects the neutrophil granulocyte, our targeting carrier, from cytotoxic effects of the drug and enhances uptake via phagocytosis. Chlorhexidine is a potentially suitable bactericidal drug showing activity even against MRSA strains²²⁸). Using neutrophils as delivery vehicle has the advantage of a rapid targeted delivery to an infection site due to a fast

inflammation response. This allows localized treatment with low drug dosages. The short lifespan of neutrophils²²⁹⁾ guarantees a quick release of the drug.

It is intriguing that this cell-delivered antibacterial therapy was efficacious in the mouse model even though only a small amount of chlorhexidine was administered (less than 60 micrograms in $1.3 \cdot 10^6$ number of neutrophils), and only one dose was administered. Multiple daily injections of the cell therapy could improve the reduction of the CFU count and may have completely eliminated all bacteria. It is also possible that the cell-based therapy discussed here could be further enhanced by combining two or more agents in the bacteria. For example, silver has been shown to greatly enhance the efficacy of antibiotics, even in cases of drug resistance²³⁰⁾.

Effective antibacterial drugs exist, even for multidrug resistant bacteria, but they are limited by severe toxicity issues. For example, colistin, a polymyxin antibiotic discovered more than fifty years ago but discontinued due to its toxicity is now again in the clinic to treat cystic fibrosis patients, for which there is no other recourse²³¹⁾. If a good retention by the drug carrying bacterial cell is given, the approach presented here could allow such drugs to be used because cells are used as a Trojan horse to shield normal tissues and cells from the drug, and only very small amounts of the drug are required, due to a localized distribution.

Bacterial resistance to antimicrobials is now a global threat to humanity. The findings presented here may offer the prospect of a new armament in the perpetual arms race against multidrug resistant bacteria, since it utilizes a cell-based targeted approach for single or combinatorial delivery of antiseptics or antibiotics that would otherwise be toxic. It is intriguing that a very small amount of drug only administered once can be leveraged into a therapeutic benefit when actively targeted to the lesion by neutrophils.

References

1. Endrich B, Reinhold HS, Gross JF, Intaglietta M. Tissue perfusion inhomogeneity during early tumor growth in rats. *J Natl Cancer Inst.* 1979;62(2):387-95.
2. Grunt TW, Lametschwandtner A, Staindl O. The vascular pattern of basal cell tumors: light microscopy and scanning electron microscopic study on vascular corrosion casts. *Microvasc Res.* 1985;29(3):371-86.
3. Dewhirst MW, Tso CY, Oliver R, Gustafson CS, Secomb TW, Gross JF. Morphologic and hemodynamic comparison of tumor and healing normal tissue microvasculature. *Int J Radiat Oncol Biol Phys.* 1989;17(1):91-9.
4. Brown JM, Giaccia AJ. The unique physiology of solid tumors: opportunities (and problems) for cancer therapy. *Cancer Res.* 1998;58(7):1408-16.
5. Vaupel P, Schlenger K, Knoop C, Höckel M. Oxygenation of human tumors: evaluation of tissue oxygen distribution in breast cancers by computerized O₂ tension measurements. *Cancer Res.* 1991;51(12):3316-22.
6. Gray LH, Conger AD, Ebert M, Hornsey S, Scott OC. The concentration of oxygen dissolved in tissues at the time of irradiation as a factor in radiotherapy. *Br J Radiol.* 1953;26(312):638-48.
7. Tannock IF. The relation between cell proliferation and the vascular system in a transplanted mouse mammary tumour. *Br J Cancer.* 1968;22(2):258-73.
8. Bedford, J. S., and J. B. Mitchell. "The Effect of Hypoxia on the Growth and Radiation Response of Mammalian Cells in Culture." *British Journal of Radiology* 47.562 (1974): 687-96. Web.
9. Thomlinson RH, Gray LH. The histological structure of some human lung cancers and the possible implications for radiotherapy. *Br J Cancer.* 1955;9(4):539-49.
10. Brown JM. Evidence for acutely hypoxic cells in mouse tumours, and a possible mechanism of reoxygenation. *Br J Radiol.* 1979;52(620):650-6.
11. Rockwell S, Sartorelli AC, Tomasz M, Kennedy KA. Cellular pharmacology of quinone bioreductive alkylating agents. *Cancer Metastasis Rev.* 1993;12(2):165-76.
12. Rauth AM, Marshall RS, Kuehl BL. Cellular approaches to bioreductive drug mechanisms. *Cancer Metastasis Rev.* 1993;12(2):153-64.
13. Brown JM, Siim BG. Hypoxia-Specific Cytotoxins in Cancer Therapy. *Semin Radiat Oncol.* 1996;6(1):22-36.

14. Delaney, Geoff, Susannah Jacob, Carolyn Featherstone, and Michael Barton. "The Role of Radiotherapy in Cancer Treatment." *Cancer* 104.6 (2005): 1129-137. Web.
15. Urruticoechea A, Alemany R, Balart J, Villanueva A, Viñals F, Capellá G. Recent advances in cancer therapy: an overview. *Curr Pharm Des.* 2010;16(1):3-10.
16. Kerbel, Robert S., and Barton A. Kamen. "The Anti-angiogenic Basis of Metronomic Chemotherapy." *Nature Reviews Cancer* 4.6 (2004): 423-36. Web.
17. Hanahan, Douglas, Gabriele Bergers, and Emily Bergsland. "Less Is More, Regularly: Metronomic Dosing of Cytotoxic Drugs Can Target Tumor Angiogenesis in Mice." *Journal of Clinical Investigation* 105.8 (2000): 1045-047. Web.
18. Bailar, John C., and Heather L. Gornik. "Cancer Undefeated." *New England Journal of Medicine* 336.22 (1997): 1569-574. Web.
19. Beatson, Georgethomas. "On The Treatment Of Inoperable Cases Of Carcinoma Of The Mamma: Suggestions For A New Method Of Treatment, With Illustrative Cases.1." *The Lancet* 148.3802 (1896): 104-07. Web.
20. Shiau, Andrew K., Danielle Barstad, Paula M. Loria, Lin Cheng, Peter J. Kushner, David A. Agard, and Geoffrey L. Greene. "The Structural Basis of Estrogen Receptor/Coactivator Recognition and the Antagonism of This Interaction by Tamoxifen." *Cell* 95.7 (1998): 927-37. Web.
21. Smith, Ian E. "Aromatase Inhibitors in Early Breast Cancer Therapy." *Seminars in Oncology* 31 (2004): 9-14. Web.
22. Benson, Jr. "Tamoxifen in Early Breast Cancer." *The Lancet* 352.9125 (1998): 404-05. Web.
23. Yarden Y, Sliwkowski MX. Untangling the ErbB signalling network. *Nat Rev Mol Cell Biol.* 2001;2(2):127-37.
24. Slamon, D., W. Godolphin, L. Jones, J. Holt, S. Wong, D. Keith, W. Levin, S. Stuart, J. Udove, A. Ullrich, and Al. Et. "Studies of the HER-2/neu Proto-oncogene in Human Breast and Ovarian Cancer." *Science* 244.4905 (1989): 707-12. Web.
25. Slamon, Dennis J., Brian Leyland-Jones, Steven Shak, Hank Fuchs, Virginia Paton, Alex Bajamonde, Thomas Fleming, Wolfgang Eiermann, Janet Wolter, Mark Pegram, Jose Baselga, and Larry Norton. "Use of Chemotherapy plus a Monoclonal Antibody against HER2 for Metastatic Breast Cancer That Overexpresses HER2." *New England Journal of Medicine* 344.11 (2001): 783-92. Web.

26. Geyer, Charles E., John Forster, Deborah Lindquist, Stephen Chan, C. Gilles Romieu, Tadeusz Pienkowski, Agnieszka Jagiello-Gruszfeld, John Crown, Arlene Chan, Bella Kaufman, Dimosthenis Skarlos, Mario Campone, Neville Davidson, Mark Berger, Cristina Oliva, Stephen D. Rubin, Steven Stein, and David Cameron. "Lapatinib plus Capecitabine for HER2-Positive Advanced Breast Cancer." *New England Journal of Medicine* 355.26 (2006): 2733-743. Web.
27. Hanahan, D., and J. Folkman. "Patterns and Emerging Mechanisms of the Angiogenic Switch during Tumorigenesis." *Cell* 86.3 (1996): 353-64. Web.
28. Bergers, Gabriele, and Laura E. Benjamin. "Angiogenesis: Tumorigenesis and the Angiogenic Switch." *Nature Reviews Cancer* 3.6 (2003): 401-10. Web.
29. Carmeliet P, Dor Y, Herbert JM, et al. Role of HIF-1 alpha in hypoxia-mediated apoptosis, cell proliferation and tumour angiogenesis. *Nature*. 1998;394(6692):485-90.
30. Sherwood, Louis M., Edith E. Parris, and Judah Folkman. "Tumor Angiogenesis: Therapeutic Implications." *New England Journal of Medicine* 285.21 (1971): 1182-186. Web.
31. Relf M, Lejeune S, Scott PA, et al. Expression of the angiogenic factors vascular endothelial cell growth factor, acidic and basic fibroblast growth factor, tumor growth factor beta-1, platelet-derived endothelial cell growth factor, placenta growth factor, and pleiotrophin in human primary breast cancer and its relation to angiogenesis. *Cancer Res*. 1997;57(5):963-9.
32. Parato, Kelley A., Donna Senger, Peter A. J. Forsyth, and John C. Bell. "Recent Progress in the Battle between Oncolytic Viruses and Tumours." *Nature Reviews Cancer* 5.12 (2005): 965-76. Web.
33. Jensen HK, Donskov F, Marcussen N, Nordmark M, Lundbeck F, Von der maase H. Presence of intratumoral neutrophils is an independent prognostic factor in localized renal cell carcinoma. *J Clin Oncol*. 2009;27(28):4709-17.
34. Wislez M, Rabbe N, Marchal J, et al. Hepatocyte growth factor production by neutrophils infiltrating bronchioloalveolar subtype pulmonary adenocarcinoma: role in tumor progression and death. *Cancer Res*. 2003;63(6):1405-12.
35. Knaapen AM, Güngör N, Schins RP, Borm PJ, Van schooten FJ. Neutrophils and respiratory tract DNA damage and mutagenesis: a review. *Mutagenesis*. 2006;21(4):225-36.
36. Dallegri F, Ottonello L, Ballestrero A, et al. Tumor cell lysis by activated human neutrophils: analysis of neutrophil-delivered oxidative attack and role of leukocyte function-associated antigen 1. *Inflammation*. 1991;15(1):15-30.

37. Fridlender Z G; Sun J; Kim S; Kapoor V; Cheng G; Ling L; Worthen G S; Albelda S M, Polarization of tumor-associated neutrophil phenotype by TGF- β : "N1" versus "N2" TAN, *Cancer Cell* 2009, 16(3), 183-194
38. Human neutrophil-mediated lysis of ovarian cancer cells, Lichtenstein A; Seelig M; Berek J; Zigelboim J, *Blood*, 1989, 74(2), 805-9
39. Oxidative burst of neutrophils against melanoma B16-F10, Zivkovic M; Poljak-Blazi M; Zarkovic K; Mihaljevic D; Schaur R J; Zarkovic , *Cancer Letters* , 2007, 246(1-2), 100-108
40. Loss of collagenase-2 confers increased skin tumor susceptibility to male mice, Balbin M; Fueyo A; Tester A M; Pendas A M; Pitiot A S; Astudillo A; Overall C M; Shapiro S D; Lopez-Otin C, *Nature Genetics* 2003, 35(3), 252-257
41. Fas Ligand on Tumor Cells Mediates Inactivation of Neutrophils, Chen Y L; Chen S H; Wang J Y; Yang B C, *Journal of Immunology*, 2003, 171(3), 1183-1191
42. The neutrophil as a cellular source of chemokines, Scapini P; Lapinet-Vera J A; Gasperini S; Calzetti F; Bazzoni F; Cassatella M A, *From Immunological Reviews*, 2000, 177, 195-203
43. Inflammation and cancer, Coussens L M; Werb Z, *Nature* , 2002, 420(6917), 860-867
44. Matrix metalloproteinase-9 from bone marrow-derived cells contributes to survival but not growth of tumor cells in the lung microenvironment, Acuff H B; Carter K J; Fingleton B; Gorden D L; Matrisian L M, *Cancer research*, 2006, 66(1), 259-66
45. Tumor-elicited polymorphonuclear cells, in contrast to "normal" circulating polymorphonuclear cells, stimulate invasive and metastatic potentials of rat mammary adenocarcinoma cells, Welch D R; Schissel D J; Howrey R P; Aeed P A, *Proceedings of the National Academy of Sciences of the United States of America*, 1989, 86(15), 5859-63
46. Differential response of primary and metastatic melanomas to neutrophils attracted by IL-8, Schaidler H; Oka M; Bogenrieder T; Nesbit M; Satyamoorthy K; Berking C; Matsushima K; Herlyn M, *International Journal of Cancer*, 2003, 103(3), 335-343
47. Growth regulated Oncogene- α expression by murine squamous cell carcinoma promotes tumor growth, metastasis, leukocyte infiltration and angiogenesis by a host CXC Receptor-2 dependent mechanism, Loukinova E; Dong G; Enamorado-Ayalya I; Thomas G R; Chen Z; Schreiber H; Van Waes C, *Oncogene*, 2000, 19(31), 3477-3486
48. Neutrophils: key mediators of tumour angiogenesis, Tazzyman S; Lewis C E; Murdoch C, *International Journal of Experimental Pathology*, 2009, 90(3), 222-231

49. Infiltrating neutrophils mediate the initial angiogenic switch in a mouse model of multistage carcinogenesis, Nozawa H; Chiu C; Hanahan D, Proceedings of the National Academy of Sciences of the United States of America 2006, 103(33), 12493-12498
50. Peritumoral neutrophils link inflammatory response to disease progression by fostering angiogenesis in hepatocellular carcinoma, Kuang D M; Zhao Q; Wu Y; Peng C; Wang J; Xu Z; Yin X Y; Zheng L, Journal of Hepatology, 2011, 54(5), 948-955
51. IL-8 induces exocytosis of arginase 1 by neutrophil polymorphonuclears in nonsmall cell lung cancer, Rotondo R; Barisione G; Mastracci L; Grossi F; Orenco A M; Costa R; Truini M; Fabbi M; Ferrini S; Barbieri O, International Journal of Cancer 2009, 125(4), 887-893
52. Bellocq A, Antoine M, Flahault A, et al. Neutrophil alveolitis in bronchioloalveolar carcinoma: induction by tumor-derived interleukin-8 and relation to clinical outcome. Am J Pathol. 1998;152(1):83-92.
53. Reiman JM, Kmiecik M, Manjili MH, Knutson KL. Tumor immunoediting and immunosculpting pathways to cancer progression. Semin Cancer Biol. 2007;17(4):275-87.
54. Imai Y, Kubota Y, Yamamoto S, et al. Neutrophils enhance invasion activity of human cholangiocellular carcinoma and hepatocellular carcinoma cells: an *in vitro* study. J Gastroenterol Hepatol. 2005;20(2):287-93.
55. Gregory AD, Houghton AM. Tumor-associated neutrophils: new targets for cancer therapy. Cancer Res. 2011;71(7):2411-6.
56. Belaouaj A, Mccarthy R, Baumann M, et al. Mice lacking neutrophil elastase reveal impaired host defense against gram negative bacterial sepsis. Nat Med. 1998;4(5):615-8.
57. Houghton AM, Rzymkiewicz DM, Ji H, et al. Neutrophil elastase-mediated degradation of IRS-1 accelerates lung tumor growth. Nat Med. 2010;16(2):219-23.
58. Huh SJ, Liang S, Sharma A, Dong C, Robertson GP. Transiently entrapped circulating tumor cells interact with neutrophils to facilitate lung metastasis development. Cancer Res. 2010;70(14):6071-82.
59. "Antibiotic Treatment." *Centers for Disease Control and Prevention*. Centers for Disease Control and Prevention, 09 July 2013. Web. 24 Aug. 2014.
60. Jyoti Tanwar, Shrayanee Das, Zeeshan Fatima, and Saif Hameed, "Multidrug Resistance: An Emerging Crisis," *Interdisciplinary Perspectives on Infectious Diseases*, vol. 2014, Article ID 541340, 7 pages, 2014.

61. Bennett, Jason W., Janelle L. Robertson, Duane R. Hospenthal, Steven E. Wolf, Kevin K. Chung, Katrin Mende, and Clinton K. Murray. "Impact of Extended Spectrum Beta-Lactamase Producing *Klebsiella Pneumoniae* Infections in Severely Burned Patients." *Journal of the American College of Surgeons* 211.3 (2010): 391-99. Web.
62. Loeffler, J., and D. A. Stevens. "Antifungal Drug Resistance." *Clinical Infectious Diseases* 36.Supplement 1 (2003): S31-41. Web.
63. Khalilzadeh S, Boloorsaz MR, Safavi A, Farnia P, Velayati AA. Primary and acquired drug resistance in childhood tuberculosis. *East Mediterr Health J*. 2006;12(6):909-14.
64. Marks, Suzanne M., Jennifer Flood, Barbara Seaworth, Yael Hirsch-Moverman, Lori Armstrong, Sundari Mase, Katya Salcedo, Peter Oh, Edward A. Graviss, Paul W. Colson, Lisa Armitige, Manuel Revuelta, and Kathryn Sheeran. "Treatment Practices, Outcomes, and Costs of Multidrug-Resistant and Extensively Drug-Resistant Tuberculosis, United States, 2005–2007." *Emerging Infectious Diseases* 20.5 (2014): n. pag. Web.
65. Lee, Chang-Ro, Ill Cho, Byeong Jeong, and Sang Lee. "Strategies to Minimize Antibiotic Resistance." *International Journal of Environmental Research and Public Health* 10.9 (2013): 4274-305. Web.
66. S, Chethana G., Hari Venkatesh K R, Farhad Mirzaei, and S. M. Gopinath. "Review On Multi Drug Resistant Bacteria And Its Implication In Medical Sciences." *Journal of Biological and Scientific Opinion* 1.1 (2013): 32-37. Web.
67. Tenover FC. Mechanisms of antimicrobial resistance in bacteria. *Am J Med*. 2006;119(6 Suppl 1):S3-10.
68. S. Dzidic, J. Suskovic, and B. Kos, "Antibiotic resistance mechanisms in bacteria: biochemical and genetic aspects," *Food Technology and Biotechnology*, vol. 46, no. 1, pp. 11–21, 2008.
69. Palmer AC, Kishony R. Opposing effects of target overexpression reveal drug mechanisms. *Nat Commun*. 2014;5:4296.
70. Pierigè, F., S. Serafini, L. Rossi, and M. Magnani. "Cell-based Drug Delivery." *Advanced Drug Delivery Reviews* 60.2 (2008): 286-95. Web.
71. Freitas RA. Phagocytes: an ideal vehicle for targeted drug delivery. *J Nanosci Nanotechnol*. 2006;6(9-10):2769-75.
72. Freitas RA. Phagocytes: an ideal vehicle for targeted drug delivery. *J Nanosci Nanotechnol*. 2006;6(9-10):2769-75.

73. Allen TM. Ligand-targeted therapeutics in anticancer therapy. *Nat Rev Cancer*. 2002;2(10):750-63.
74. Huwyler, J. "Brain Drug Delivery of Small Molecules Using Immunoliposomes." *Proceedings of the National Academy of Sciences* 93.24 (1996): 14164-4169. Web.
75. Chowdhary RK, Shariff I, Dolphin D. Drug release characteristics of lipid based benzoporphyrin derivative. *J Pharm Pharm Sci*. 2003;6(1):13-9.
76. Allen, T. M. "Drug Delivery Systems: Entering the Mainstream." *Science* 303.5665 (2004): 1818-822. Web.
77. Bolotin, Elijah M., Rivka Cohen, Liliana K. Bar, Noam Emanuel, Sami Ninio, Yechezkel Barenholz, and Danilo D. Lasic. "Ammonium Sulfate Gradients for Efficient and Stable Remote Loading of Amphipathic Weak Bases into Liposomes and Ligandoliposomes." *Journal of Liposome Research* 4.1 (1994): 455-79. Web.
78. Cullis, Pieter R., Michael J. Hope, Marcel B. Bally, Thomas D. Madden, Lawrence D. Mayer, and David B. Fenske. "Influence of PH Gradients on the Transbilayer Transport of Drugs, Lipids, Peptides and Metal Ions into Large Unilamellar Vesicles." *Biochimica Et Biophysica Acta (BBA) - Reviews on Biomembranes* 1331.2 (1997): 187-211. Web.
79. Woodle MC, Newman MS, Cohen JA. Sterically stabilized liposomes: physical and biological properties. *J Drug Target*. 1994;2(5):397-403.
80. Cabanes A, Briggs KE, Gokhale PC, Treat JA, Rahman A. Comparative *in vivo* studies with paclitaxel and liposome-encapsulated paclitaxel. *Int J Oncol*. 1998;12(5):1035-40.
81. Meerum terwoegt JM, Groenewegen G, Pluim D, et al. Phase I and pharmacokinetic study of SPI-77, a liposomal encapsulated dosage form of cisplatin. *Cancer Chemother Pharmacol*. 2002;49(3):201-10.
82. Tollemar J, Andersson S, Ringdén O, Tydén G. A retrospective clinical comparison between antifungal treatment with liposomal amphotericin B (AmBisome) and conventional amphotericin B in transplant recipients. *Mycoses*. 1992;35(9-10):215-20.
83. Gelmon KA, Tolcher A, Diab AR, et al. Phase I study of liposomal vincristine. *J Clin Oncol*. 1999;17(2):697-705.

84. Tardi P, Choice E, Masin D, Redelmeier T, Bally M, Madden TD. Liposomal encapsulation of topotecan enhances anticancer efficacy in murine and human xenograft models. *Cancer Res.* 2000;60(13):3389-93.
85. Vasey PA, Kaye SB, Morrison R, et al. Phase I clinical and pharmacokinetic study of PK1 [N-(2-hydroxypropyl)methacrylamide copolymer doxorubicin]: first member of a new class of chemotherapeutic agents-drug-polymer conjugates. Cancer Research Campaign Phase I/II Committee. *Clin Cancer Res.* 1999;5(1):83-94.
86. Maeda H, Wu J, Sawa T, Matsumura Y, Hori K. Tumor vascular permeability and the EPR effect in macromolecular therapeutics: a review. *J Control Release.* 2000;65(1-2):271-84.
87. Hashizume, Hiroya, Peter Baluk, Shunichi Morikawa, John W. Mclean, Gavin Thurston, Sylvie Roberge, Rakesh K. Jain, and Donald M. McDonald. "Openings between Defective Endothelial Cells Explain Tumor Vessel Leakiness." *The American Journal of Pathology* 156.4 (2000): 1363-380. Web.
88. Schiffelers RM, Storm G, Bakker-woudenberg IA. Host factors influencing the preferential localization of sterically stabilized liposomes in *Klebsiella pneumoniae*-infected rat lung tissue. *Pharm Res.* 2001;18(6):780-7.
89. Edens HA, Levi BP, Jaye DL, et al. Neutrophil transepithelial migration: evidence for sequential, contact-dependent signaling events and enhanced paracellular permeability independent of transjunctional migration. *J Immunol.* 2002;169(1):476-86.
90. Northfelt DW, Dezube BJ, Thommes JA, et al. Pegylated-liposomal doxorubicin versus doxorubicin, bleomycin, and vincristine in the treatment of AIDS-related Kaposi's sarcoma: results of a randomized phase III clinical trial. *J Clin Oncol.* 1998;16(7):2445-51.
91. Jain, Rakesh K. "Transport of Molecules across Tumor Vasculature." *Cancer And Metastasis Review* 6.4 (1987): 559-93. Web.
92. Yuan F, Leunig M, Huang SK, Berk DA, Papahadjopoulos D, Jain RK. Microvascular permeability and interstitial penetration of sterically stabilized (stealth) liposomes in a human tumor xenograft. *Cancer Res.* 1994;54(13):3352-6.
93. Wu NZ, Da D, Rudoll TL, Needham D, Whorton AR, Dewhirst MW. Increased microvascular permeability contributes to preferential accumulation of Stealth liposomes in tumor tissue. *Cancer Res.* 1993;53(16):3765-70.
94. Netti, Paolo A., Sylvie Roberge, Yves Boucher, Laurence T. Baxter, and Rakesh K. Jain. "Effect of Transvascular Fluid Exchange on Pressure–Flow Relationship

- in Tumors: A Proposed Mechanism for Tumor Blood Flow Heterogeneity." *Microvascular Research* 52.1 (1996): 27-46. Web.
95. Gabizon, Alberto, Hilary Shmeeda, and Yechezkel Barenholz. "Pharmacokinetics of Pegylated Liposomal Doxorubicin." *Clinical Pharmacokinetics* 42.5 (2003): 419-36. Web.
 96. Lavan, David A., Terry McGuire, and Robert Langer. "Small-scale Systems for *in Vivo* Drug Delivery." *Nature Biotechnology* 21.10 (2003): 1184-191. Web.
 97. Guo X, Szoka FC. Chemical approaches to triggerable lipid vesicles for drug and gene delivery. *Acc Chem Res.* 2003;36(5):335-41.
 98. Bressler, Neil M. "Verteporfin Therapy of Subfoveal Choroidal Neovascularization in Age-related Macular Degeneration: Two-year Results of a Randomized Clinical Trial including Lesions with Occult with No Classic Choroidal Neovascularization—verteporfin in Photodynamic Therapy Report 2." *American Journal of Ophthalmology* 133.1 (2002): 168-69. Web.
 99. Glantz MJ, Jaeckle KA, Chamberlain MC, et al. A randomized controlled trial comparing intrathecal sustained-release cytarabine (DepoCyt) to intrathecal methotrexate in patients with neoplastic meningitis from solid tumors. *Clin Cancer Res.* 1999;5(11):3394-402.
 100. Zhang AY, Wu C, Zhou L, et al. Transduced monocyte/macrophages targeted to murine skin by UV light. *Exp Dermatol.* 2006;15(1):51-7.
 101. Aboody KS, Najbauer J, Schmidt NO, et al. Targeting of melanoma brain metastases using engineered neural stem/progenitor cells. *Neuro-oncology.* 2006;8(2):119-26.
 102. Gorantla, S., H. Dou, M. Boska, C. J. Destache, J. Nelson, L. Poluektova, B. E. Rabinow, H. E. Gendelman, and R. L. Mosley. "Quantitative Magnetic Resonance and SPECT Imaging for Macrophage Tissue Migration and Nanoformulated Drug Delivery." *Journal of Leukocyte Biology* 80.5 (2006): 1165-174. Web.
 103. Dou H, Destache CJ, Morehead JR, et al. Development of a macrophage-based nanoparticle platform for antiretroviral drug delivery. *Blood.* 2006;108(8):2827-35.
 104. Dutta, Tathagata, Hrushikesh B. Agashe, Minakshi Garg, Prahlad Balasubramaniam, Madhulika Kabra, and Narendra K. Jain. "Poly (propyleneimine) Dendrimer Based Nanocontainers for Targeting of Efavirenz to Human Monocytes/macrophages." *Journal of Drug Targeting* 15.1 (2007): 89-98. Web.

105. Hirota K, Hasegawa T, Hinata H, et al. Optimum conditions for efficient phagocytosis of rifampicin-loaded PLGA microspheres by alveolar macrophages. *J Control Release*. 2007;119(1):69-76.
106. Vyas, Suresh P., and Kapil Khatri. "Liposome-based Drug Delivery to Alveolar Macrophages." *Expert Opinion on Drug Delivery* 4.2 (2007): 95-99. Web.
107. Sou K, Goins B, Takeoka S, Tsuchida E, Phillips WT. Selective uptake of surface-modified phospholipid vesicles by bone marrow macrophages *in vivo*. *Biomaterials*. 2007;28(16):2655-66.
108. Hillaireau H, Le doan T, Appel M, Couvreur P. Hybrid polymer nanocapsules enhance *in vitro* delivery of azidothymidine-triphosphate to macrophages. *J Control Release*. 2006;116(3):346-52.
109. Lecaroz C, Gamazo C, Blanco-prieto MJ. Nanocarriers with gentamicin to treat intracellular pathogens. *J Nanosci Nanotechnol*. 2006;6(9-10):3296-302.
110. Cohen-sela E, Dangoor D, Epstein H, et al. Nanospheres of a bisphosphonate attenuate intimal hyperplasia. *J Nanosci Nanotechnol*. 2006;6(9-10):3226-34.
111. Cervasi B, Paiardini M, Serafini S, et al. Administration of fludarabine-loaded autologous red blood cells in simian immunodeficiency virus-infected sooty mangabeys depletes pSTAT-1-expressing macrophages and delays the rebound of viremia after suspension of antiretroviral therapy. *J Virol*. 2006;80(21):10335-45.
112. Zarabi, Bahar, Anjan Nan, Jiachen Zhuo, Rao Gullapalli, and Hamidreza Ghandehari. "Macrophage Targeted-(2-Hydroxypropyl)methacrylamide Conjugates for Magnetic Resonance Imaging." *Molecular Pharmaceutics* 3.5 (2006): 550-57. Web.
113. Owais M, Gupta CM. Targeted drug delivery to macrophages in parasitic infections. *Curr Drug Deliv*. 2005;2(4):311-8.
114. Lloyd, David H., Jacqueline Viac, Dirk Werling, Christophe A. Rème, and Hugues Gatto. "Role of Sugars in Surface Microbe-host Interactions and Immune Reaction Modulation." *Veterinary Dermatology* 18.4 (2007): 197-204. Web.
115. Anand RJ, Kohler JW, Cavallo JA, Li J, Dubowski T, Hackam DJ. Toll-like receptor 4 plays a role in macrophage phagocytosis during peritoneal sepsis. *J Pediatr Surg*. 2007;42(6):927-32.
116. Hirano, Masayuki, Randall S. Davis, W. David Fine, Shugo Nakamura, Kentaro Shimizu, Hirokazu Yagi, Koichi Kato, Robert P. Stephan, and Max D.

- Cooper. "IgE Immune Complexes Activate Macrophages through FcγRIV Binding." *Nature Immunology* 8.7 (2007): 762-71. Web.
117. Greaves DR, Gough PJ, Gordon S. Recent progress in defining the role of scavenger receptors in lipid transport, atherosclerosis and host defence. *Curr Opin Lipidol.* 1998;9(5):425-32.
 118. Aderem A, Underhill DM. Mechanisms of phagocytosis in macrophages. *Annu Rev Immunol.* 1999;17:593-623.
 119. Prior S, Gander B, Blarer N, et al. *In vitro* phagocytosis and monocyte-macrophage activation with poly(lactide) and poly(lactide-co-glycolide) microspheres. *Eur J Pharm Sci.* 2002;15(2):197-207.
 120. Schöler N, Zimmermann E, Katzfey U, Hahn H, Müller RH, Liesenfeld O. Effect of solid lipid nanoparticles (SLN) on cytokine production and the viability of murine peritoneal macrophages. *J Microencapsul.* 2000;17(5):639-50.
 121. Kagan VE, Bayir H, Shvedova AA. Nanomedicine and nanotoxicology: two sides of the same coin. *Nanomedicine.* 2005;1(4):313-6.
 122. Medina C, Santos-martinez MJ, Radomski A, Corrigan OI, Radomski MW. Nanoparticles: pharmacological and toxicological significance. *Br J Pharmacol.* 2007;150(5):552-8.
 123. Lee, Sungmun. "Monocytes: A Novel Drug Delivery System Targeting Atherosclerosis." *Journal of Drug Targeting* (2013): 1-8. Web.
 124. Serafini, S., L. Rossi, A. Antonelli, A. Fraternali, A. Cerasi, R. Crinelli, L. Chiarantini, G.f. Schiavano, and M. Magnani. "Drug Delivery through Phagocytosis of Red Blood Cells." *Transfusion Medicine and Hemotherapy* 31.2 (2004): 92-101. Web.
 125. Kay MM, Goodman SR, Sorensen K, et al. Senescent cell antigen is immunologically related to band 3. *Proc Natl Acad Sci USA.* 1983;80(6):1631-5.
 126. Riedmann EM, Kyd JM, Cripps AW, Lubitz W. Bacterial ghosts as adjuvant particles. *Expert Rev Vaccines.* 2007;6(2):241-53.
 127. Kudela P, Koller VJ, Lubitz W. Bacterial ghosts (BGs)--advanced antigen and drug delivery system. *Vaccine.* 2010;28(36):5760-7.
 128. Chellat F, Merhi Y, Moreau A, Yahia L. Therapeutic potential of nanoparticulate systems for macrophage targeting. *Biomaterials.* 2005;26(35):7260-75.
 129. Smith, D. H., J. R. Adams, S. R. D. Johnston, A. Gordon, M. F. Drummond, and C. L. Bennett. "A Comparative Economic Analysis of Pegylated

- Liposomal Doxorubicin versus Topotecan in Ovarian Cancer in the USA and the UK." *Annals of Oncology* 13.10 (2002): 1590-597. Web.
130. Peters BG, Goeckner BJ, Ponzillo JJ, Velasquez WS, Wilson AL. Pegaspargase versus asparaginase in adult ALL: a pharmaco-economic assessment. *Formulary*. 1995;30(7):388-93.
 131. Alberts DS, Garcia DJ. Safety aspects of pegylated liposomal doxorubicin in patients with cancer. *Drugs*. 1997;54 Suppl 4:30-5.
 132. Senter PD, Springer CJ. Selective activation of anticancer prodrugs by monoclonal antibody-enzyme conjugates. *Adv Drug Deliv Rev*. 2001;53(3):247-64.
 133. Samuels BL, Vogelzang NJ, Ruane M, Simon MA. Continuous venous infusion of doxorubicin in advanced sarcomas. *Cancer Treat Rep*. 1987;71(10):971-2.
 134. Lotem M, Hubert A, Lyass O, et al. Skin toxic effects of polyethylene glycol-coated liposomal doxorubicin. *Arch Dermatol*. 2000;136(12):1475-80.
 135. Aderem A. Phagocytosis and the inflammatory response. *J Infect Dis*. 2003;187 Suppl 2:S340-5.
 136. Grasso, P. *Essentials of Pathology for Toxicologists*. London: Taylor & Francis, 2002. Print.
 137. Metschnikoff E. Lecture on Phagocytosis and Immunity. *Br Med J*. 1891; 1(1570):213-7.
 138. Ernst, Joel D., and Olle Stendahl. *Phagocytosis of Bacteria and Bacterial Pathogenicity*. Cambridge, UK: Cambridge UP, 2006. Print.
 139. Rabinovitch, Michel. "Professional and Non-professional Phagocytes: An Introduction." *Trends in Cell Biology* 5.3 (1995): 85-87. Web.
 140. Fridman WH. Fc receptors and immunoglobulin binding factors. *FASEB J*. 1991; 5 (12):2684-90.
 141. Harris, H. "Chemotaxis of Granulocytes." *The Journal of Pathology and Bacteriology* 66.1 (1953): 135-46.
 142. Harris H. Role of chemotaxis in inflammation. *Physiol Rev*. 1954; 34 (3):529-62.
 143. Roitt, Ivan M., and Peter J. Delves. *Roitt's Essential Immunology*. Malden, MA: Blackwell Pub., 2006. Print.

144. Janeway CA Jr, Travers P, Walport M, et al. Immunobiology: The Immune System in Health and Disease. 5th edition. New York: Garland Science; 2001. Induced innate responses to infection. Available from: <http://www.ncbi.nlm.nih.gov/books/NBK27122/>
145. Ono, Santa Jeremy, Takao Nakamura, Dai Miyazaki, Masaharu Ohbayashi, Maria Dawson, and Masako Toda. "Chemokines: Roles in Leukocyte Development, Trafficking, and Effector Function." *Journal of Allergy and Clinical Immunology* 111.6 (2003): 1185-199. Web.
146. Fang, Ferric C. "Antimicrobial Reactive Oxygen and Nitrogen Species: Concepts and Controversies." *Nature Reviews Microbiology* 2.10 (2004): 820-32. Web.
147. Janeway CA Jr, Travers P, Walport M, et al. Immunobiology: The Immune System in Health and Disease. 5th edition. New York: Garland Science; 2001. The course of the adaptive response to infection. Available from: <http://www.ncbi.nlm.nih.gov/books/NBK27125/>
148. Dale, D. C., L. Boxer, and W. C. Liles. "The Phagocytes: Neutrophils and Monocytes." *Blood* 112.4 (2008): 935-45. Web.
149. Robinson, John M. "Phagocytic Leukocytes and Reactive Oxygen Species." *Histochemistry and Cell Biology* 131.4 (2009): 465-69. Web.
150. Shatwell, Karolyn P., and Anthony W. Segal. "NADPH Oxidase." *The International Journal of Biochemistry & Cell Biology* 28.11 (1996): 1191-195. Web.\
151. Vanaporn, M., M. Wand, S. L. Michell, M. Sarkar-Tyson, P. Ireland, S. Goldman, C. Kewcharoenwong, D. Rinchai, G. Lertmemongkolchai, and R. W. Titball. "Superoxide Dismutase C Is Required for Intracellular Survival and Virulence of Burkholderia Pseudomallei." *Microbiology* 157.8 (2011): 2392-400. Web.
152. Fridovich I. Superoxide radical and superoxide dismutases. *Annu Rev Biochem.* 1995;64:97-112.
153. Klebanoff SJ. Myeloperoxidase: friend and foe. *J Leukoc Biol.* 2005;77(5):598-625.

154. Tzong-Hsien Lee, Kristopher Hall, Adam Mechler, Lisandra Martin, Jonathan Popplewell, Gerry Ronan, Marie-Isabel Aguilar Molecular Imaging and Orientational Changes of Antimicrobial Peptides in Membranes American Peptide Society (2007) Peptides for Youth. Eds. Emanuel Escher, William D. Lubell, Susan Del Valle
155. Ibrahim, Hisham Radwan, Akio Kato, and Kunihiro Kobayashi. "Antimicrobial Effects of Lysozyme against Gram-negative Bacteria Due to Covalent Binding of Palmitic Acid." *Journal of Agricultural and Food Chemistry* 39.11 (1991): 2077-082. Web.
156. Farnaud, Sebastien, and Robert W. Evans. "Lactoferrin—a Multifunctional Protein with Antimicrobial Properties." *Molecular Immunology* 40.7 (2003): 395-405. Web.
157. Brix K. Lysosomal Proteases: Revival of the Sleeping Beauty. In: Madame Curie Bioscience Database [Internet]. Austin (TX): Landes Bioscience; 2000-. Available from: <http://www.ncbi.nlm.nih.gov/books/NBK6348/>
158. Green, Shawn J., Sylvie Mellouk, Stephen L. Hoffman, Monte S. Meltzer, and Carol A. Nacy. "Cellular Mechanisms of Nonspecific Immunity to Intracellular Infection: Cytokine-induced Synthesis of Toxic Nitrogen Oxides from L-arginine by Macrophages and Hepatocytes." *Immunology Letters* 25.1-3 (1990): 15-19. Web.
159. Krown, K. A., M. T. Page, C. Nguyen, D. Zechner, V. Gutierrez, K. L. Comstock, C. C. Glembotski, P. J. Quintana, and R. A. Sabbadini. "Tumor Necrosis Factor Alpha-induced Apoptosis in Cardiac Myocytes. Involvement of the Sphingolipid Signaling Cascade in Cardiac Cell Death." *Journal of Clinical Investigation* 98.12 (1996): 2854-865. Web.
160. Mosser, David M., and Justin P. Edwards. "Exploring the Full Spectrum of Macrophage Activation." *Nature Reviews Immunology* 8.12 (2008): 958-69. Web.
161. Warheit DB, Hill LH, George G, Brody AR. Time course of chemotactic factor generation and the corresponding macrophage response to asbestos inhalation. *Am Rev Respir Dis*. 1986; 134 (1):128-33.

162. Mak, Tak W., and Mary E. Saunders. *The Immune Response: Basic and Clinical Principles*. Amsterdam: Elsevier/Academic, 2006. Print.
163. Summers, Charlotte, Sara M. Rankin, Alison M. Condliffe, Nanak Singh, A. Michael Peters, and Edwin R. Chilvers. "Neutrophil Kinetics in Health and Disease." *Trends in Immunology* 31.8 (2010): 318-24. Web.
164. Zucker-franklin D. The percentage of monocytes among "mononuclear" cell fractions obtained from normal human blood. *J Immunol*. 1974; 112 (1):234-40.
165. Mehraj, V., J. Textoris, A. Ben Amara, E. Ghigo, D. Raoult, C. Capo, and J.-L. Mege. "Monocyte Responses in the Context of Q Fever: From a Static Polarized Model to a Kinetic Model of Activation." *Journal of Infectious Diseases* 208.6 (2013): 942-51. Web.
166. Randolph, Gwendalyn J., Kayo Inaba, Davide F. Robbiani, Ralph M. Steinman, and William A. Muller. "Differentiation of Phagocytic Monocytes into Lymph Node Dendritic Cells *In Vivo*." *Immunity* 11.6 (1999): 753-61. Web.
167. Hijdra, Daniëlle, Adriane D. M. Vorselaars, Jan C. Grutters, Anke M. E. Claessen, and Ger T. Rijkers. "Phenotypic Characterization of Human Intermediate Monocytes." *Frontiers in Immunology* 4 (2013): n. pag. Web.
168. Krombach, Fritz, Silvia Munzing, Anne-Marie Allmeling, J. Tilman Gerlach, Jurgen Behr, and Martina Dorger. "Cell Size of Alveolar Macrophages: An Interspecies Comparison." *Environmental Health Perspectives* 105 (1997): 1261. Web.
169. Cannon GJ, Swanson JA. The macrophage capacity for phagocytosis. *J Cell Sci*. 1992;101 (Pt 4):907-13.
170. Unanue ER. Antigen-presenting function of the macrophage. *Annu Rev Immunol*. 1984;2:395-428.
171. Underhill, D. M. "Dynamic Interactions of Macrophages with T Cells during Antigen Presentation." *Journal of Experimental Medicine* 190.12 (1999): 1909-914. Web.
172. Harding CV, Geuze HJ. Class II MHC molecules are present in macrophage lysosomes and phagolysosomes that function in the phagocytic

- processing of *Listeria monocytogenes* for presentation to T cells. *J Cell Biol.* 1992; 119 (3):531-42.
173. Mills CD. Macrophage arginine metabolism to ornithine/urea or nitric oxide/citrulline: a life or death issue. *Crit Rev Immunol.* 2001; 21 (5):399-425.
174. Gonzalez-mejia ME, Doseff AI. Regulation of monocytes and macrophages cell fate. *Front Biosci (Landmark Ed).* 2009; 14: 2413-31.
175. Bratton, Donna L., and Peter M. Henson. "Neutrophil Clearance: When the Party Is Over, Clean-up Begins." *Trends in Immunology* 32.8 (2011): 350-57. Web.
176. Brown, Simon, Isabelle Heinisch, Ewan Ross, Kate Shaw, Chris D. Buckley, and John Savill. "Apoptosis Disables CD31-mediated Cell Detachment from Phagocytes Promoting Binding and Engulfment." *Nature* 418.6894 (2002): 200-03. Web.
177. Friedl P, Borgmann S, Bröcker EB. Amoeboid leukocyte crawling through extracellular matrix: lessons from the Dictyostelium paradigm of cell movement. *J Leukoc Biol.* 2001;70(4):491-509.
178. Condeelis, John, and Jeffrey E. Segall. "Intravital Imaging of Cell Movement in Tumours." *Nature Reviews Cancer* 3.12 (2003): 921-30. Web.
179. Kumar, V., and A. Sharma. "Neutrophils: Cinderella of Innate Immune System." *International Immunopharmacology* 10.11 (2010): 1325-334. Web.
180. Pillay, J., I. Den Braber, N. Vrisekoop, L. M. Kwast, R. J. De Boer, J. A. M. Borghans, K. Tesselaar, and L. Koenderman. "In Vivo Labeling with 2H2O Reveals a Human Neutrophil Lifespan of 5.4 Days." *Blood* 116.4 (2010): 625-27. Web.
181. Lee A, Whyte MK, Haslett C. Inhibition of apoptosis and prolongation of neutrophil functional longevity by inflammatory mediators. *J Leukoc Biol.* 1993; 54(4):283-8.
182. Tofts, P. S., T. Chevassut, M. Cutajar, N. G. Dowell, and A. M. Peters. "Doubts concerning the Recently Reported Human Neutrophil Lifespan of 5.4 Days." *Blood* 117.22 (2011): 6050-052. Web.

183. Zweiman, Burton, Paul C. Atkins, Anne Moskovitz, Carolyn Von Allmen, Michael Ciliberti, and Scott Grossman. "Cellular Inflammatory Responses during Immediate, Developing, and Established Late-phase Allergic Cutaneous Reactions: Effects of Cetirizine." *Journal of Allergy and Clinical Immunology* 100.3 (1997): 341-47. Web.
184. Fridlender, Z. G., and S. M. Albelda. "Tumor-associated Neutrophils: Friend or Foe?" *Carcinogenesis* 33.5 (2012): 949-55. Web.
185. Downey GP, Doherty DE, Schwab B, Elson EL, Henson PM, Worthen GS. Retention of leukocytes in capillaries: role of cell size and deformability. *J Appl Physiol.* 1990;69(5):1767-78.
186. Lieber JG, Webb S, Suratt BT, et al. The *in vitro* production and characterization of neutrophils from embryonic stem cells. *Blood.* 2004; 103 (3):852-9.
187. Cartwright GE, Athens JW, Wintrobe MM. THE KINETICS OF GRANULOPOIESIS IN NORMAL MAN. *Blood.* 1964; 24:780-803.
188. Scheel-toellner D, Wang K, Craddock R, et al. Reactive oxygen species limit neutrophil life span by activating death receptor signaling. *Blood.* 2004; 104(8):2557-64.
189. Lee, G. Richard., and Maxwell M. Wintrobe. *Wintrobe's Clinical Hematology.* Philadelphia: Lea & Febiger, 1993 p201, 386. Print.
190. Borregaard N, Cowland JB. Granules of the human neutrophilic polymorphonuclear leukocyte. *Blood.* 1997;89(10):3503-21.
191. Bainton, D. F. "Sequential Degranulation Of The Two Types Of Polymorphonuclear Leukocyte Granules During Phagocytosis Of Microorganisms." *The Journal of Cell Biology* 58.2 (1973): 249-64. Web.
192. Brinkmann, V. "Neutrophil Extracellular Traps Kill Bacteria." *Science* 303.5663 (2004): 1532-535. Web.
193. Buss JL, Greene BT, Turner J, Torti FM, Torti SV. Iron chelators in cancer chemotherapy. *Curr Top Med Chem.* 2004;4(15):1623-35.

194. Kalinowski DS, Richardson DR. The evolution of iron chelators for the treatment of iron overload disease and cancer. *Pharmacol Rev.* 2005;57(4):547-83.
195. Finch RA, Liu M, Grill SP, et al. Triapine (3-aminopyridine-2-carboxaldehyde- thiosemicarbazone): A potent inhibitor of ribonucleotide reductase activity with broad spectrum antitumor activity. *Biochem Pharmacol.* 2000;59(8):983-91.
196. Abeysinghe RD, Greene BT, Haynes R, et al. p53-independent apoptosis mediated by tachpyridine, an anti-cancer iron chelator. *Carcinogenesis.* 2001;22(10):1607-14.
197. Guimaraes DP, Hainaut P. TP53: a key gene in human cancer. *Biochimie.* 2002;84(1):83-93.
198. Lowe SW. Cancer therapy and p53. *Curr Opin Oncol.* 1995;7(6):547-53.
199. O'connor PM, Jackman J, Bae I, et al. Characterization of the p53 tumor suppressor pathway in cell lines of the National Cancer Institute anticancer drug screen and correlations with the growth-inhibitory potency of 123 anticancer agents. *Cancer Res.* 1997;57(19):4285-300.
200. Thelander L, Reichard P. Reduction of ribonucleotides. *Annu Rev Biochem.* 1979;48:133-58.
201. Whitnall M, Howard J, Ponka P, Richardson DR. A class of iron chelators with a wide spectrum of potent antitumor activity that overcomes resistance to chemotherapeutics. *Proc Natl Acad Sci USA.* 2006;103(40):14901-6.
202. Le NT, Richardson DR. Iron chelators with high antiproliferative activity up-regulate the expression of a growth inhibitory and metastasis suppressor gene: a link between iron metabolism and proliferation. *Blood.* 2004;104(9):2967-75.
203. Bandyopadhyay S, Pai SK, Gross SC, et al. The Drg-1 gene suppresses tumor metastasis in prostate cancer. *Cancer Res.* 2003;63(8):1731-6.
204. Yuan J, Lovejoy DB, Richardson DR. Novel di-2-pyridyl-derived iron chelators with marked and selective antitumor activity: *in vitro* and *in vivo* assessment. *Blood.* 2004;104(5):1450-8.
205. Trinder D, Zak O, Aisen P. Transferrin receptor-independent uptake of differic transferrin by human hepatoma cells with antisense inhibition of receptor expression. *Hepatology.* 1996;23(6):1512-20.
206. Gupte A, Mumper RJ. Elevated copper and oxidative stress in cancer cells as a target for cancer treatment. *Cancer Treat Rev.* 2009;35(1):32-46.

207. Lovejoy DB, Jansson PJ, Brunk UT, Wong J, Ponka P, Richardson DR. Antitumor activity of metal-chelating compound Dp44mT is mediated by formation of a redox-active copper complex that accumulates in lysosomes. *Cancer Res.* 2011;71(17):5871-80.
208. Momparler RL, Karon M, Siegel SE, Avila F. Effect of adriamycin on DNA, RNA, and protein synthesis in cell-free systems and intact cells. *Cancer Res.* 1976;36(8):2891-5.
209. Silvestrini R, Lenaz L, Di Fronzo G, Sanfilippo O. Correlations between cytotoxicity, biochemical effects, drug levels, and therapeutic effectiveness of daunomycin and adriamycin on Sarcoma 180 ascites in mice. *Cancer Res.* 1973;33(11):2954-8.
210. Bonadonna G, Zucali R, Monfardini S, De Lena M, Uslenghi C. Combination chemotherapy of Hodgkin's disease with adriamycin, bleomycin, vinblastine, and imidazole carboxamide versus MOPP. *Cancer.* 1975;36(1):252-9.
211. Goodman MF, Bessman MJ, Bachur NR. Adriamycin and daunorubicin inhibition of mutant T4 DNA polymerases. *Proc Natl Acad Sci USA.* 1974;71(4):1193-6.
212. Wang JJ, Chervinsky DS, Rosen JM. Comparative biochemical studies of adriamycin and daunomycin in leukemic cells. *Cancer Res.* 1972;32(3):511-5.
213. Zunina F, Gambetta R, Di Marco A. The inhibition *in vitro* of DNA polymerase and RNA polymerases by daunomycin and adriamycin. *Biochem Pharmacol.* 1975;24(2):309-11.
214. Barry E, Alvarez JA, Scully RE, Miller TL, Lipshultz SE. Anthracycline-induced cardiotoxicity: course, pathophysiology, prevention and management. *Expert Opin Pharmacother.* 2007;8(8):1039-58.
215. Jones CG. Chlorhexidine: is it still the gold standard?. *Periodontol 2000.* 1997;15:55-62.
216. Martin AR. A technique for studying the action of antiseptics on bacteria in subcutaneous tissues, with special reference to chlorhexidine. *J Clin Pathol.* 1959;12(1):48-51.
217. Brooks SE, Walczak MA, Hameed R, Coonan P. Chlorhexidine resistance in antibiotic-resistant bacteria isolated from the surfaces of dispensers of soap containing chlorhexidine. *Infect Control Hosp Epidemiol.* 2002;23(11):692-5.
218. Cookson BD, Bolton MC, Platt JH. Chlorhexidine resistance in methicillin-resistant *Staphylococcus aureus* or just an elevated MIC? An *in vitro* and *in vivo* assessment. *Antimicrob Agents Chemother.* 1991;35(10):1997-2002.

219. Van meerloo J, Kaspers GJ, Cloos J. Cell sensitivity assays: the MTT assay. *Methods Mol Biol.* 2011;731:237-45.
220. "Support Protocols." General Annexin V Staining Procedure. N.p., n.d. Web. 29 July 2014.
221. Perera AS, Wang H, Basel MT, Pokhrel MR, Gamage PS, et al. (2013) Channel Blocking of MspA Revisited. *Langmuir* 29: 308-315.
222. Narayanan SK, Chengappa MM, Stewart GC, Nagaraja TG. Immunogenicity and protective effects of truncated recombinant leukotoxin proteins of *Fusobacterium necrophorum* in mice. *Vet Microbiol.* 2003;93(4):335-47.
223. Rowe, R., Todd, R., Waide, J., 1977. Microtechnique for mostprobable-number analysis. *Appl. Environ. Microbiol.* 333, 675– 680.
224. Reiss M, Roos D. Differences in oxygen metabolism of phagocytosing monocytes and neutrophils. *J Clin Invest.* 1978;61(2):480-8.
225. Critchlow, D. E. and Fligner, M. A. (1991), "On Distribution-Free Multiple Comparisons in the One-Way Analysis of Variance," *Communications in Statistics—Theory and Methods*, 20, 127–139.
226. Dwass, M. (1960), *Contributions to Probability and Statistics*, chapter Some k-Sample Rank-Order Tests, 198–202, Stanford, CA: Stanford University Press.
227. Steel, R. G. D. (1960), "A Rank Sum Test for Comparing All Pairs of Treatments," *Technometrics*, 2, 197–207.
228. Brooks, Steven E., Mary A. Walczak, Rizwanullah Hameed, and Patrick Coonan. "Chlorhexidine Resistance in Antibiotic-Resistant Bacteria Isolated From the Surfaces of Dispensers of Soap Containing Chlorhexidine, *Infection Control and Hospital Epidemiology* 23.11 (2002): 692-95. Web.
229. Pillay, J., I. Den Braber, N. Vrisekoop, L. M. Kwast, R. J. De Boer, J. A. M. Borghans, K. Tesselaar, and L. Koenderman. "*In Vivo* Labeling with $^2\text{H}_2\text{O}$ Reveals a Human Neutrophil Lifespan of 5.4 Days." *Blood* 116.4 (2010): 625-27. Web.

230. Morones-Ramirez, J. R., J. A. Winkler, C. S. Spina, and J. J. Collins. "Silver Enhances Antibiotic Activity Against Gram-Negative Bacteria." *Science Translational Medicine* 5.190 (2013): 190ra81. Web.
231. Li, Jian, Roger L. Nation, John D. Turnidge, Robert W. Milne, Kingsley Coulthard, Craig R. Rayner, and David L. Paterson. "Colistin: The Re-emerging Antibiotic for Multidrug-resistant Gram-negative Bacterial Infections." *The Lancet Infectious Diseases* 6.9 (2006): 589-601. Web.
232. Holian A, Daniele RP. Stimulation of oxygen consumption and superoxide anion production in pulmonary macrophages by N-formyl methionyl peptides. *FEBS Lett.* 1979;108(1):47-50.
233. C. R. Wilke, P Chang, Correlation of diffusion coefficients in dilute solutions, *AIChE Journal*, Volume 1, Issue 2, pages 264–270, June 1955
234. Ping Han and David M. Bartels, Temperature Dependence of Oxygen Diffusion in H₂O and D₂O, *The Journal of Physical Chemistry* 1996 100 (13), 5597-5602
235. Hass, Volker C., and Ralf Pörtner. *Praxis Der Bioprozesstechnik: Mit Virtuellem Praktikum*. Heidelberg: Spektrum, Akad. Verl., 2011. Print.
236. Benson, Bruce B., and Daniel Krause. "The Concentration and Isotopic Fractionation of Oxygen Dissolved in Freshwater and Seawater in Equilibrium with the Atmosphere." *Limnology and Oceanography* 29.3 (1984): 620-32. Web.
237. Miller WM, Wilke CR, Blanch HW. Effects of dissolved oxygen concentration on hybridoma growth and metabolism in continuous culture. *J Cell Physiol.* 1987;132(3):524-30.
238. Robinson JM. Reactive oxygen species in phagocytic leukocytes. *Histochem Cell Biol.* 2008;130(2):281-97.
239. Joshi GN, Knecht DA. Silica phagocytosis causes apoptosis and necrosis by different temporal and molecular pathways in alveolar macrophages. *Apoptosis.* 2013;18(3):271-85.

Appendix A - R-code for student's t-test

R-code used for students t-test:

```
two.sample.t.test.with.summary.data=function(x1bar,x2bar,s1,s2,n1,n2, mu,
                                             var.equal=FALSE, alternative ='less'){
  if( var.equal==FALSE )
  { se = sqrt( (s1^2/n1) + (s2^2/n2) )
    # welch-satterthwaite df
    df = ( (s1^2/n1 + s2^2/n2)^2 )/( (s1^2/n1)^2/(n1-1) + (s2^2/n2)^2/(n2-1) )
  } else
  { # pooled standard deviation, scaled by the sample sizes
    se = sqrt( (1/n1 + 1/n2) * ((n1-1)*s1^2 + (n2-1)*s2^2)/(n1+n2-2) )
    df = n1+n2-2
  }
  tobs=(x1bar-x2bar- mu)/ se
  if (alternative =='less') pvalue= pt(tobs, df=df)
  if (alternative =='greater') pvalue= 1-pt(tobs, df=df)
  if (alternative =='two.sided') pvalue= 2*( 1-pt(abs(tobs), df=df) )
  list(test.stat=tobs, pvalue=pvalue, alternative=alternative)
}
x1bar=#insert_value# ; x2bar=#insert_value#; s1=#insert_value#;
s2=#insert_value#; n1= #insert_value#; n2= #insert_value#; mu=0
two.sample.t.test.with.summary.data(x1bar,x2bar,s1,s2,n1,n2, mu,
                                    var.equal=TRUE, alternative ='less')
```